Three-Dimensional Patterning Using Ultraviolet Curable Nanoimprint Lithography

by

Khairudin Mohamed

A thesis submitted in partial fulfillment

of the requirements for the Degree of

Doctor of Philosophy

in Electrical and Computer Engineering

at the University of Canterbury, Christchurch, New Zealand.

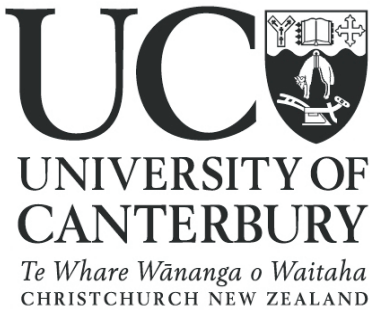

October 2009

For my beloved family...

Abstract

Although a large number of works on nanoimprint lithography (NIL) techniques have been reported, the the ability for three-dimensional (3-D) patterning using NIL has not been fully addressed in terms of the mold fabrication and imprint processes. Patterning 3-D and multilevel features are important because they eliminate multiple steps and complex interlevel alignments in the nanofabrication process. In this thesis, the 3-D and multilevel mold design and fabrication, and imprint processes have been studied and investigated.

Semiconductor industries through the International Technology Roadmap for Semiconductor (ITRS) organization have identified NIL, especially ultraviolet curable nanoimprint lithography (UV-NIL) as a strong candidate for the next generation lithography (NGL) technology for nodes down to 5 nm. In the UV-NIL technique, a transparent mold with micro/nanostructure patterns on its surface is allowed to be replicated on UV curable polymer without the need of high applied pressure or temperature. UV-NIL has the potential to fabricate micro/nanostructures with high resolution, high reproducibility, low cost, high throughput and is capable of 3-D patterning. Its resolution is not limited by diffraction as in optical lithography or electron scattering as in electron beam lithography (EBL).

This research focuses on two aspects; the development of mold making and imprint processes. The development of the 2-D mold making process of high aspect ratio structures was used as a platform to understand the underlying science and engineering prior to the development of more challenging 3-D mold making processes of geometrical shapes such as pyramid, cones and hemisphere. Similarly, the development of the 2-D imprint process was used to characterize and optimize the imprint process parameters such as resist ma-

terials, imprint pressure and sticking issues. The subsequent development of 3-D imprint processes has been simplified with the knowledge developed in 2-D processes. This approach has paved the way for successful 3-D UV-NIL.
Quartz is of particular interest as a mold substrate because of its known superior properties in UV transmission. It can withstand high temperatures and is an extremely hard material.
In the process of making a master mold, an EBL technique was employed for writing patterns on e-beam resists. PMMA positive resist was used for 2-D patterning and ma-N2403 negative resist from Microresist Technology was used for 3-D patterning. After being developed, the 3-D mold pattern was transferred onto quartz substrate using a single-step reactive ion etching (RIE) technique.
A number of challenging issues such as surface charging, electron scattering and proximity effects surfaced during the EBL pattern writing on insulating and transparent molds. Built up charges will cause e-beam deflection and proximity effects have a limiting influence when patterning dense patterns. A number of new approaches have been developed for suppressing the charging effects in the 2-D and 3-D patterning. Using thin metallic coating on the quartz substrates or on top of the resist, or conductive polymer coating using PEDOT/PSS on top of the resist has demonstrated excellent results in a 2-D structure with a high aspect-ratio of 1:10 and feature sizes down to 60 nm. In 3-D patterning, two approaches have been followed; the critical energy method and/or a top coating of conductive polymer (PEDOT/PSS) layer. Isolated 3-D structures with feature sizes down to 500 nm were successfully fabricated using the first method while by using the second method, dense 3-D structures patterns with feature sizes down to 300 nm, on 400 nm pitch have been demonstrated.
In UV-NIL, the surface roughness $R_{q(rms)}$ should be less than 5 nm. This is especially important for replicating optical structures and devices. In this work, the RIE process been optimized to yield 2 nm roughness on a patterned quartz surface. This was achieved by optimizing the RIE process pressure of below 6 mTorr.

The other part of this thesis is on replication or imprinting of 2-D and 3-D structures. In the process of replicating the master mold profiles, the imprint processes were carried out using a vacuum operated manual imprint tool which was attached to a Mask Aligner UV illumination system. The replication of the profiles of a 2-D mold requires a single step imprint, but two imprint steps are involved in the replication of a 3-D mold structure. In 2-D imprinting, resist sticking on the vertical side wall was the main issue, especially on high aspect ratio structures. Meanwhile in 3-D imprinting, the imprint results have shown good reproducibility in up to 15 imprint cycles, where the issue of Ormocomp soft/daughter mold cracking after long UV exposure had limited the repetition of the imprint cycles.

In this thesis, the 2-D and 3-D resist patterning on insulating substrates using the EBL technique have been demonstrated with the assistance of a number of developed charge suppression methods. Single-step RIE pattern transfer onto quartz substrates with surface roughness below 5nm has been achieved. Replication of 3-D and multilevel structures reliably make the UV-NIL technique suitable for future applications such as surface texturing, optical devices and many other complex structures including MEMS.

Acknowledgements

Sincere thanks go to my supervisor Associate Professor Maan Alkaisi, for his endless efforts in coaching me throughout postgraduate studies since the first day of my enrolment in the Master of Engineering course in March 2003. His advice, comments, input and recommendations have had a significant impact on the quality of this research work.

Special thanks go to my co-supervisor Professor Richard J. Blaikie, for keeping track of the progress of the students and providing brilliant comments on the publications of research work.

Many thanks go to Helen Devereux and Gary Turner for providing technical assistance during the nanofabrication laboratory work. Similarly Dr Marko Vogler from Microresist Technology Gmbh is also thanked, for countless discussions regarding resist materials.

This appreciation is also extended to post doctoral fellows, Dr. Euan Boyd (Physics Dept.), Dr. Liu Xiang Ming (Chemistry Dept.) and former postgraduates in the Electrical and Computer Engineering department, Dr Kumar Ganesh, Dr. James Muys, and Dr. Lin Ling for fruitful discussion on research matters.

Many thanks go to peer postgraduates Volker Nock and Elliot Cheng for our endless discussion about issues in our research work and David Garret (Chemistry Dept) for helping in surface wetting experiments. A third professional year student, Tuan Hassan, is also thanked for his assistance in accomplishing some special tasks in this study of further shrinking of 3-D structures.

I would like to acknowledge the Mac Diarmid Institute for providing facilities for this research work and funds to attend conferences locally and overseas. The author is grateful to University Sains Malaysia (USM) and the Ministry of Higher Education of Malaysia (MOHE) for providing the scholarship and travel

funds during the studies.

Last but not least, my sincere thanks go to my dear wife Zarita Abdul Razak, our children Nur Balqis, Nur Zahirah, Mukhriz, Harris, Idris and Jazmyn for their endless love, understanding, support and great patience. Also a million thanks to my family members back home in Malaysia and local friends for their advice, motivation and encouragement.

Preface

This thesis was written based on author's research work in the Nanoimprint Lithography research area. His Master of Engineering degree (M.E.) with a thesis titled "Resist Deformation in Nanoimprint Lithography (NIL)" was completed at the University of Canterbury, Christchurch, New Zealand in April 2005. He continued this research area with PhD studies entitled "Three-Dimensional Patterning using Ultraviolet Curable Nanoimprint Lithography".

This new research area has many opportunities and unlimited potential applications. As NIL technology is still far from maturity, there are so much to be understood and so much to be explored. However, the knowledge of nanoscience and technologies, especially in NIL research area is developing quickly, suggesting that tracking the progress of this research area is essential. This research work is referring to the latest developments of NIL research area as well as contributing the new findings and ideas into this research community.

This thesis has contributed significantly in NIL research area especially in design, fabrication and testing of three-dimensional patterning at nanoscale structures using Nanoimprint lithography. The knowledge developed in the research work was published in a master's thesis, book chapter, journal publications, conference proceedings, oral presentations and poster presentations. Below are the list of the author's publications during the studies.

Thesis

1. Khairudin Mohamed, "Resist deformation in nanoimprint lithography (NIL)", Master of Engineering (ME) Thesis, Electrical and Computer Engi-

neering Department, University of Canterbury, New Zealand, April 2005.

Book Chapter

1. Maan Alkaisi and Khairudin Mohamed, "3D Patterning using UV-NIL" in "Lithography", Aleksandar Lazinica Ed., IN-TECH, Vienna Austria, ISBN 978-953-7619-X-X. (In Review), 2009.

Journal Publications

1. K. Mohamed, M. M. Alkaisi and J. Smaill, "Resist deformation at Low Temperatures in Nanoimprint lithography", Current Applied Physics, 6, pp 486-490, 2006.

2. K. Mohamed, M. M. Alkaisi and R. J. Blaikie, "The fabrication of three dimensional structures for UV curable nanoimprint (UV-NIL) mold using variable dose control with critical energy electron beam exposure", Journal Vacuum Science and Technology B., 25(6), pp 2357-2360, Nov/Dec 2007.

3. K. Mohamed, M. M. Alkaisi and R. J. Blaikie, "The replication of three dimensional structures using UV Curable nanoimprint lithography (UV-NIL)", Journal of Vacuum Science and Technology B., 26(6), pp 2500-2503, Nov/Dec 2008.

4. K. Mohamed, M. M. Alkaisi and R. J. Blaikie, "Surface charging suppression using PEDOT/PSS in the fabrication of three dimensional structures on quartz substrate", Microelectronic Engineering, 86, pp 535-538, 2009.

5. K. Mohamed and M. M. Alkaisi, "Three-dimensional pattern transfer on quartz substrates", Microelectronic Engineering, (In Review).

Proceedings

1. K. Mohamed, M. M. Alkaisi and R. J. Blaikie, ”The ultraviolet curable nanoimprint lithography (UV-NIL) technique for replicating three dimensional structures”, Proceedings of United Kingdom-Malaysia Engineering Conference (UK-MEC 2008), University College of London, pp19-22, 2008.

2. K. Mohamed, M. M. Alkaisi and R. J. Blaikie, ”A three dimensional UV curable nanoimprint lithography”, AIP Conference Proceedings of the Fourth International Conference on Advanced Materials and Nanotechnology (AMN-4), Dunedin, New Zealand, Feb 8-12, pp114-117, 2009.

3. A. Ali, K. Mohamed, S. L. Ranford, and H. Zhang, ”Developments towards a Surface Acoustic Wave (SAW) sensor for detecting volatiles and its evaluation system”, AIP Conference Proceedings of the Fourth International Conference on Advanced Materials and Nanotechnology (AMN-4), Dunedin, New Zealand, Feb 8-12, pp110-113, 2009.

Oral Presentations

1. K. Mohamed, M. M. Alkaisi and R. J. Blaikie, ”Three dimensional UV-NIL”, The Third International Conference on Advanced Materials and Nanotechnology (AMN-3), Wellington, New Zealand, Feb 11-16, 2007.

2. K. Mohamed, M. M. Alkaisi and R. J. Blaikie, ”The fabrication of three dimensional mold structures for UVNIL”, Nanolithography Workshop, University of Canterbury, Feb 19 & 20, 2007.

3. K. Mohamed, M. M. Alkaisi and R. J. Blaikie, ”The ultraviolet curable nanoimprint lithography (UV-NIL) technique for replicating three dimensional structures”, Proceeding of United Kingdom-Malaysia Engineering Conference (UK-MEC 2008), University College of London, United Kingdom, July 14 & 15, 2008.

Poster Presentations

1. K. Mohamed, M. M. Alkaisi and J. Smaill, ”Resist deformation in Nanoimprint lithography”, The Second International Conference on Advanced Materials and Nanotechnology (AMN-2), Queenstown, New Zealand, Feb 6-11, 2005.

2. K. Mohamed, M. M. Alkaisi and R. J. Blaikie, ”The fabrication of three dimensional mold structures for UV-NIL”, The Fifth International Conference of Nanoimprint and Nanoprint Technology (NNT ’06), San Francisco, USA, Nov 15- 17, 2006.

3. K. Mohamed, M. M. Alkaisi and R. J. Blaikie, ”The fabrication of three dimensional structures for UV curable nanoimprint (UV-NIL) mold using variable dose control with critical energy electron beam exposure”, The 51st International Conference of Electron, Ion, Photon and Nanotechnology Conference (EIPBN 2007), Denver, Colorado, USA, May 29 - Jun 1, 2007.

4. K. Mohamed, M. M. Alkaisi and R. J. Blaikie, ”The fabrication of 3D structures with multilevel features”, UC Postgraduate Showcase ’07, University of Canterbury, Christchurch, New Zealand, Aug 29, 2007.

5. K. Mohamed, M. M. Alkaisi and R. J. Blaikie, ”The replication of three dimensional microstructures using Ultraviolet Curable Nanoimprint Lithography (UV-NIL)”, UC College of Engineering’s MacDiarmid Poster Competition ’08, University of Canterbury, Christchurch, New Zealand, Mar 2008.

6. K. Mohamed, M. M. Alkaisi and R. J. Blaikie, ”Three dimensional nanolithography using Ultraviolet Curable Nanoimprint Lithography (UV-NIL)”, The 52nd International Conference of Electron, Ion, Photon and Nanotechnology (EIPBN 2008), Portland, Oregon, USA, May 27 - 30, 2008.

7. K. Mohamed, M. M. Alkaisi and R. J. Blaikie, ”Surface charging suppression using PEDOT/PSS in the fabrication of three dimensional structures on quartz substrate”, The 34th International Conference on Micro and Nano Engineering (MNE 2008), Athens, Greece, Sept 15 - 18, 2008.

8. K. Mohamed, M. M. Alkaisi and R. J. Blaikie, ”Patterning of three dimensional structures using UV curable nanoimprint lithography (UV-NIL)”, The Fourth International Conference on Advanced Materials and Nanotechnology (AMN-4), Dunedin, New Zealand, Feb 8-12, 2009.

9. A. Ali, K. Mohamed, S. L. Ranford, and H. Zhang, ”The development of a Surface Acoustic Wave (SAW) sensor for detecting volatiles and its evaluation system”, The Fourth International Conference on Advanced Materials and Nanotechnology (AMN-4), Dunedin, New Zealand, Feb 8-12, 2009.

10. K. Mohamed and M. M. Alkaisi, ”Three-dimensional pattern transfer on quartz substrate”, The 35th International Conference on Micro and Nano Engineering (MNE 2009), Ghent, Belgium, Sept 28 - 30, 2009.

11. K. Mohamed and M. M. Alkaisi, ”The high aspect ratio pattern transfer on quartz substrate”, The 35th International Conference on Micro and Nano Engineering (MNE 2009), Ghent, Belgium, Sept 28 - 30, 2009.

Table of Contents

Chapter 1: INTRODUCTION **1**

1.1 Next Generation Lithography (NGL) 2

1.2 Overview of Nanoimprint Lithography Techniques 5

1.3 The Ultraviolet Curable Nanoimprint Lithography (UV-NIL) . . . 10

1.4 Nanoimprint Process 12

1.5 Nanoimprint Lithography: Opportunities and Applications . . . 13

1.6 Research Background 15

1.7 The Objectives of the Thesis 18

1.8 Thesis Outline 19

Chapter 2: EXPERIMENTAL TECHNOLOGIES **21**

2.1 Process and Apparatus 22

2.1.1 Pattern Definition Using the EBL Technique 23

2.1.2 Pattern Development 28

2.1.3 Metal Deposition Techniques 28

2.1.3.1 Metal Thermal Evaporator 29

2.1.3.2 E-beam Evaporator 31

2.1.3.3 Magnetron Sputtering 31

2.1.4 Surface Profiler 33

2.1.5 Lift off 34

2.1.6 Surface Imaging Techniques 35

2.1.6.1 Scanning Electron Microscopy (SEM) 36

2.1.6.2 Atomic Force Microscopy (AFM) 37

2.1.7 Pattern Transfer 39

2.1.8 Imprint Tools 42

2.1.9 Surface Wetting 44

2.2 Materials 46
2.2.1 Substrate Material 46
2.2.2 Cleaning in the Mold Making Process 47
2.2.3 Resists for Mold Fabrication 48
2.2.4 Resists for Imprint Processes 51
2.2.5 Anti-Sticking Layers 53
2.2.6 Conductive Polymer 55
2.3 Summary 55

Chapter 3: MOLD FABRICATION 57
3.1 The Fabrication of Two-Dimensional Structures 58
3.1.1 Preparation 59
3.1.2 The Fabrication Techniques 60
3.1.2.1 Thin Metallic Coating on Quartz Substrate 61
3.1.2.2 Thin Metal Coating on Top of Resist 62
3.1.2.3 Conductive Polymer Coating on Top of Resist . . 65
3.1.3 Pattern Definition using EBL 68
3.1.4 The 2-D Pattern Transfer 69
3.1.4.1 Etching Chemistry 71
3.1.4.2 Etching Analysis 73
3.2 The Fabrication of Three-Dimensional Structures 78
3.2.1 Preparation 78
3.2.2 Fabrication Techniques 80
3.2.2.1 The Critical Energy or Critical Accelerating Voltage 82
3.2.2.2 Top Conductive Dissipation Layer using PEDOT/PSS 87
3.2.3 Three-Dimensional Pattern Transfer 90
3.2.3.1 Etching Chemistry 92
3.2.3.2 Etching Analysis 95
3.3 Summary 102

Chapter 4: IMPRINTS 105
4.1 The Imprint of Two-Dimensional Structures 107
4.1.1 Preparation 107

4.1.2 Imprint Process 108
4.1.2.1 Imprint using Transparent Molds 110
4.1.2.2 Imprint using Transparent Molds with a NiCr Absorber 111
4.1.3 Final Pattern Transfer 112
4.1.4 2-D Imprint Analysis 113
4.2 The Imprint of Three-Dimensional Structures 117
4.2.1 Preparation 117
4.2.2 Imprint Process 119
4.2.2.1 Imprint 1 121
4.2.2.2 Imprint 2 125
4.2.3 Final Pattern Transfer 126
4.2.4 3-D Imprint Analysis 128
4.3 Summary 130

Chapter 5: DISCUSSION AND RECOMMENDATIONS 131
5.1 General NIL Issues 132
5.1.1 Particle Related Defects 132
5.1.2 Irregularities in Polymers 133
5.1.3 Overlay Accuracies 134
5.1.4 Throughput 134
5.2 Limitations of This Work 135
5.3 Recommendations for Future Work 136
5.3.1 Processes and Equipments 137
5.3.2 Materials 138
5.4 Future of NIL Technology 138
5.5 Summary 140

Chapter 6: CONCLUSIONS 143

Chapter Appendices 163

Chapter A: List of equipment used in this research work 165

Chapter B: Chemicals used in this research work **171**

Chapter C: Other Images **173**

List of Figures

1.1 The schematic diagram of the Extreme Ultra Violet Lithography system. 4
1.2 The International Technology Roadmap for Semiconductor (2008 Update) 5
1.3 Type of nanoimprint lithography technique 7
1.4 The schematic of NIL processes based on step and repeat sequence. 9
1.5 The schematic of micro contact printing (μCP) process flow. 9
1.6 The schematic process flow of reversal imprint lithography. 10
1.7 Type of UV curable nanoimprint lithography technique for mass production 12
1.8 The schematic of imprint analysis for 2-D and 3-D imprint processes. 14
1.9 Examples of 3-D structures fabricated using different lithographic techniques 16
1.10 Recent work on surface texturing on silicon substrate using the RIE technique. 17

2.1 The schematic diagram of the electron beam lithography system . 24
2.2 The schematic of electron beam configuration of the area step size and single pass line (SPL) 26
2.3 The example of the proximity correction on a 2-D pattern during pattern writing using EBL. 27
2.4 The different method of 3-D patterning using the EBL technique. 27
2.5 Electron beam induced chain scission and crosslinking reaction of resists. 29
2.6 The schematic diagram of a metal/thermal evaporator 30
2.7 The schematic diagram of a magnetron sputtering system 32

2.8 The schematic diagram of a profiler system 34
2.9 The schematic diagram of patterning on PMMA bi-layer using lift off method 34
2.10 Various morphology characterization using different imaging and analytical techniques 36
2.11 The schematic diagram of atomic force microscope detection using the laser beam deflection method 38
2.12 SEM images of AFM tips used in this work. 39
2.13 Plasma etch processes on chamber pressure scale 40
2.14 The plasma etching mechanism 41
2.15 The schematic view of an RIE system 42
2.16 The second (vacuum operated) manual imprint tool used in this research work. 43
2.17 The first manual imprint tool used in this research work. 43
2.18 The analysis of a water drop in the contact angle measurement method. 45
2.19 The contact angle measurements of some materials used in this work. 45
2.20 A study of e-beam dosages versus the height of the developed negative resist structure. 49
2.21 Raw data of e-beam dosages versus the height of the developed structure. 50
2.22 The contrast curves of negative resist ma-N2403 for SPL, DPL and QPL exposure schemes. 51
2.23 Spin curves of Ormocomp resist that were diluted in an Ormothin solvent 53
2.24 The UV transmission data on Ormocer series resist 54
2.25 The self assembled monolayer (SAM) using a natural convection deposition method of FOTS in a petri dish. 55

3.1 The 2-D pattern transfer methods 59
3.2 The contact angle measurements on quartz substrates 60

3.3 The fabrication of 2-D structures on quartz substrate using a common method of depositing a thin metal layer on the substrate . . 63
3.4 The fabrication of 2-D structures on quartz substrate using metal coating on top of the resist layer 64
3.5 The fabrication of 2-D structures on quartz substrate using conductive polymer (PEDOT/PSS) coating on top of the resist. . . . 66
3.6 Optical images of the contact angle measurement on PMMA surfaces 66
3.7 Optical images of incomplete removal of an e-beam exposed PEDOT/PSS layer using DIW on PMMA resist with a feature size of about 1 micron 67
3.8 AFM image of the developed 2-D pattern of 60 nm lines on PMMA bilayer resist. 69
3.9 Schematic of RIE mechanism for a 2-D structure 73
3.10 SEM image of a pillar showing sidewall passivation and trenching effects at the bottom of the structure when operating pressures are below 30 mTorr. 73
3.11 SEM images of a few results of continuous deep RIE on quartz substrate. Structure heights are about 150 nm and about 80 to 85 degrees of vertical angle. 74
3.12 SEM images of the fabricated 2-D high aspect-ratio structures on quartz substrate. 75
3.13 SEM images of the fabricated 2-D structures on quartz substrate . 76
3.14 Issue of metal deposition on a feature size below 50 nm using PMMA bi-layer resist 77
3.15 SEM image of the etched 40 nm feature on quartz substrate which failed to preserve the flat top profile. 77
3.16 The SPL writing scheme for 3-D patterns 79
3.17 Schematic diagram of e-beam interaction volumes of low keV as compared to high keV 80
3.18 The fabrication process flow options for fabricating the 3-D structures on insulating substrates 81

3.19 Schematic diagram of critical energy 82
3.20 Electron trajectories of various e-beam acceleration voltages across a 600 nm thick ma-N2403 resist layer and quartz substrate by employing Monte Carlo simulation using CASINO software. 84
3.21 Accelerating voltages required for zero surface charging in various resist thickness compared to the estimated penetration depth at those voltages. 85
3.22 AFM images of the developed 3-D structures on the negative resist 86
3.23 A comparison of the appearance SEM images of the resist surface without and with a PEDOT/PSS conductive polymer layer 88
3.24 Schematic diagram showing electron trajectories when the e-beam was exposed on the resist 88
3.25 The EBL writing scheme for 3-D patterns and the associated results 89
3.26 The comparison of the highest pattern density of two pattern writing methods. 91
3.27 The 3-D etching chemistry 93
3.28 The 3-D etching mechanism 94
3.29 The SEM and AFM cross sectional view of trenching effects on 3-D ring mold structure. 95
3.30 SEM images of the 3-D structures on quartz substrate after etching with different plasma power densities. 97
3.31 The etching product that created a nanomasking effects resulting in a nanopillar surface finish 98
3.32 The surface roughness versus RIE operating pressure 99
3.33 The surface roughness analysis using AFM 100
3.34 SEM images of the 3-D structures on quartz substrate. 101
3.35 The profile analysis for 3-D ring profiles before and after the RIE process. 102
3.36 The SEM images of various 3-D shaped structures on quartz substrate. 103

4.1 The contact angles on the surface of Ormocomp resist at normal conditions and after being coated with an anti adhesive monolayer 108
4.2 Two types of transparent molds used for 2-D imprints. 109
4.3 The schematic of the manual de-molding process. 110
4.4 The 2-D imprint of two types of feature sizes on Ormocomp resist 111
4.5 The 2-D imprint procedures using a transparent mold and a transparent mold with a NiCr absorber. 112
4.6 The AFM images of the examples of the final 2-D structures on quartz substrate. 113
4.7 The AFM image showing the missing and broken imprinted structures after de-molding process. 114
4.8 The schematic diagram showing an analysis of de-molding failures. 115
4.9 The simulation of resist reflow into a 2-D cavity using ABAQUS finite element software 116
4.10 The contact angle measurement of the materials in normal conditions and after being coated with a FOTS anti adhesive monolayer 119
4.11 The master mold of a 3-D ring structure 120
4.12 The master mold of a multilevel pyramid structure 120
4.13 The schematic of the first imprint of the 3-D imprint step (Imprint 1) 121
4.14 The optical images of the inverted shapes of the master mold on Ormocomp resist after the Imprint 1 process 122
4.15 The replication of of a 3-D ring structure on Ormocomp resist after the Imprint 1 process 123
4.16 The replication of a multilevel pyramid structure on Ormocomp resist after the Imprint 1 process 124
4.17 The schematic of the second imprint of the 3-D imprint step (Imprint 2) 125
4.18 The molding of the 3-D ring soft mold structure on the mr-UVCur06 resist. 126
4.19 The molding of multilevel pyramids soft mold structure on the mr-UVCur06 resist 126

4.20 The schematic of the 3-D final pattern transfer) 127
4.21 The final 3-D structure etched by the final RIE pattern transfer . . 128
4.22 The sticking of 3-D imprinted structure on Ormocomp resist. . . 129

5.1 The defect density monitored by Molecular Imprint Inc. 133
5.2 The contact angle measurement on PP-MOCVD titania surface . . 139
5.3 Shown on far left are 5 nm lines with pitch of 12 nm imprinted by Nanonex Inc. 139

A.1 The Laurell Technologies spinner system 166
A.2 The newly installed spinner system 166
A.3 The ultrasonic bath from Unisonics 166
A.4 The in-house designed wafer scriber/cleaver tool. 166
A.5 The Raith-150 electron beam lithography (EBL) system 167
A.6 The atomic force microsopy (AFM) system 167
A.7 The Karl Suss mask aligner system (MA-6) 167
A.8 The newly installed EVG620 UV Curable Nanoimprint Lithography system 167
A.9 The Edward 500 Magnetron sputtering system 168
A.10 The Balzers BA 510A metal evaporator system 168
A.11 The conventional Oxford Plasma 80plus reactive ion etching system 168
A.12 The Veeco Dektak 150 profilometer system 168
A.13 The old ET Plasmafab oxygen plasma system 169
A.14 The newly installed Emitech K1050X oxygen plasma system . . . 169
A.15 The Tempress 602 dice saw system 169
A.16 The stirrer system from Grant Instrument 169
A.17 The mask writer system from Heidelberg Instrument 170
A.18 The mini furnace from Orton 170
A.19 The UC contact angle measurement system 170
A.20 The manual ellipsometer system 170

C.1 The multilevel shape of a hemisphere on top of square block. . . . 174
C.2 A single hemisphere shape. 174

C.3 The multilevel structure of a hemisphere placed on top of the square block. 174
C.4 The silicon tip fabricated after the pattern transfer of a 3-D pyramid shape onto a silicon substrate. 174
C.5 The multilevel structure of pyramid array on silicon substrate. . . 174
C.6 The multilevel structure of pyramid array on silicon nitride substrate. 174
C.7 The SEM image of 3-D multilevel with 3-level structures. 175
C.8 The AFM image of the imprinted 3-level structure on an Ormocomp resist. 175
C.9 The SEM image of various 3-D geometrical shapes on quartz mold.175
C.10 The AFM image of the imprinted 3-D geometrical shapes on Ormocomp resist. 175

List of Tables

2.1 The physical properties of the quartz supplied by TOSOH Quartz Inc. 47

3.1 RIE recipes for descumming the residual layer and removal of the tungsten (W) layer using SF_6 etchant 62
3.2 The recipe of O_2 plasma surface treatment on the PMMA surface . 67
3.3 EBL parameters for defining a fine 2-D pattern on PMMA resist . 68
3.4 RIE recipe for etching 2-D structures on quartz substrate 70
3.5 The optimized CHF_3/Ar RIE parameter for 3-D pattern transfer onto quartz substrate 92

4.1 The RIE parameter for surface treatment 119
4.2 The optimized CHF_3/O_2 RIE parameter for final 3-D pattern transfer onto quartz substrate 127

B.1 The list of chemicals for resists, developer and solvents. 171
B.2 The list of chemicals for etching and coating. 172
B.3 The recipe for wet etching chemicals. 172

Chapter 1

INTRODUCTION

The nanotechnology revolution has opened up new potential for producing miniaturized devices with less cost, less materials, and better performance. For example, in the last 50 years, cars, aircraft, houses and furniture have changed moderately in their capabilities and costs, but DNA and microelectronics technologies have exploded, expanding their basic capabilities by factors of more than a billion [1].

Miniaturized devices such as microprocessors, micro optics, biochips, microarrays and microfluidics consist of micro/nanostructures of functional materials which can be made in numerous ways either using the 'bottom up' or 'top down' approach. The bottom up approach fabricates materials and devices at the atomic or molecular scale, possibly using self-assembly methods, while the top down approach etches or mills the smaller structures from larger ones [2].

Currently, the fabrication processes of most micro/nanostructures for micro/nano devices are based on an established semiconductor industries manufacturing technology. In this technology, lithography is the key technique whereby the circuit patterns are defined on an imaging layer using an optical lithography technique and then transferred onto a substrate using etching process. For multi-layer/level circuits, semiconductor industries employ optical lithography's planar fabrication technology in which integrated circuits are built by stacking one layer of circuit elements on top of another. These make the fabrication process complicated and expensive. Roughly 35% of device costs are attributed to repetitive lithography processes [3].

Optical or photo lithography which was used to fabricate printing plates prior to the semiconductor era, has been the technology of semiconductor manufacturing since its feature sizes of more than 2 microns until the current 32 nm CMOS technology. Optical lithography is widely used because it has high throughput, good resolution, low cost, and ease of operation. This is only possible with the help of resolution enhancement technologies (RET) such as phase-shifting mask (PSM), optical proximity correction (OPC) and many others [4].
Recently, the introduction of water immersion lithography [5] has further extended the life span of optical lithography which manufactures nodes down to 45 nm with a 65 nm half pitch. A 32 nm node with a 45 nm half pitch is possible with this technique by using fluid with a higher refractive index [6], polarized illumination, solid mask immersion and double exposures. However, this technique faces enormous problems in shrinking the feature size further, owing to such defects as water stain, bubbles and particle contamination.
It is becoming costly and complicated going to even smaller scale as demanded by the industry. Therefore new lithography technologies that are high resolution (beyond 32 nm), less complicated, and low cost are sought after.
Beyond a 32 nm half pitch, the optical lithography may not materialize because it is no longer economical to continue with technology that has approached its ultimate limits. From this point on, one can probably count down the days till optical lithography ends. It may not be able to survive on its own and has to be integrated into other technology, such as mix-and-match lithography [7] in order to extend its life span.
There are a number of lithographic technologies that have potential as the successor to optical lithography. The next generation lithography (NGL) techniques will be discussed next.

1.1 Next Generation Lithography (NGL)

Considerable efforts have been devoted to NGL techniques by various research laboratories and industries around the globe. Extreme Ultraviolet Lithography

(EUVL), Electron Beam Lithography (EBL), Focused Ion Beam (FIB), High Index Immersion Lithography, Nanoimprint Lithography (NIL) and X-Ray Lithography (XRL) are some of the candidates for NGL. Amongst them, the two most promising candidates for NGL are EUVL and NIL.

EUVL is the favourite of semiconductor industries and has been backed by major players in the semiconductor industry such as AMD, Intel and Motorola [8], because this technology is based on an extended optical lithography technique, but with a shorter wavelength (13.4 nm) of light illumination. However, a wavelength of 13 nm is a long x-ray and as such is easily absorbed in most materials. In this system, refractive optics are no longer feasible, instead, reflective optics such as the Bragg reflector system are used. Figure 1.1 shows the schematic of the EUVL system where the EUV light is generated from a 45 eV plasma created when a 1700 Watts pulsed Ytterbium-Aluminium-Garnet (YAG) solid state laser illuminates a supersonic jet of Xenon gas. The EUV light is collected and focused on a 4X reflective mask by a series of condenser mirrors (C1 - C4). The mask image is projected onto the wafer by a 4X reduction camera (M1 - M4) while the mask and wafer are simultaneously scanned. The entire operation takes place in a high-vacuum environment enclosure. All other offline optical lithography tools are still relevant to this technology, but the unresolved issues such as debris in laser source power, brightness of mask defect inspection system and immature resist performance have delayed the deployment of this technology into high volume manufacturing line [9].

On the other side, NIL is an ancient patterning technique, as shown by an imprint of the pre-historic creatures found on the fossils. In this technique, a hard mold shape is replicated by pressing it onto a soft imaging layer. It is a simple, low cost and high throughput technology, but this technology is considered a newcomer to semiconductor industries. Industries may have to modify the process layout and some tools related to the optical lithography in adopting the NIL processes in their manufacturing lines.

The International Technology Roadmap for Semiconductor (ITRS) in the year 2003 [11] had mapped out an imprint as one of the lithography candidates for nodes beyond 32 nm. This has attracted research around the world to explore

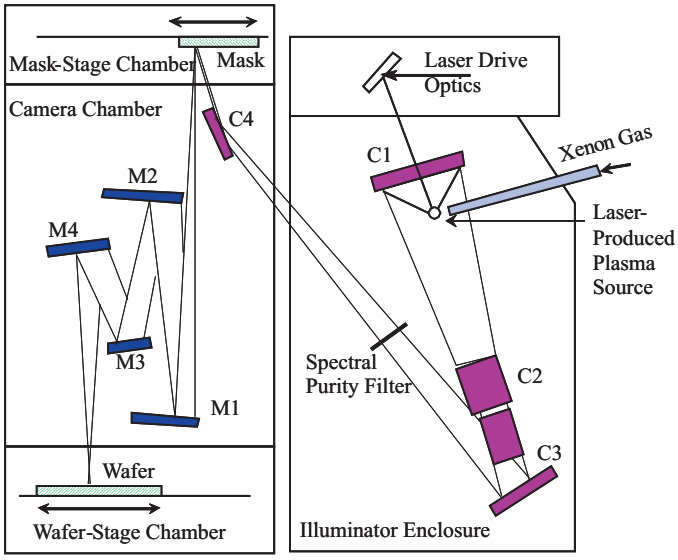

Figure 1.1: The schematic diagram of the Extreme Ultra Violet Lithography system [10]

its potential. In ITRS 2005, a more detailed lithography expectation of the UV-NIL process was defined [12], especially on the mold fabrication specification. The requirements have been updated since then and the latest ITRS 2008 [13] for UV-NIL is illustrated in Figure 1.2. For NIL technology, the major ITRS concerns are over surface roughness, the defect level of the fabricated molds as well as the timelines and the capability of equipment infrastructure. Another drawbacks of this technology such as contaminations, resist sticking on mold surfaces, mold crack, and bubbles have been addressed by various research groups.

Globally, we can find a large number of investments from government agencies, technology companies and higher education institutions, in setting up businesses and researches based on NIL technologies. In the USA, Molecular Imprint Incorporated and Nanonex Corporation are examples of early spin-off companies as NIL experts in equipment, processes and NIL related materials. Similar companies such as EV Group (Austria), Obducat AB (Sweden) and Suss Microtec (Germany) in Europe and many others around the world are progressing in this technology. Huge investments have been poured into it, and nowadays we can find many research and manufacturing tools for NIL technologies available in the market.

In the latest developments, NIL has demonstrated its capability for applica-

UV-NIL-specific Mask Requirements	*2008*	*2009*	*2010*	*2011*	*2012*	*2013*	*2014*	*2015*	*2016*	*2017*	*2018*	*2019*	*2020*	*2021*	*2022*
Defect size impacting CD (nm) x, y [J]	4.5	4.0	3.6	3.2	2.8	2.5	2.3	2.0	1.8	1.6	1.4	1.3	1.1	1.0	0.9
Defect size impacting CD (nm) z [K]	9.0	8.0	7.1	6.4	5.7	5.1	4.5	4.0	3.6	3.2	2.8	2.5	2.3	2.0	1.8
Mask substrate flatness (nm peak-to-valley) [L]	298	252	192	180	153	126	110	88	72	56	45	36	29	24	21
Trench depth, mean (nm) [M]	75–119	67–104	60–90	53–81	47–72	42–64	37–57	33–51	30–45	26–41	23–36	21–32	18–29	17-26	15-22
Etch depth uniformity (nm) [N]	3.8–5.9	3.4–5.2	3.0–4.5	2.7–4.0	2.4–3.6	2.1–3.2	1.9–2.8	1.7–2.5	1.5–2.3	1.3–2.0	1.2–1.8	1.1–1.6	0.9–1.4	0.9-1.3	0.8-1.1
Trench wall angle (degrees) [O]	87	87.3	87.6	87.9	88.1	88.3	88.5	88.7	88.8	88.9	89.1	89.2	89.2	89.3	89.4
Trench width roughness (nm, 3 sigma) [P]	4.3	3.7	3.2	2.8	2.5	2.2	2.0	1.8	1.6	1.4	1.3	1.1	1.0	0.9	0.8
Corner radius, bottom of feature (nm) [Q]	6.3	5.6	5	4.5	4	3.5	3.2	2.8	2.5	2.2	2	1.8	1.6	1.3	1.1
Corner radius, top of feature (nm) [R]	1.4	1.2	1.1	0.9	0.8	0.7	0.7	0.6	0.5	0.5	0.4	0.4	0.3	0.3	0.3
Trench bottom surface roughness (nm, 3 sigma) [S]	7.6	6.7	6	5.4	4.8	4.2	3.8	3.4	3	2.7	2.4	2.1	1.9	1.5	1.2
Template absorption [T]	<2%	<2%	<2%	<2%	<2%	<2%	<2%	<2%	<2%	<2%	<2%	<2%	<2%	<2%	<2%
Near surface defect (nm) [U]	53	47	41	36	32	29	26	23	20	18	16	14	13	11	10
Defect size, patterned template (nm) [V]	35	30	30	20	20	20	20	10	10	10	10	10	10	10	10
Defect density (#/cm^2) [W]	0.03	0.03	0.03	0.01	0.01	0.01	0.01	0.01	0.01	0.01	0.01	0.01	0.01	0.01	0.01
Dual Damascene overlay: metal/via on template (nm, 3 sigma) [X]	11.9	10.3	9.0	8.0	7.1	6.4	5.7	5.1	4.5	4.0	3.6	3.2	2.8	2.5	2.3

Manufacturable solutions exist, and are being optimized
Manufacturable solutions are known
Manufacturable solutions are NOT known

Source : ITRS 2008 Update for Lithography

Figure 1.2: The International Technology Roadmap for Semiconductor (2008 Update) expectations regarding the UV-NIL mold fabrication process.

tions toward 22 nm node CMOS devices [14]. Obviously, these promising NIL technologies have potential for unlimited future applications especially for the fabrication of nanostructures. The progress made in the last years has shown that NIL is not only a serious NGL candidate, but also a platform for one of ten technologies in the MIT Technology Review being evaluated to change the world [15].

On the other side, EUVL has been under development for more than 20 years, however as of now, only a few beta EUVL tools are available in the world; located in the USA [16], Europe(ASML, IMEC)[17, 18] and Japan [19, 20, 21] for process characterization purposes. The large costs of electrical consumption, large footprint, costly parts, and process stability issues have hindered the progress of this technology. Based on this information, we can easily discover which NGL candidate is at the leading edge.

1.2 Overview of Nanoimprint Lithography Techniques

Imprint technologies normally used in the stamping and molding of plastics products have been around for decades. These are called 'imprint' in the USA or 'hot embossing' in Europe and were low cost technology capable of emboss-

ing down to the micro scale level. In the mid 1990s, Stephen Y. Chou and co-workers had demonstrated that this technique was still embossing perfectly down to 25 nm feature sizes [22]. A silicon dioxide (SiO_2) mold was used in imprinting a heated Polymethylmetacrylate (PMMA) resist above its glass transition temperature (T_g) and later work had demonstrated that imprinting down to 10 nm feature sizes was achievable [23]. This work had been considered a major breakthrough in patterning at nanoscale level and nanoimprint lithography (NIL) technology was then officially established based on this technique.
There are three basic components of NIL: molds or stamps, material to be printed and a tool for printing. The equipment used for NIL technologies is in general low cost, high throughput and has better process compatibility [24].
In 1996, a group from Phillips Research Laboratories, led by Jan Haisma, had published a work of patterning with dimensions 100 nm or less on a thin UV curable resist layer by a technique called mold lithography [25]. A transparent mold was used for imprinting a pattern on the UV curable monomer and then cured by UV exposure. This technique is the basis of UV curable nanoimprint lithography (UV-NIL) technology.
In general, NIL can be categorized into two major types; thermal NIL and UV assisted/curable NIL (UV-NIL). In thermal NIL as shown in Figure 1.3(a), the thermoplastic polymer resist that is coated on the substrate is heated by a heater or an ultrasonic source [26] to above T_g, to soften the resist prior to the imprint being pressed by the patterned mold. Pressure is held constantly while the sample is cooled to below T_g to freeze the replicated pattern of the mold. After being released from the mold, an oxygen dry etching is normally used to remove the resist residual layer.
There is also a thermal NIL technique that uses a laser source to directly soften the substrate material [27]. In this laser assisted direct imprint (LADI) technique, no resist is used and the laser is exposed through the transparent quartz mold to heat the substrate surface to a very high temperature. The quartz mold that can withstand high temperatures is then directly pressed onto the softened substrate surface. The mold is then released after the sample has cooled down. Figure 1.3(b) shows a schematic of the simple UV-NIL process steps. In this

technique viscous UV-curable monomer is used as a compliant layer instead of the thermoplastic polymer and imprinted at room temperature. This reduces the imprint pressure significantly, improving the resist reflow and avoiding time consuming and stress inducing temperature cycles [15]. After imprinting, broadband UV light crosslinks the resist directly through the back side of the transparent mold or substrate.

UV-NIL technique has many advantages compared to Thermal NIL. Low pressure and room temperature are important for processing soft materials such as plastics, organic, thin films and materials that do not tolerate high temperatures. Increasing the process temperature also induces stresses between materials in the device system that have different thermal expansion coefficients. Moreover, the temperature cycle is a troublesome, low throughput and costly process in the manufacturing environment where the elimination of the temperature cycle process means a huge reduction of process costs.

NIL is a simple technique which creates features by the mechanical deforma-

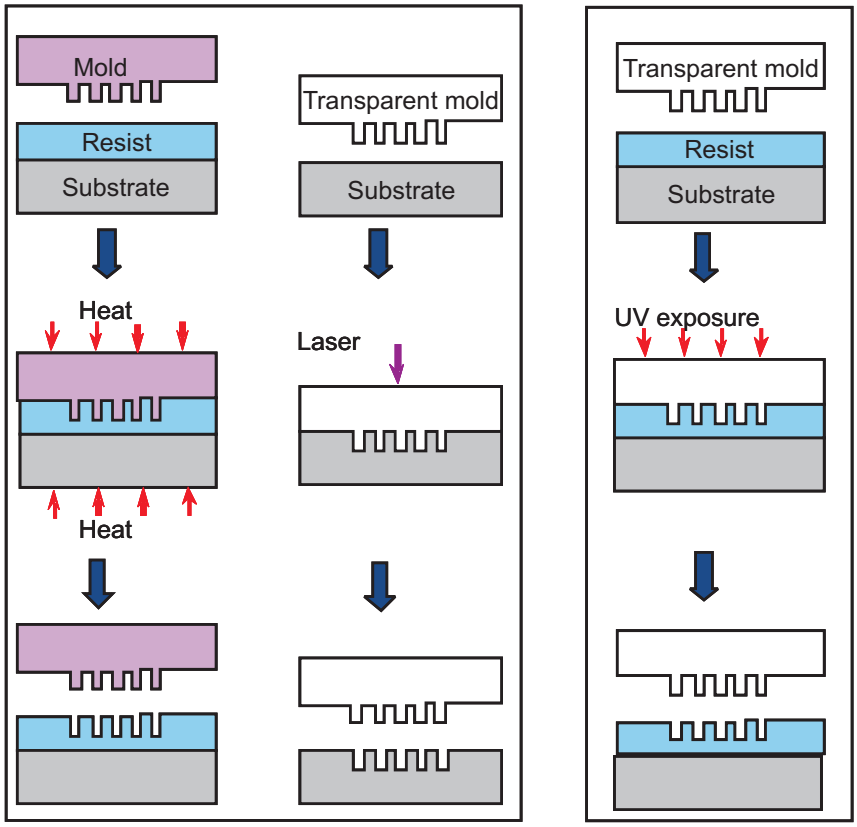

(a) Thermal NIL (b) UV-NIL

Figure 1.3: Type of nanoimprint lithography technique

tion of a resist layer using a mold rather than by changing the chemical properties of the resist as in other lithography techniques. NIL techniques have been investigated extensively by various laboratories worldwide for more than a decade, however a standard for NIL processing has not yet been established. Stringent requirements by current device manufacturing industries on defect levels have delayed the deployment of this technology. It has mainly used as research tool more than as industrial manufacturing technology owing to many applications having different requirements in terms of acceptable defect level, resolution, design, resist and pattern transfer. NIL process can be customized to suit certain application and it is a flexible technique that is suited to various potential applications.

Many other alternative lithographic techniques have been developed based on the NIL concept such as step and stamp imprint lithography (SSIL) [28, 29], step and flash imprint lithography (SFIL) [30], microcontact printing (MCP or μCP) [31], laser assisted NIL [32] and reversal imprint [33].

There are two different approaches that have been suggested for large area lithography: large area parallel imprinting and sequential imprinting. In parallel imprinting, a large area mold of up to 150 mm (6 inches) diameter of patterned wafer can be imprinted on a similar size substrate wafer in a single imprint step [28]. While in sequential technique, SSIL uses a small patterned mold size to imprint the large surface area in stepping mode as illustrated in Figure 1.4(a). In this method, the mold is heated to above the T_g of the polymer resist and then the imprint pressure is applied to the top of the mold onto the polymer resist. The mold and resist are later cooled down to a temperature below T_g before the demolding process takes place. The polymer resist and substrate are consistently heated to a temperature of below T_g [29]. These pressure and temperature cycles processes are repeated at the next location until the whole substrate area is imprinted.

The step and flash imprint lithography (SFIL) is another NIL technique that uses the step and repeat sequence approach as illustrated in Figure 1.4(b). In this method, the transparent mold is imprinted on a low viscosity UV curable resist and then illuminated with UV exposure to cure the polymer resist. This

process is repeated at the next location and it operates at a room temperature avoiding high temperature and pressure cycles.

μCP is basically an inking approach, using self-assembled monolayers (SAMs)

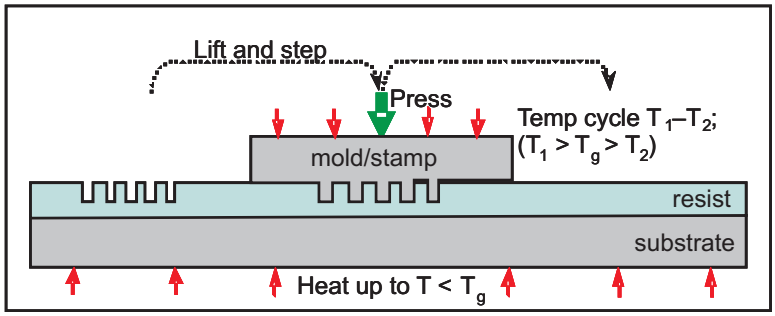

(a) Step and stamp imprint lithography (SSIL)

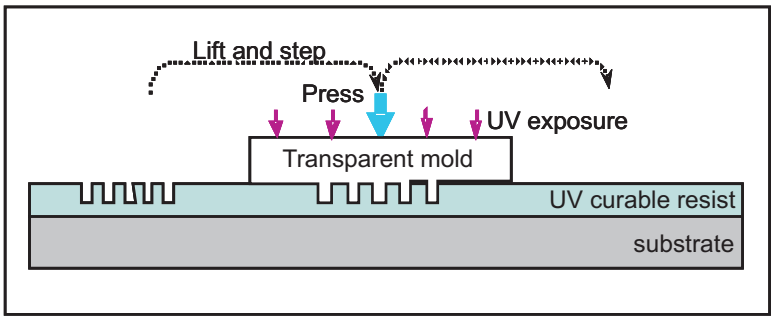

(b) Step and flash imprint lithography (SFIL)

Figure 1.4: The schematic of NIL processes based on step and repeat sequence.

as the ink, and elastomeric mold such as PolyDiMethylSiloxane (PDMS) to define the features onto a substrate [31] as illustrated in Figure 1.5. The patterns are later transferred onto a gold masking layer by employing a wet etching process.

Reversal imprint lithography (RIL) is another NIL technique where resist layer

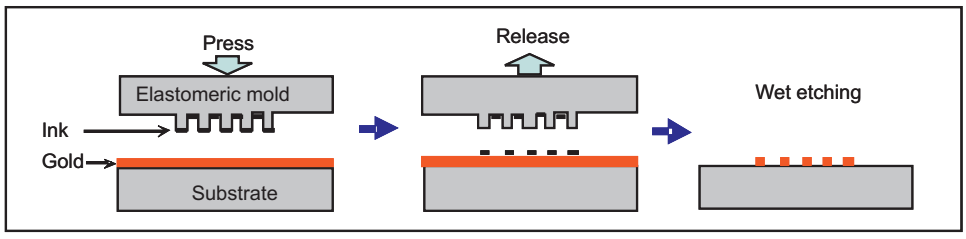

Figure 1.5: The schematic of micro contact printing (μCP) process flow.

is spun coated on a mold and transferred to a bare substrate by imprinting under suitable temperature and pressure as illustrated in Figure 1.6. This method

offers a unique advantage as compared to conventional NIL by allowing imprinting onto substrates that are difficult to be spun coated with resist material, such as flexible or nonflat substrates [33].

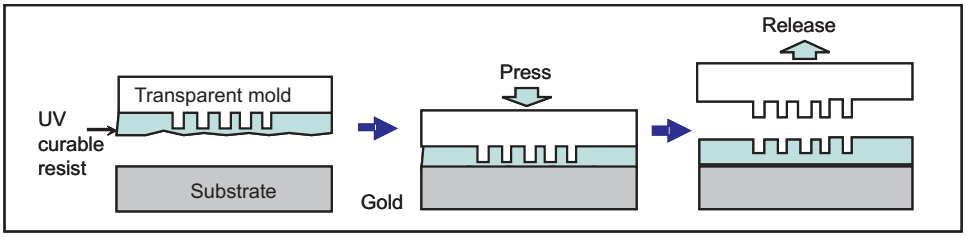

Figure 1.6: The schematic process flow of reversal imprint lithography.

1.3 The Ultraviolet Curable Nanoimprint Lithography (UV-NIL)

The UV-NIL advantages such as low imprint pressure, low residual resist layer, the avoidance of thermal cycles by operating at room temperatures, low tool cost, large wafer imprint capability, high throughput and structural flexibility make it a leader in NGL technologies. UV-NIL is considered a candidate for mass manufacturing technology. It normally uses spin coated resist on the substrate prior to imprinting and UV exposure. This is close to the existing processing technologies in the current microelectronic industries which mostly operate at room temperature.

The disadvantages are on a large imprint area, where a trade off between precision and imprint area needs to be dealt with. An ultra rigid quartz mold is essential in achieving high resolution, alignment accuracy and pattern fidelity, however, if standard wafers are used, surface waviness hinders full contact between mold and resist. Homogenous residual resist thickness can no longer be fulfilled along with the large imprint pressure required for a large imprint area. Hence, full wafer patterning with rigid molds can be performed using a method of so called step and repeat sequence as discussed earlier.

In this approach, a small mold is used for imprinting over a large area by im-

print and UV exposure steps, and the process cycle is repeated by indexing to the next location until the whole area is completed. The advantage of the small mold is that it is easy to fabricate to achieve a high quality standard, low imprint pressure and wafer deformation during imprint is minimized. Moreover, the Step and Flash Imprint Lithography $(S - FIL^{TM})$ technique which was introduced by Colburn et al. [30] offers a reliable technique and a capable process even for integrated circuit fabrication [34]. In the latest development, a more reliable "drop on demand" approach using an inkjet printer head has been used as a method to dispense the UV curable resist on the substrate more uniformly by following the volume requirements of the pattern design. Figure 1.7(a) shows the schematic of the $(S - FIL^{TM})$ process. Currently, most of the available UV-NIL high volume manufacturing systems in the market are based on this technique. The major concern of this technique is the relatively low throughput because of using a small mold and multiple stepping and UV flashes to complete the imprint for the whole wafer area. Other related issues such as overlay accuracies, particle related defects and irregularities in polymers have been investigated by various research groups and are improving from time to time.

Stitching free full wafer patterning within one step can be achieved by reducing the rigidity of the mold. Flexible molds are able to adapt their surface to the waviness of a wafer surface to achieve an homogenous residual resist layer. Polymeric materials such as Polydimethylsiloxane (PDMS), Polymethylmethacrylate (PMMA), Polytetrafluoroethylene or Teflon (PTFE) and Polyurethane (PU) are suitable materials for cast molding to replicate the soft mold from a rigid master mold. This technique is called Soft-UV-NIL.

One of the techniques that uses this approach is called roller imprint [36] or the roll-to-roll nanoimprint lithography (R2RNIL) [35]. Figure 1.7(b) shows a schematic diagram of a customized R2RNIL system to produce the diffraction grating. This technique is useful for a very large imprint area and high throughput requirement such as display manufacturing. The only disadvantage is the difficulty in achieving a high quality pattern across the large mold area.

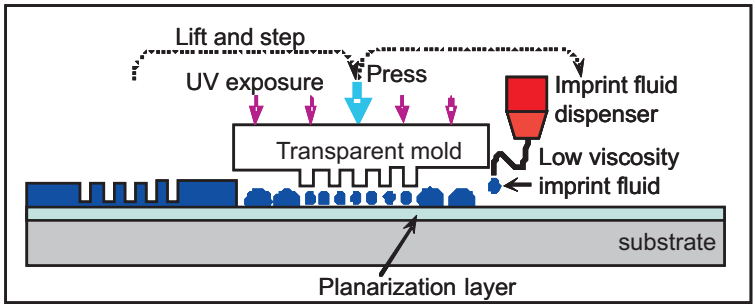

(a) The schematic process flow of Step & Flash Imprint Lithography $(S - FIL^{TM})$

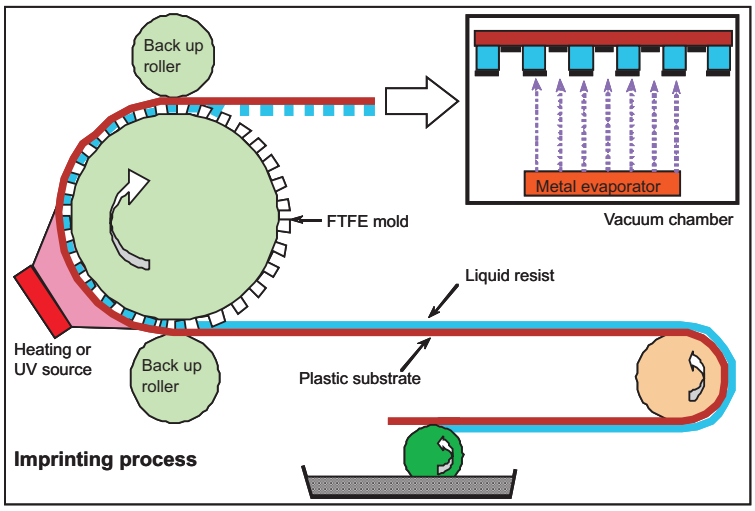

(b) The schematic of roll-to-roll nanoimprint lithography (R2RNIL) [35]

Figure 1.7: Type of UV curable nanoimprint lithography technique for mass production

1.4 Nanoimprint Process

In the nanoimprint process, the imprint pressure, ambient pressure, temperature, resist viscosity, initial resist thickness and mold features are the important input parameters, while the residual resist thickness, the height of the imprinted structures or cavity filling, and stickiness between mold and resist are some of the important output parameters.

In the two dimensional (2-D) imprint analysis is illustrated in Figure 1.8(a). Applying the continuity equation with the assumption that the mold is rigid and the resist material is incompressible (conservation of polymer volume), the volume of the initial resist before the imprint is equal to the volume of the resist

after the imprint. Therefore,

$$t_o \sum (s_i + w_i) = t_r \sum (s_i + w_i) + h_r \sum w_i \tag{1.1}$$

The total width $W = \sum (s_i + w_i)$ and L is the length.
wheret_o is the initial resist thickness, t_r is the residual resist thickness, w_i is the width of the mold cavity and h_r is the height of the imprinted resist structure. Therefore, the required initial resist thickness for 2-D imprint is;

$$t_o = t_r + \frac{h_r}{W} \sum w_i \tag{1.2}$$

For example, if the width of the analyzed mold/substrate boundary W is one micron, the desired residual resist thickness t_r is 100 nm, the total width of the mold cavities $\sum w_i$ is 500 nm and the height of the imprinted resist structure h_r is 700 nm. By using equation 1.1, the calculated initial resist thickness t_o is 450 nm. This is a close approximation for optimizing the imprinting process parameter.
Similarly in 3-D imprint analysis as illustrated in Figure 1.8(b), by assuming a rigid mold and incompressible resist material, the total volume of resist before imprint is equal to the total volume of the imprinted resist.

$$WLt_o = WLt_r + \sum v_i \tag{1.3}$$

where WL is the boundary area and v_i is the volume of the mold cavity.
Therefore by assuming 100% 3-D mold cavity filling, the required initial resist thickness for 3-D imprint is;

$$t_o = t_r + \frac{1}{WL} \sum v_i \tag{1.4}$$

1.5 Nanoimprint Lithography: Opportunities and Applications

At the moment, optical lithography is still the dominant lithography technology, but its future is uncertain. Its survival relies on the latest developments

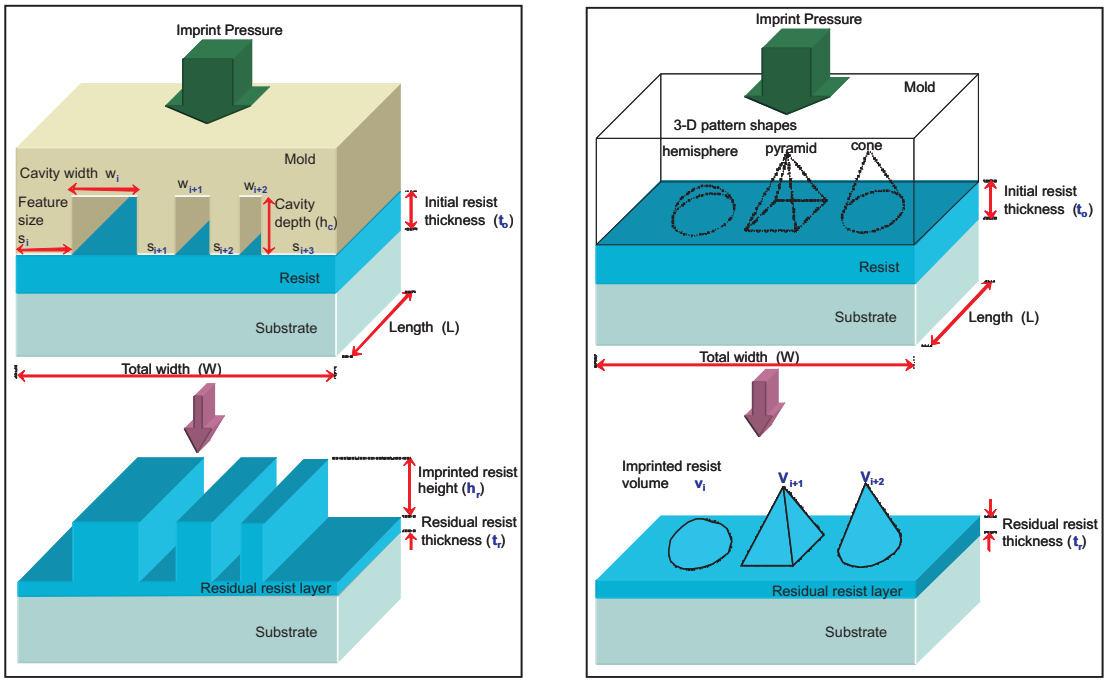

(a) 2-D imprint (b) 3-D imprint

Figure 1.8: The schematic of imprint analysis for 2-D and 3-D imprint processes.

of the integration with other techniques (mix and match) to overcome its physical limit. Even though EUVL was the first candidate to appear in the NGL elite group and had been named as a potential heir to lithography technology, its cost has ruined its reputation. Apparently not many parties could afford to own an EUVL system because of its high cost of about $USD 50 million per system, meaning only a few giant companies had the privilege of owning the EUVL system.

On the other hand, NIL technologies offer a promising low cost alternative lithography technology that is suitable for those with limited investment in future technologies such as small companies, small research laboratories and small scale manufacturing. They are also suitable as a research and development tool for developing countries and small countries like New Zealand. This technology is very useful for future new devices or product developments where providing samples for product characterization is a costly exercise in current technology. NIL replication may save costs in preparing the device or product samples. As an alternative lithography, NIL has created huge opportunities as a low cost and flexible technique for future applications.

These challenges and opportunities have initiated the race to the new leading edge of lithography technologies. NIL technology has been demonstrated and it is open to many possible applications in making devices ranging from optics [37, 38], patterned media data storage [39], bio-sensor/MEMS , microfluidics [40, 41], to molecular electronics [42].

In processor chip technology, the device speed is not scaling below the 65-nm node the way it has historically scaled. Leakage current has been the gating factor for progress of below 45-nm node and optical lithography solutions for beyond 32 nm nodes are still problematic. Since 2-D scaling faces numerous technological issues, 3-D integration could be the next scaling engine. The ability to create 3-D device stacks appears promising as a way to integrate more devices into a chip [43]. 3-D chips require a 3-D fabrication technology that is reliable, low cost, of high accuracy and with high throughput. Here, NIL could offer its 3-D patterning capability for the progress of 3-D chip technology.

The major impact of NIL technology is on the large area replication of nanometer features where high density and high fidelity pattern replications have been demonstrated [44, 45].

In 2005, basic nanoimprint tools were sold with price tags begin at US$100,000 compared to US$25-to-US$40 million price for the latest 193-nm immersion lithography tool [46]. More sophisticated nanoimprint tools have been manufactured since then but not too high in cost. It was estimated that the latest beyond 32-nm nodes NIL line equipment is only one fifth of normal optical lithography line equipment. The combination of NIL with other techniques also extends itself to many other potential applications. Because of its flexibility for customized applications, it is most suitable for the future lithography technique of complex structures.

1.6 Research Background

In general, 3-D micro/nanostructures, including 3-D NIL molds, can be fabricated using various techniques such as multistep lithography , maskless gray-

scale lithography [47], FIB writing [48], proton beam writing [49], XRL [50, 51], or EBL. Figure 1.9(a) shows an example of 3-D structures which are eight-level fresnel zone lenses. They were fabricated using multi-step lithography [52] which resulted in very rough multi-step structures. Figure 1.9(b) shows an example of lens structure fabricated using grey scale lithography [47] and the structures are relatively large for nanoscale applications.

Another method of fabricating 3-D structures is by the surface texturing method.

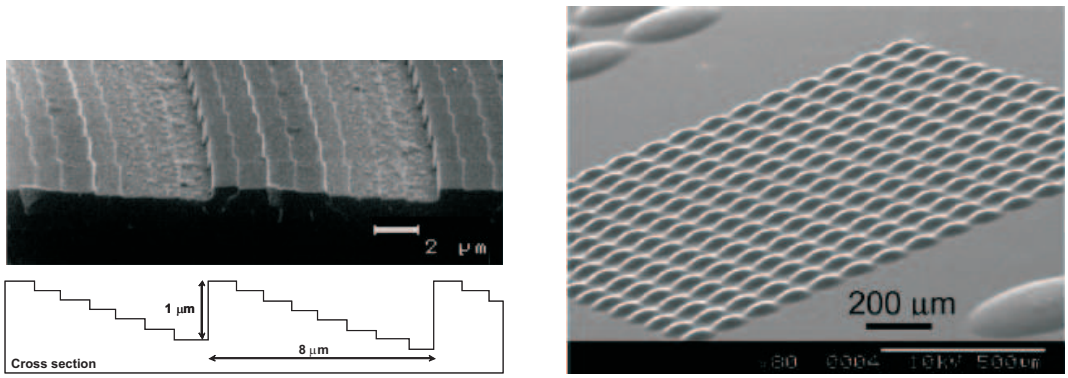

(a) multi step lithography [52] (b) grey scale lithography [47]

Figure 1.9: Examples of 3-D structures fabricated using different lithographic techniques

Figure 1.10(a)shows one of the 3-D surface textures for solar cells which was fabricated using an intentionally over-etched RIE process [53]. Figure 1.10(b) shows a 3-D sub-wavelength surface texturing using interferometric lithography patterning and RIE [54]. 3-D structures down to sub-wavelength scale can be fabricated using an advanced lithography technique, but the reproducibility in mass production will be the major concern.

As an alternative lithography technology, a key advantage of the NIL technique is its simplicity and it has been used to fabricate devices for many applications. Thermal NIL is an established technology but operates at high pressure and temperature cycles. Some device fabrication may disadvantaged by these process conditions as explained in section 1.2. A process that operates at room temperature is most preferable in the manufacturing environment, hence, UV-NIL is the technique that will further investigated.

Even though so many works in NIL techniques such as SSIL, SFIL, μCP, LADI and RIL have been published, not many works have emphasized patterning

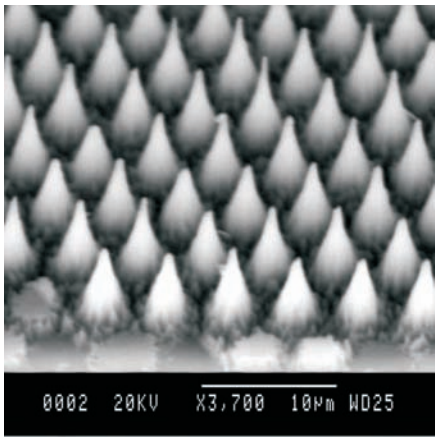

(a) 3-D surface texture for solar cells fabricated using an over-etching technique [53]

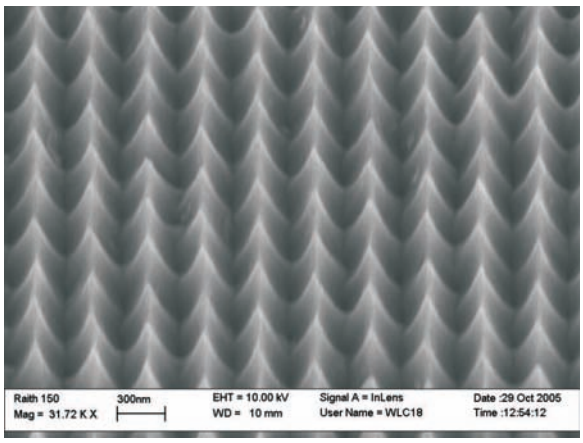

(b) 3-D surface texture using an advanced surface texturing technique [54]

Figure 1.10: Recent work on surface texturing on silicon substrate using the RIE technique.

and replicating 3-D structures especially on mold making processes. Most of the reports of NIL techniques are on the replication of 2-D structures. So far only a limited number of 3-D NIL works have been published; yet so many applications are seeking the capability of 3-D patterning.

Recently, 3-D and multilevel nanoimprint lithography [55] has attracted significant interest for use in a number of applications including microfluidic devices, micro-optics, biochemistry and microsystems. Some complicated designs require 3-D structures with multilevel features to eliminate multiple process steps and complex alignments.

The high resolution and high throughput lithography techniques developed by the semiconductor industries are becoming very expensive for fabricating nanoscale features. The problem is even larger for printing 3-D structures at the nanometer scale. These are the research areas that require immediate attention in progressing the NIL technologies.

1.7 The Objectives of the Thesis

Since not much work is being done on 3-D nanoimprint especially on mold making processes, this thesis emphasizes developing the 3-D mold making processes as well as the 3-D imprint processes. The UV-NIL technique is employed to avoid a process with high pressure and high temperature cycles. Pattern writing, pattern transfer and imprint are the three major areas that are investigated. The molds are made using a high-resolution but low-throughput EBL technique and subsequent imprint lithography is employed for the replication of the micro/nanostructures. An EBL is used for patterning and the pattern transfer onto mold substrate is achieved using an RIE technique. The mold profiles are replicated onto imprint resists using manual imprint tools.

Equipment and process used in this research work are selected based on their resolution, limitations, capability and functionality. Material characterization process is carried out to define suitable materials for this work.

The 3-D pattern profiles are created on a negative photoresist using a Raith 150 EBL tool in a single step variable e-beam dose controlled exposure. Resist contrast curves are obtained with a negative photoresist (ma-N2403) and a single pass line (SPL) pattern writing scheme is employed to create a 3-D pattern profile. Specially designed test patterns are used to demonstrate the capability of UV-NIL in replicating the 3-D and multilevel structures.

Surface charging, electron back scattering and proximity effects on insulating materials such as quartz during e-beam exposure are investigated. Multiple approaches for suppressing the charging, electrons backscattering and proximity effects are developed. Monte Carlo simulation using CASINO software is employed to investigate the effects of accelerating voltages on electron trajectories during the e-beam exposure.

As a substrate material that has numerous applications at micro/nano scale, quartz is the center of the material processing research, especially if used as a transparent imprint mold. The fabrication of 2-D high aspect-ratio structures and 3-D pattern transfer onto quartz substrate are the aim of the mold making process. The optimization process to achieve a very low surface roughness of below 5 nm is the prime focus in the pattern transfer process. This work could

result in a better understanding of the underlying science of etching hard materials such as quartz.
In this research work, manual operated imprint tools are used for imprint processes, to demonstrate that low cost and an unsophisticated system that are fabricated in a general workshop can produce high quality lithography results. The materials, methods, conditions and problems of the imprint processes are studied. The resist reflow, cavity filling, sticking phenomena during imprint are investigated by the assistance of simulation using ABAQUS finite element software.

1.8 Thesis Outline

The thesis starts by outlining the challenges in semiconductor industries and the assessment of 3-D UV-NIL as a candidate for future nanolithography technology. Each chapter begins with an introduction, background and details of the subject, and concludes with a summary of the important findings or accomplishments.
Chapter 1 presents the challenges for current and future manufacturing technologies. The overview of NIL as candidate for NGL and its promising characteristics for future technology are described. The future of NIL technology and its opportunities became the motivation for this research work. The research background and the objective of this research work are also discussed.
The experimental technologies adopted in this research work are discussed in Chapter 2. The justification for equipment, process and material selections are explained and a number of nanofabrication equipments in the UC Nanolab facility that are utilized in this research work are discussed. The characterization of the materials used in this work are also discussed.
Chapter 3 describes the major challenge of this research which is the mold making process. A variable controlled e-beam dosages method has been employed in 3-D pattern writing using EBL. A linear contrast curve as a relationship between the e-beam dosages and the associated height of the developed resist

structure has been established. The obstacles in writing the pattern on the insulator substrate such as quartz using EBL have been overcome with a number of newly developed approaches for fabricating 2-D and 3-D structures. In fabricating 2-D structures, thin metallic and conductive polymer coatings were employed while for 3-D structures, special techniques called critical energy and top conductive polymer coating have been developed to suppress the surface charging, electrons backscattering and proximity effects. The 2-D and 3-D pattern transfer processes onto quartz substrate are investigated and explained in detail.

The replication processes of 2-D and 3-D structures are described in detail in Chapter 4. In 2-D imprinting, two imprint procedures using transparent molds and transparent molds with NiCr absorber layer were described. The materials used and the conditions of the imprint process are elaborated. Issues related to this process such as sticking and de-molding failures are also discussed.

Chapter 5 discusses the some of important issues of NIL technology in general as well as the limitations and issues which emerged in this research work. The recommendation for further improvement of this technology is also discussed. The prospects of this technology as the candidate for future nanolithography technology are outlined.

Lastly in chapter 6, as conclusions, the findings and accomplishments of this research work are summarized.

Chapter 2

EXPERIMENTAL TECHNOLOGIES

In this thesis, a number of fabrication techniques/processes/equipments were employed. In this chapter, these equipments will be investigated and processes developed will be illustrated and explained. The main equipment used for defining nanometer scale patterns was EBL where 3-D patterns and multilevel structures were built on quartz substrates. For metal deposition, thermal and e-beam evaporators were used to evaporate metallic thin film such as NiCr and aluminium, and magnetron sputtering was used to deposit metallic materials such as tungsten and metal oxide materials including titanium dioxide. A scanning electron microscope (SEM) and an atomic force microscope (AFM) were normally used for imaging the resultant structures. For pattern transfer, RIE using fluorinated plasma was used to etch quartz substrate. Imprint was performed using simple imprint tools designed for this purpose. A UC contact angle system was used to measure the surface contact angle as a tool to estimate the wettability of the material surfaces such as substrates and imprint resists.
The Nanofabrication Laboratory at the University of Canterbury (UC Nanolab), Christchurch, New Zealand contains facilities for semiconductor material processing, nanofabrication and device development. This is the main fabrication facility for the MacDiarmid Institute for Advanced Materials and Nanotechnology. The equipment in the UC Nanolab covers most aspects of semiconductor device fabrication, from materials growth to device characterization. UC Nanolab hosts key fabrication equipment including an Electron Beam Lithography machine (Raith-150), a high precision optical Mask Aligner (Karl Suss

MA-6) and a versatile sputtering system with DC/RF co-sputtering and electron beam evaporation capability (Edward Auto500).
The suitable process and equipment were defined upfront based on their resolution, functionalities and capabilities. Trial and error, and systematic methods were applied to define the process window for certain processes and subsequently a proper design of experiment was carried out to define optimum parameters for the processes.
A material selection and characterization process were carried out to define suitable materials to be used in this research. Most of the materials such as the imprint resists used in this research are relatively new and much remains to be understood. Conductive polymer was used as the charge dissipation layer in comparison to the thin metallic layer.
This research work was divided into two phases; mold making and replication using the imprint technique. For mold making, the patterns were defined using the EBL technique and the samples were developed using appropriate developer to realize the patterns. The patterns were then transferred onto substrate using the RIE pattern transfer process. The UV-NIL was employed using a manual imprint tool to replicate the master mold onto an imprint resist. The patterns were transferred onto a final substrate using the RIE pattern transfer process.

2.1 Process and Apparatus

Lithography is a key technique in making micro/nanostructures. Making a device or structure at micro/nanoscale involves a number of nanofabrication process steps. Patterns are defined on an imaging layer and later transferred onto a substrate using an etching process.
Mold making was the major task in this research, where most of the major nanofabrication equipment such as EBL and RIE was utilized in this phase. The mold fabrication process begins with substrate preparation/cleaning, resist coating using resist spinner, and pre-baked in an oven or a hot plate. DEK-

TAK or Veeco profilometer were used to measure the resist layer thickness. This followed by pattern definition using an EBL technique. Patterns were realized after an exposed sample was developed in an appropriate developer. High resolution AFM and SEM were employed as pattern imaging technique.
For 2-D pattern transfer using additive pattern transfer method which will be explained in section 3.1, a thin metallic layer was deposited using thermal evaporator system. In 3-D pattern transfer, the developed resist patterns were directly transferred onto substrate using the RIE pattern transfer techniques.
In the imprinting, manual imprint tools were employed to replicate the master mold onto the imprint resist. During imprint , the negative resist was cured using an UV exposure tool such as Karl Suss MA-6. Molds were released from the imprinted resits by using manual de-molding process. Equipment was carefully selected based on its resolutions, limitations and functionalities. Pictures of all tools and equipment that were used in this research work are listed in Appendix A.

2.1.1 Pattern Definition Using the EBL Technique

Electron beams (e-beam) have been used for lithography purposes since the 1960s. A lithography system can be easily added to nearly all modern electron or ion microscopes, including scanning electron microscopes (SEM), scanning transmission microscopes (STEM), FIB and dual SEM/FIB microscope models [56]. Most microscope models have inputs for external control of the XY beam position. A beam blanker is an accessory for lithography purpose, where beam-on/beam-off events can be controlled while writing from one pattern element to another pattern element without exposing the resist in between the patterns. For lithography (pattern writing), this system normally uses the vector writing approach, where the beam moves in any direction and scans only areas to be exposed (pattern).
Figure 2.1 illustrates a schematic of a typical SEM-based lithography system. The electron gun is on the top of the column, produces the electrons which are accelerated by electrostatic fields towards the sample surface at a specified ac-

celerating voltage or energy in keV unit. Electromagnetic lenses and apertures are used to focus the e-beam and to form a focused e-beam spot on the sample surface. A high-vacuum environment allows electron travel without scattering by the air. The sample stage, e-beam scanning coils, signal detection, and processing system provide real-time observation and image recording of the specimen surface.

In this work, the Raith-150 EBL system as shown in Appendix A - Figure A.5

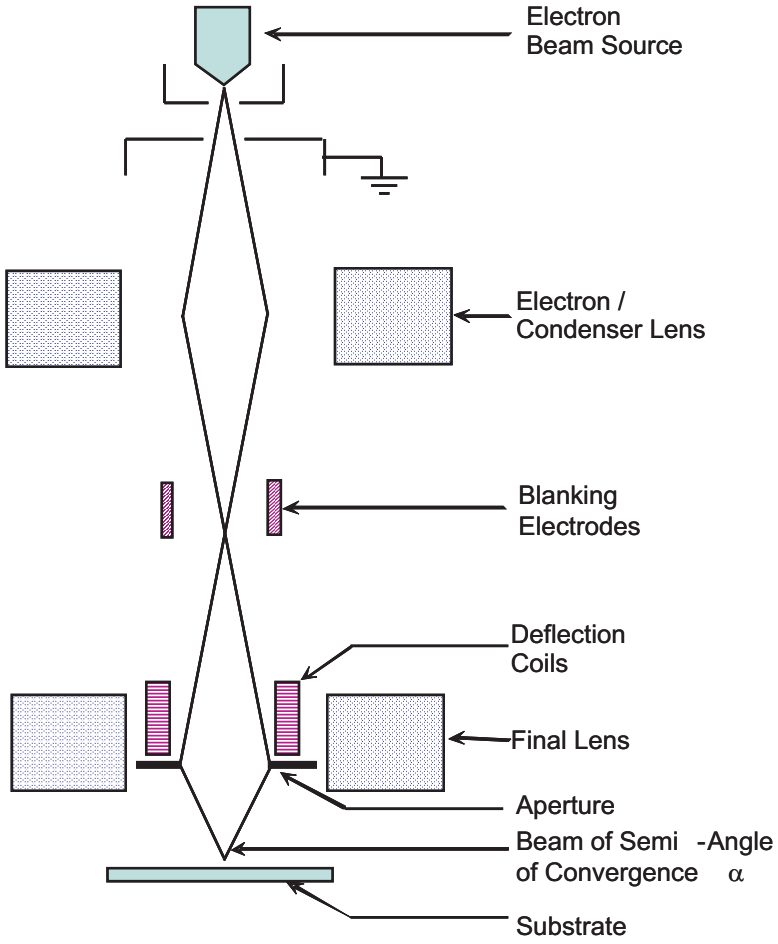

Figure 2.1: The schematic diagram of the electron beam lithography system

was employed in pattern writing on a negative and positive photoresists. This is the SEM-based lithography system that uses a field-emission electron gun and is capable of exposing e-beam from a few keV up to 30 keV.

EBL was the choice for the patterning task of this research work owing to its well-known high resolution and 3-D capabilities. Unlike optical lithography, no costly masks are required for patterning using EBL. The only disadvantage is that the throughput is very low, but it has been traded off with the high reso-

lution and precision requirements.

The parameter setting of e-beam exposure such as write field size, working distance, accelerating voltage, aperture size, beam current, and dosages (writing speed) are dependent on the pattern design and resist requirements. The write field size is determined by the magnification of the microscope. If a large area of fine features is desired, several fields can be positioned so that the field edges align with each other, normally known as stitching. This work uses a 25 μm x 25 μm write field size for exposing feature sizes below 100 nm. The working distance influences the minimum spot size that is achievable and for this work the working distance of 6 mm has been used. High accelerating voltages will produce a high electron penetration depth, thus lowering the number of scattered electrons in the resist, resulting in fine e-beam line width. For 2-D patterning work, an accelerating voltage of 20 keV and 20 μm aperture size has been used to achieve patterns with feature sizes of below 100 nm and for normal feature sizes of above 100 nm, accelerating voltage of 10 keV and aperture size 30 μm have been used. The measured e-beam currents using a Faraday cup are determined by a combination of accelerating voltage and aperture size used. At accelerating voltage of 20 keV and aperture size of 20 μm, a beam current of about 25 pA has been measured. E-beam dosage is the amount of electrons exposed (in $Coulomb$) per unit length (cm) for single pass line (SPL) or per unit area (cm^2) for area exposure. In pattern writing, an e-beam dosage is increased when the e-beam dwelling time is increased in which the e-beam scanning/writing speed (in cm/s) is decreased.

Figure 2.2 shows the e-beam scanning configuration. A SPL scanning or writing normally uses half a beam/spot size stepping $(d/2)$. In exposing a pattern area, area step size (y) is the distance of a SPL from the adjacent SPL scanning/writing.

The electron beam is scattered in the resist and substrate. The scattered electrons expose some resist outside the intended pattern area which called proximity effect. The proximity effects on the exposed patterns can be minimized by the proximity correction capability in the Raith-150 software. Figure 2.3(a) illustrates an example of a 2-D pattern of 200 nm features which is designed using

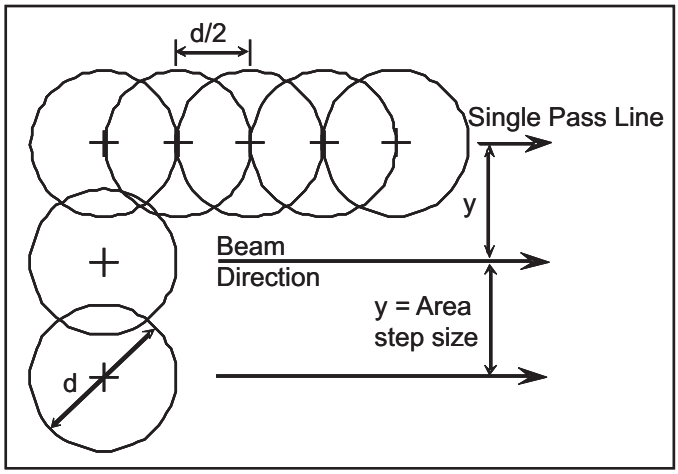

Figure 2.2: The schematic of electron beam configuration of the area step size and single pass line (SPL)

L-Edit pattern layout software. To achieve this pattern on PMMA bi-layer resist with thickness of 200 nm, accelerating voltage of 10 keV and 30 microns aperture normally used in EBL. In this work, basic correction by using a prepared substructuring Frame command with parameters α (the spread of the electrons from beam point) of 0.1 microns, β (backscattering range) of about 0.2 microns and η (the ratio of back scattering energy to forward scattering energy) of 0.4 was performed. Figure 2.3(b) illustrated the shape modifications for area exposure that carried out by the Raith 150 proximity correction software to achieve the intended pattern.

For 3-D patterning, there are two methods of defining a 3-D pattern using EBL: variable accelerating voltage and variable exposure dosage. The variable accelerating voltage technique [57] uses a specific voltage assigned to a specific pattern design layer where the limitation might be on the maximum number of the possible assigned design layers in the design layout software such as L-Edit. If the positive resist is exposed to the e-beam, the depth of the e-beam penetration is a factor of the e-beam accelerating voltage as illustrated in Figure 2.4(a). In this method, for example, the depths of the developed 3-D pattern are controlled by the magnitude of the uniform accelerating voltage assigned to each pattern layer. After pattern development, the depths of the cavities formed are a factor of the uniform accelerating voltage assigned to each design layer.

On the other hand, the variable dosage technique employs an e-beam expo-

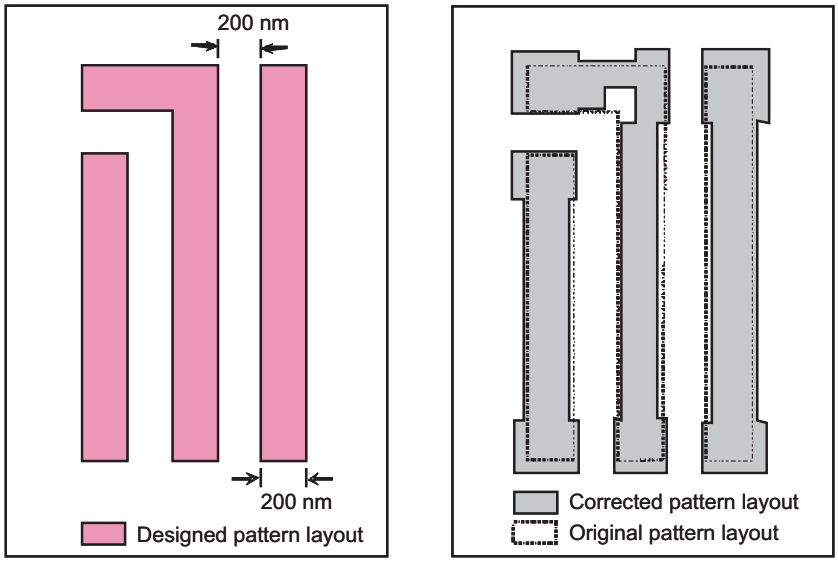

(a) Original pattern design

(b) Pattern modification after the proximity correction

Figure 2.3: The example of the proximity correction on a 2-D pattern during pattern writing using EBL.

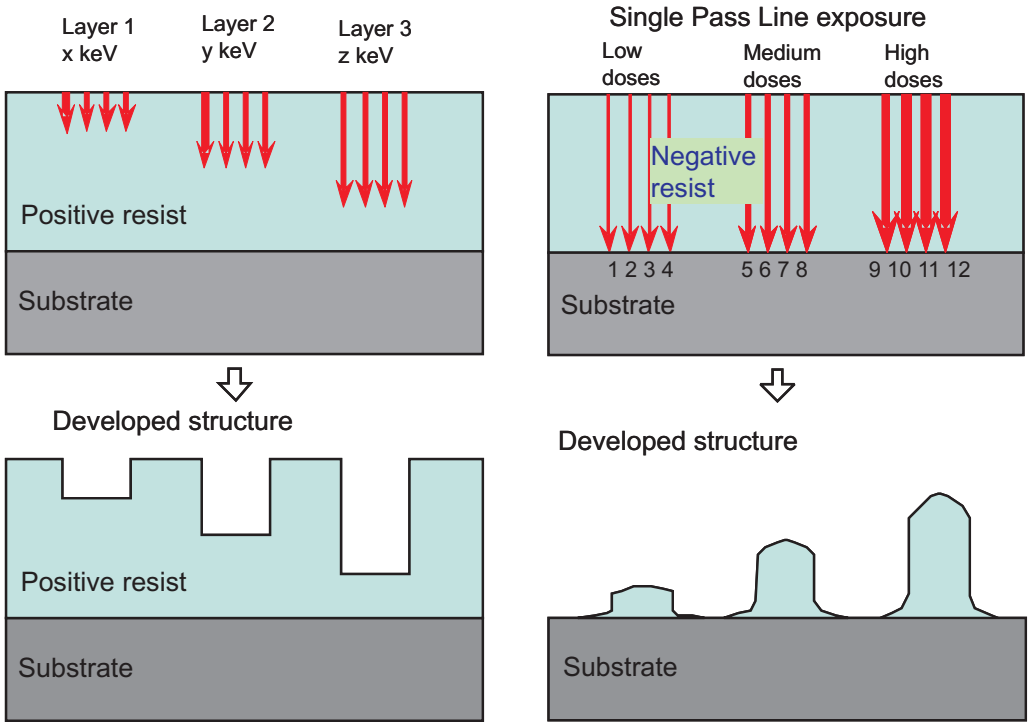

(a) Variable voltage

(b) Variable dosage

Figure 2.4: The different method of 3-D patterning using the EBL technique.

sure with path by path routing using a SPL scheme, with a specifically assigned dosage for each path as illustrated in Figure 2.4(b). In this method everything

is designed in a single design layer. The 3-D profiles can be achieved on negative resist by bringing SPL paths close (not less than e-beam size) and parallel to each other. There is no limitation on the number of paths and all paths are designed in a single design layer for any 3-D pattern design [58].

2.1.2 Pattern Development

There are two types of photo or e-beam sensitive resist material; positive resist and negative resist. Positive resist undergoes main chain scission when it is exposed to irradiation as illustrated in Figure 2.5(a) while negative resist chains are crosslinked when exposed to irradiation as illustrated in Figure 2.5(b) [59]. The developing agent dissolves the more soluble areas (the short and untangled polymer chains) to produce the desired pattern. The less soluble areas will also be dissolved if the resist is left too long in the developer. Hence, to have consistent results, developing time must also be consistent. Moreover, the development rate is dependent on the developer temperature. The soluble resist dissolves faster at a higher temperature as compared to a lower temperature. The developing time and temperature are two important development parameters. For example, in 2-D work, the PMMA bi-layer samples are developed in a MIBK:IPA 1:3 developer for 30 seconds at a temperature of 23^oC.

2.1.3 Metal Deposition Techniques

There are various methods of thin metal film deposition, such as evaporative methods, glow discharge processes, gas-phase chemical processes and liquid-phase chemical techniques [60]. Among them, chemical vapour deposition (CVD) and thermal evaporation are commonly used methods because their process are simple, low cost and compatible with conventional semiconductor device fabrication. In this work, evaporative methods are used for material deposition by employing a metal thermal evaporator system, an e-beam evaporator and/or a sputtering system depending on the application of the deposited

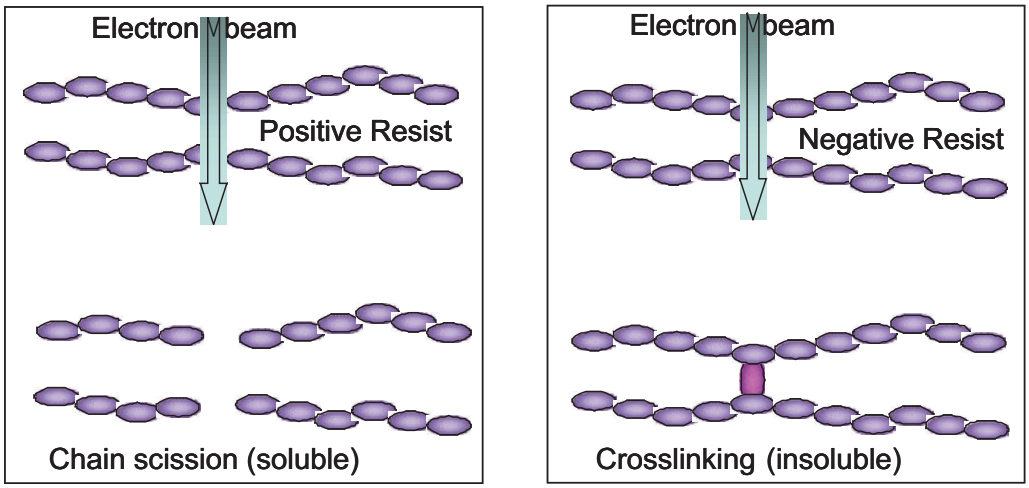

(a) positive resist: chain scission (b) negative resist: crosslinking

Figure 2.5: Electron beam induced chain scission and crosslinking reaction of resists [59].

thin film.

2.1.3.1 Metal Thermal Evaporator

Since early semiconductor technologies, the metal layers have been deposited by evaporation. Physical metal deposition uses heat to evaporate metals in a vacuum environment. Figure 2.6 shows a schematic of the metal evaporator system. It is similar to a light bulb concept as a material is loaded onto the filament boat and a high current is applied to flow through the boat in a vacuum environment. The high filament boat resistance generates heat to a very high temperature. The combination of vacuum pressure and power applied to generate heat to above the metal melting point will evaporate the metal material. The material vapour finally condenses in the form of a thin film on the cold substrate surface and on the vacuum chamber wall.

In this work, the Balzer metal evaporator system (Appendix A - Figure A.10) with resistive heating has been used for depositing most metallic thin films which requires a highly uniform flat surface and depositing metal for the purpose of the lift-off process at a later stage. The vacuum chamber size is about 600 mm in diameter and the distance between the evaporation source to the samples is about 300 mm.

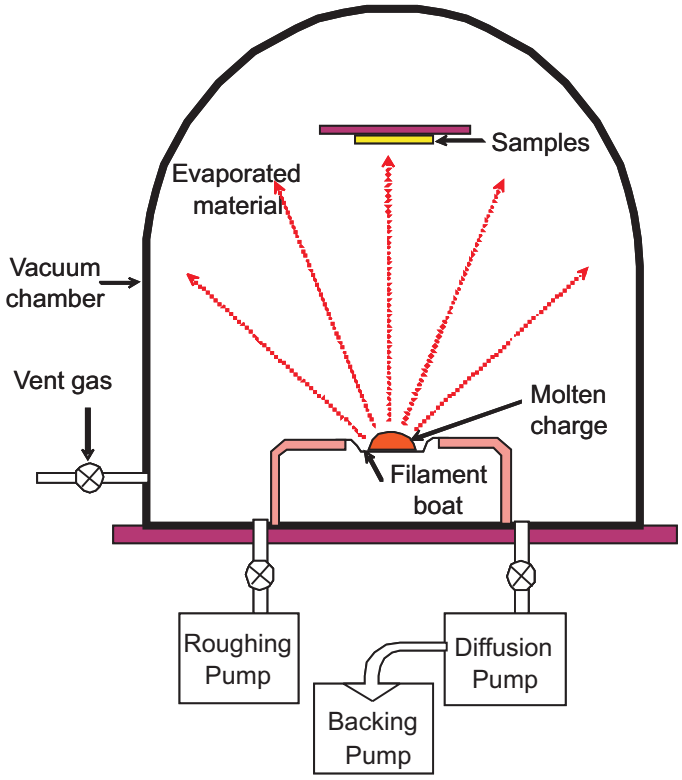

Figure 2.6: The schematic diagram of a metal/thermal evaporator

To achieve a directional deposition for the lift off patterned samples, the evaporated material particles must travel in a straight line from the evaporation source to the patterned samples. This condition can be estimated using the mean free path approach. The mean free path (l) is the average distance traveled by a particle before collision with other moving particles.

$$l = \frac{kT}{\sqrt{2}\pi d^2 P} \tag{2.1}$$

where k is the Boltzmann constant $1.38066x10^{-23}J/K$, T is the temperature in $Kelvin$, d is the particle size and P is the vacuum pressure in kPa.

Nichrome $(NiCr80/20wt.\%)$ which normally used as a masking layer in the 2-D plasma etching, has melting point of 1360^oC and density $8.5g/cm$. In vacuum condition, its vapour temperature is 1217^oC at vacuum pressure of $10^{-4}Torr$, and vapour temperature of 987^oC at vacuum pressure of $10^{-6}Torr$ [61]. Using the above formula with assumptions of a 3.5 nm particle size and a high vacuum pressure of around $10^{-4}kPa$ or $10^{-5}Torr$, the mean free path of the vapour atom is about 322 mm which is almost the same order as the vacuum chamber

dimension (300 mm in radius). At this condition, the NiCr particles travel in straight lines from the evaporation source towards the samples. Steep sidewall structures will not be coated. This is essential for coating material which requires a lift-off process at a later stage.
In this work, a 40 nm thick NiCr was coated on the patterned samples in 10 minutes, at applied power of 5.0 from a range of 0 to 10, and vacuum chamber pressure of $10^{-5}Torr$.

2.1.3.2 E-beam Evaporator

In e-beam deposition technique, metal source is placed in a crucible and a high e-beam is accelerated onto the material to heat it up to a very high temperature above its melting point. The application of this method of material deposition is dependent on the distance between the sample and the target material. In the UC Nanolab, this system is associated with the Edward Auto500 Magnetron sputtering system. The distance between the sample and the source of the evaporated material (in a 20 mm diameter crucible) is about 120 mm. This distance is too close for the atomized/evaporated materials to hit the sample surface from perpendicular angle. This system is not suitable for depositing materials to lift off samples. In this work, a 20 nm thick of aluminium layer was deposited on the PMMA bi-layer resist surface as a charge dissipation layer by using this technique. Thin metallic layer can also be coated on sample surface using magnetron sputtering technique which will be explained next.

2.1.3.3 Magnetron Sputtering

Sputtering is a process whereby atoms are ejected from a solid target material due to bombardment of the target by energetic ions in a vacuum environment. Sputter deposition is a method of depositing thin film where sputtered atoms ejected into the gas phase tend to deposit on all surfaces in the vacuum chamber. Magnetron sputtering is where the application of a magnetic field in a plasma causes the electrons to spiral around the direction of magnetic field

lines. Figure 2.7 illustrates a schematic of the magnetron sputtering system. The orbit of the electrons increases the probability that they will collide with neutral species and create ions. This increases the ion density and increases the rate of ion bombardment of the target [62]. This deposition technique is popular to achieve a high material purity and fine particles.

DC magnetron sputtering is mostly used for metal deposition and RF magnetron sputtering is normally used for the deposition of non-metal materials such as ceramics and metal oxides. This sputtering system also been used for depositing metal oxides by sputtering pure metals in an oxygen environment (reactive sputtering). In this work, the Edward Auto500 Magnetron Sputtering system as shown in Appendix A - Figure A.9, has been used for depositing metallic and non-metallic materials. The target-substrate distance is about 110 mm which enable proper coverage of the surface topology conformally. This is called conformal coating or sometimes called steep coverage which is useful for coating the 2-D and 3-D surfaces uniformly. Target size, surface diffusion also play a role in conformality of the coating process. This system also has a capability of RF/DC co-sputtering where magnetron can be operated in the DC mode with a maximum power of 500W and/or in the RF mode with a maximum power of 300 W.

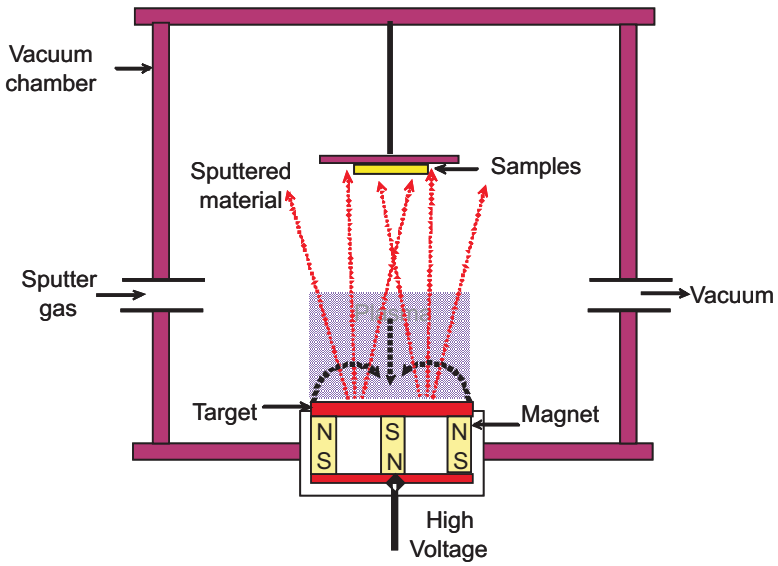

Figure 2.7: The schematic diagram of a magnetron sputtering system

In this work, DC sputtering has been used for depositing a 5 nm thick tungsten layer on quartz samples as a charge dissipation layer prior to e-beam exposure or SEM imaging. RF magnetron sputtering has been used for depositing a 4 nm TiO_2 layer on top of Ormocomp resist layer as a permanent anti-sticking coating. For this sensitive ceramic target, the RF power was ramped up from 25 W to 100 W in 20 minutes to avoid the target cracked because of unbalanced and sudden heat expansion at a high RF power. The system was running at a constant RF power of 100 W during evaporation and later ramped down from 100 W to 0 W in 30 minutes for proper cooling down.

2.1.4 Surface Profiler

Another system used in this work to measure the surface profiles is Veeco Dektak 150 profiler system as shown in Appendix I - Figure A12. This system is a step height measurement tool capable of measuring steps below 100 Angstrom and is used to profile the surface topography and waviness as well as surface roughness in nanometer range.

In this system, as illustrated in Figure 2.8, as the stage moves the sample, the stylus rides over the sample surface. Surface variations causes the stylus to be translated vertically and electrical signals corresponding to stylus movement are produced as the core position of the linear variable differential transformer (LVDT) changes. The digitized signals are then stored in computer for further manipulations.

In a standard configuration, a medium (L) diamond-tipped stylus force ranges from about 1 mg to 15 mg allows profiling on soft and hard surfaces. This system also capable of tracing lateral distance of up to 55 mm. In this work, it has been used to measure the coating thicknesses such as resists in a range of 30 nm to 900 nm and the deposited materials layer using evaporative techniques in a range of 5 nm to 200 nm.

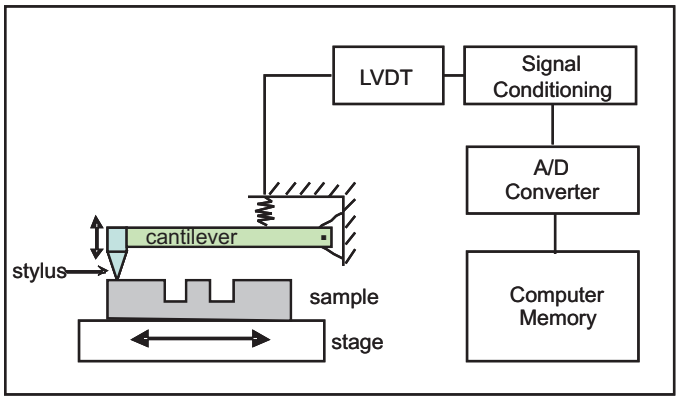

Figure 2.8: The schematic diagram of a profiler system

2.1.5 Lift off

In additive pattern transfer process which will be explained in section 3.1, a solid metal film is deposited onto a substrate through a resist mask. In the lift-off process as illustrated in Figure 2.9, the resist acts as a vertical standoff evaporation mask to separate the desired metal pattern from the extraneous material [63]. The resist layer under the metal film is removed together with the metal film by soaking in a solvent, while the metal film which is deposited on the substrate remains unchanged.

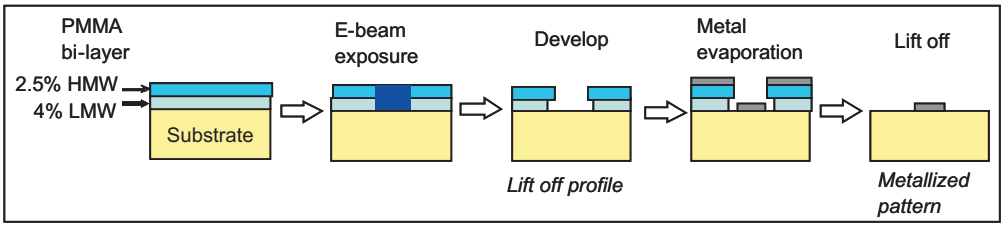

Figure 2.9: The schematic diagram of patterning on PMMA bi-layer using lift off method

In the lithography of lift-off, an e-beam positive resist such as PMMA is frequently used because it is high resolution and soluble in organic lifting solvent such as acetone. In this work, the PMMA bi-layer resist with overall layer thickness of about 180 nm was patterned with periodic lines ranges from 60 nm to 500 nm using EBL technique.

In PMMA bi-layer, the bottom layer used 4 % low molecular weight (LMW)

PMMA and the top layer used 2.5 % high molecular weight (HMW) PMMA. Both layers were spun coated at a spinning speed of 4000 rpm for one minute to achieve an overall thickness of about 180 nm. The sample was pre baked at a temperature of 185^oC for 30 minutes for each layer coating.
An e-beam exposed pattern sample was developed in MIBK:IPA 1:3 developer for 30 seconds at a temperature of 23^oC. The exposed pattern of LMW PMMA (bottom layer) dissolves faster as compared to HMW PMMA in the developer. This creates the undercut profiles as shown in Figure 2.9 which minimizes the residual resist layer after the development process as well as improves the metal deposition process.
The sample was later coated with a 40 nm NiCr layer using thermal evaporator. In lift-off process, the sample was soaked in acetone solvent for 3 hours to remove the resist and the unwanted metal layer. Replacing the acetone with NMP solvent was found to give better results in term of sample cleanliness.

2.1.6 Surface Imaging Techniques

In the investigation of micro/nanostructure, the imaging (microscopy) and analysis (spectroscopy) are common methods of surface characterization. In this work, the morphology of the micro/nanostructure is the first information required using the imaging techniques.
Surface imaging is an important technique in providing information to understand the relationship between the nanofabrication process, the structure produced and the resulting physical and mechanical properties [64]. Imaging a surface topography at nanoscale is a challenging task and optical imaging is limited to a few thousand magnifications only, and resolution down to about 200 nm [65]. Beyond that, special methods such as scanning electron microscopy (SEM), atomic force microscopy (AFM) and near-field scanning optical microscopy (NSOM) are normally employed [66]. Recently, magnetic resonance force microscope (MRFM) technique, which was developed in IBM [67], has been used for detecting the resonant force of single photons in order to image the nanostructures in three-dimension. Figure 2.10 shows the general

morphology characterization techniques in term of their lateral and depth resolutions [68]. In this work, SEM and AFM techniques were employed for the 2-D and 3-D surface imaging.

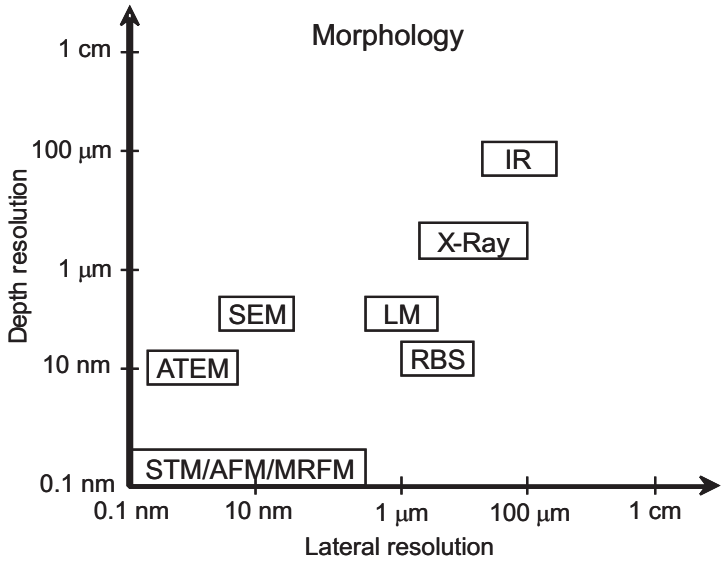

Figure 2.10: Various morphology characterizations using different imaging and analytical techniques in terms of their lateral and depth resolutions [65].

2.1.6.1 Scanning Electron Microscopy (SEM)

SEM is one of the most versatile instruments available for the imaging and analysis of the microstructure morphology and chemical composition characterizations [65]. The fundamental operation of SEM is illustrated in Figure 2.1. In this imaging technique, the reflection of secondary electrons (SE) or back scattering electrons (BSE) from surface topography are detected by a specialized detector and processed for the surface topography appearance.

For conventional imaging in the SEM, samples must be electrically conductive, at least on the surface and electrically grounded to prevent the build up of electrostatic charges at the surface. Samples require an ultra thin conductive layer that is conformal coated to realize the surface topography. This can be done by coating the sample surface with metallic thin film such as tungsten using sputtering technique as discussed earlier.

In this work, the Raith-150 SEM system of UC Nanolab and the JEOL SEM sys-

tem at the UC Mechanical Engineering Department have been used for imaging the NiCr patterns after the lift off process and the etched quartz substrate after the pattern transfer process. For Raith-150, accelerating voltage of 10 keV and 30 microns aperture are normally used for SEM imaging.

2.1.6.2 Atomic Force Microscopy (AFM)

The atomic force microscope (AFM) is probably the most versatile member of a family of microscopes known as scanning probe microscopes (SPMs). These instruments generate image by 'feeling' rather than 'looking' at specimens. They visualize surfaces using sharp probes/tips attached to the microscale cantilever, where images are obtained by measuring changes in the magnitude of the interaction between the tip and the specimen surface as the surface is scanned beneath the tip. Figure 2.11 shows the schematic of the AFM detection using the common method of laser beam deflection. The Digital Instrument's AFM system model DI3100 as shown in Appendix A - Figure A.6 was used in this research work.

There are many imaging modes when scanning surfaces using AFM. They are often differentiated as static (contact) mode and dynamic (non-contact) modes. Contact mode is where a constant pressure is applied by a probe onto the specimen surface during scanning. It is generally harder to get good images with a traditional contact mode. In non-contact mode, the oscillating cantilever never actually touches the surfaces of the sample, but hovers a few nanometers above it. Another non-contact mode is the tapping mode where a stiff rectangular cantilever is deliberately excited by an electrical oscillator to amplitudes of up to approximately 100 nm, so that it bounces up and down (taps) as it travels over the sample. It is like a blind person tapping his white stick on the foot path. This mode reduces the lateral force on the sample because the tip spends less time on the surface of the sample, which is useful for delicate surface profiles. The resolution will depend on the sharpness of the probe tip, the slope of cantilever, the tip orientation and the sampling regime [69]. The AFM tips' sensitivity can be significantly affected by the slope of the cantilever and the interactive

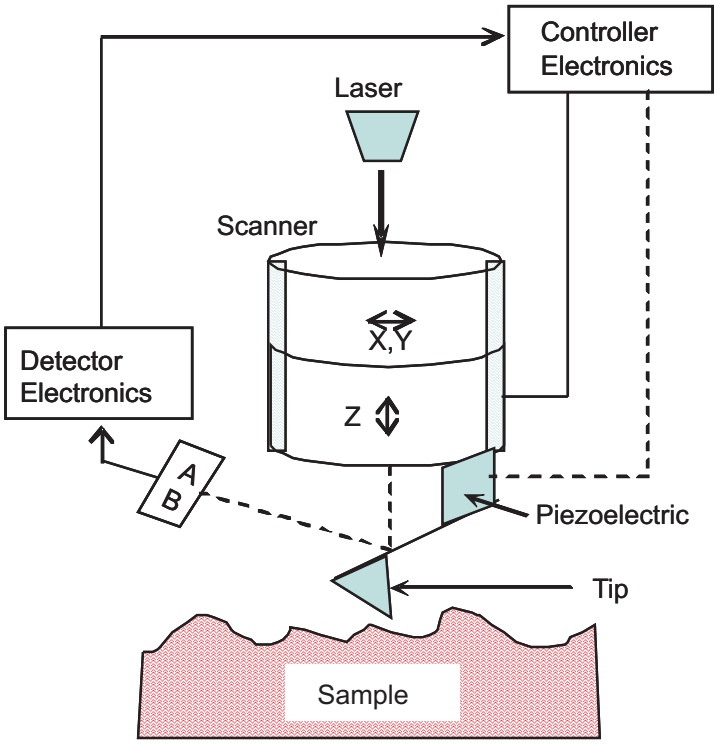

Figure 2.11: The schematic diagram of atomic force microscope detection using the laser beam deflection method

damping occurring between the cantilever tip and sample surface [70]. With a proper optimization, AFM is capable of 'atomic' resolution of a material surface and able to be used to identify even single atoms and molecules [71].

This method of imaging does not just produce topography of the surface but a more detailed picture of the material surface can be measured. In amplitude modulation, changes in the phase of oscillation can be used to discriminate between different types of materials on the surface. Another major application is force spectroscopy, the method that has been used to measure nanoscale contact, atomic bonding, Van der Waals forces etc.

There are various types of cantilever and probe tips available commercially for various applications. The shape of the tip used in AFM is an important consideration and the choice of tip shape is closely linked to the properties of the sample under study [72]. Figure 2.12(a) shows a configuration of a common tip for general use and Figure 2.12(b) shows the STING tip or High-Resolution tip that is used in this work to scan the high aspect ratio and 3-D structures. Normally, the common AFM silicon probe has its tip dimension of about 10 nm

and angle of about 30 degrees. The STING tip is a common AFM tip with additional sting structure of up to 100 nm on top of the common tip. So far this is the best probe we could get from market to be used in this work, even though this probe still not good enough for tracing the high aspect ratio and vertical sidewall structures as explained in section 3.2.3.2.

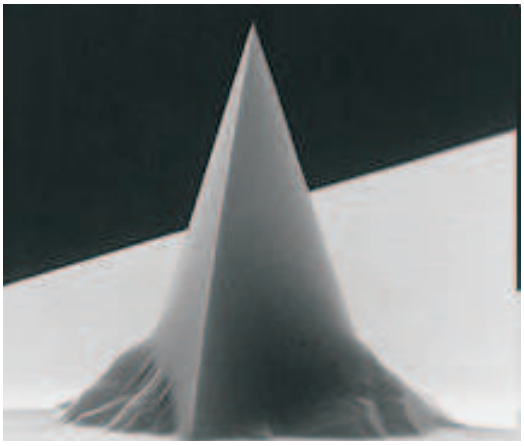

(a) AFM typical tip for normal application

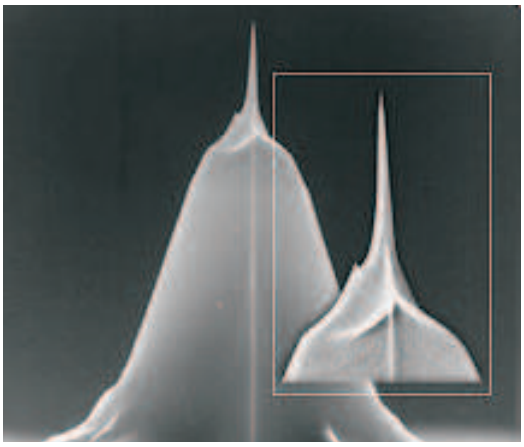

(b) AFM 'STING' tip for special application

Figure 2.12: SEM images of AFM tips used in this work.

2.1.7 Pattern Transfer

Pattern transfer is the process to transfer the developed resist pattern onto substrates. Wet chemical etching with acid or base solutions is normally used to transfer a pattern onto semiconductor materials. It involves either the oxidation or reduction of the semiconductor surface followed by removal of the soluble

reaction products. Wet etching is generally fast, with low damage and low cost. However, the isotropic etches obtained with wet chemical etchants are difficult to control and have poor resolution [73].

High quality 'dry' plasma etching was developed to overcome the limitations of etching the nano scale structures using wet chemical etching. This etching consists of a chemical reaction and physical damage by ion bombardment. Operating pressure of the plasma etching plays an important role in the way the plasma reacts to the material. Figure 2.13 shows the range of etching processes related to the operating pressure [62]. Wet etching presumably on the far left is 100% chemical reaction, while across to the far right ion milling is 100% physical etching. Plasma etching, reactive ion etching (RIE) and high density plasma etching are achieved by combinations of chemical and physical etching.

Pressure has direct influence on the major phenomena that controls plasma

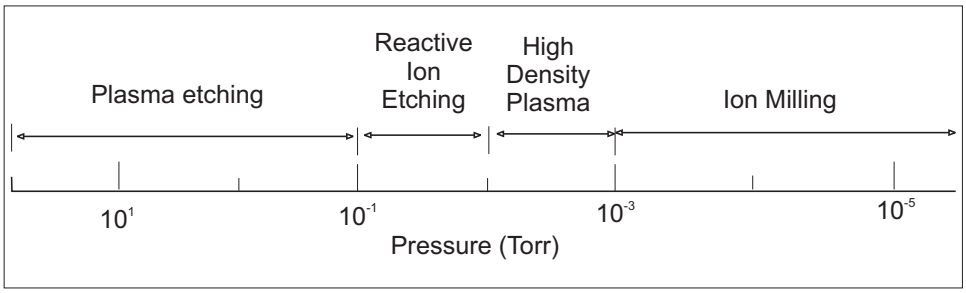

Figure 2.13: Plasma etch processes on chamber pressure scale [62]

etching [74]. Among them are: (1) The sheath potentials and energy of ions bombarding surfaces, (2)The electron energy, (3) the ion-to-neutral abundance ratio and fluxes of these species to surfaces, (4) the relative of higher to lower order chemical kinetics, (5) surface coverage by physical absorption, and (6) the relative of mass transport process. At a very low etching pressure (to the right of Figure 2.13), the sheath potentials and energy, electron energy, ion-to-neutral ratio, and mass transport are getting higher. Only chemical kinetics decreases with lowering etching pressure.

Plasma etching proceeds in five steps as illustrated in Figure 2.14 [75]. First, the etchant species is generated in the plasma, then transported by diffusion through a stagnant gas layer to the surface. After the reactant is adsorbed on the surface, a chemical reaction (along with physical ion bombardment effects)

forms volatile compounds. Finally, the compounds are desorbed from the surface, diffused into the bulk gas, and pumped out by the vacuum system.

RIE utilizes an ion-enhanced etch process where the plasma is normally gener-

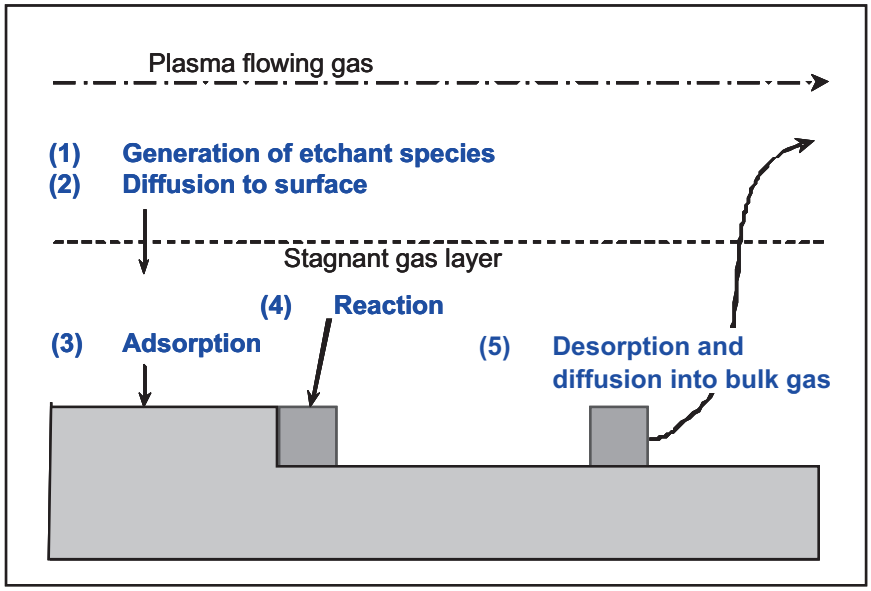

Figure 2.14: The plasma etching mechanism [75].

ated at a radio frequency (RF) of 13.56 MHz between two parallel electrodes in a reactive gas as shown in Figure 2.15 [76]. The larger grounded electrode combined with the low operating pressure $(< 500mTorr)$ causes the samples to be subjected to a heavy bombardment of energetic ions from the plasma as a result of the large negative self-bias at the sample surface which causes anisotropic (directional) etching.

The Oxford Plasma 80plus RIE system as shown in Appendix A - Figure A.11 was used in this research work for various purposes such as for quartz etching, as plasma asher for resist removal, removing tungsten layer from quartz surface, and treatments of resists and quartz surfaces. The developed RIE process recipe for particular purposes which consists of mixture of gases, temperature, RF power and pressure, will be explained in detail in chapter 3, section 3.1.4 and section 3.2.3.

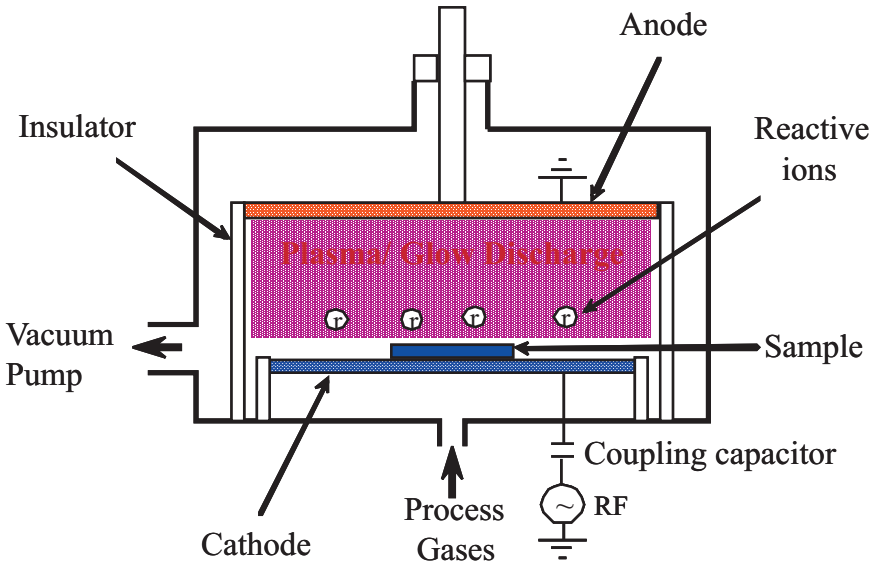

Figure 2.15: The schematic view of an RIE system

2.1.8 Imprint Tools

Two simple manual tools were designed and employed to perform the imprint processes on 10 x 10 mm^2 samples. This is a demonstration of a simple and low cost tool anybody can fabricate in general workshops. Figure 2.16(a) illustrates the schematic of a cross sectional view of the first tool used in this work which is the vacuum operated manual imprint tool. It was attached into a Karl Suss Mask Aligner MA-6 exposure module as shown in Appendix A - Figure A7, to function as the UV-NIL tool. Figure 2.16(b) shows the optical image of the vacuum operated imprint tool which was specially designed and fabricated in-house using aluminium. The vacuum line of the imprint tool is connected to the MA-6's vacuum line that used to clamp the mask onto mask holder. In this work, a vacuum pressure of 4 $mbar$ and a 365 nm UV illumination were used to perform the imprints.

Figure 2.17(a) illustrates the schematic of a cross sectional view of the second manual imprint tool used in this work. The tool was fabricated in the department's workshop using a stainless steel material. The top holder of this imprint tool that weighted about 350 gram, is used as an applied load/force onto the 10 x 10 mm^2 molds during the imprint process. Figure 2.17 shows the optical image of this self loaded imprint tool. A resist substrate and patterned mold were manually aligned and placed into the slot with a Teflon cushion. The top holder

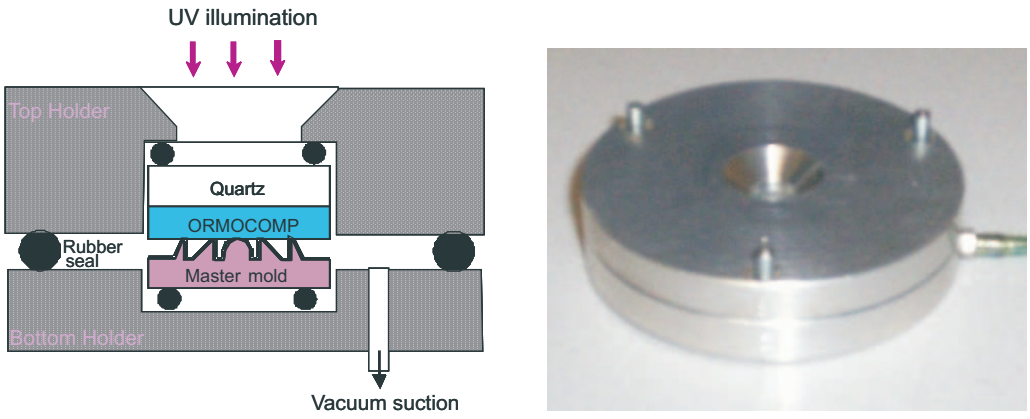

(a) The schematic view (b) The angle view

Figure 2.16: The second (vacuum operated) manual imprint tool used in this research work.

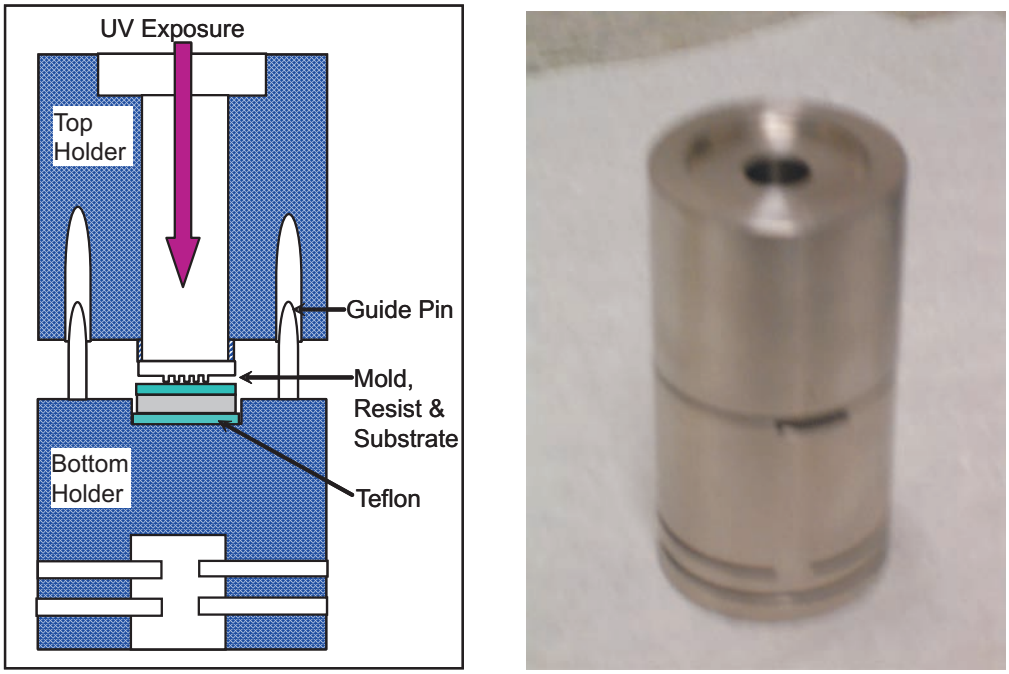

(a) The schematic view (b) The angle view

Figure 2.17: The first manual imprint tool used in this research work.

load was then gradually applied on the mold and resist sample. The imprint tool was placed inside the UC Nanolab UV box for a 365 nm UV exposure. Both manual imprint tools have been used in the development of imprint processes.

2.1.9 Surface Wetting

In resist coating and imprint processes, the non-sticking and sticking phenomena between molds, resists and substrates are a well known problem to be considered. Surface chemistries and surface energies are the properties that cause such phenomena.

When chemical reactions occurs at the interface, it changes the surface properties which lead to the change in surface energy. Surface energy is the interaction between the forces of cohesion and the forces of adhesion. Analysis of the surface properties can be performed using many methods. A surface wettability measurement is one way of estimating the surface properties. Wetting is the ability of a liquid to maintain contact with a solid and surface wettability can be determined by contact angle measurement. The contact angle provides an inverse measure of wettability. High surface energy is displayed by low contact angle on the surface and low surface energy is displayed by high contact angle on the surface.

A contact angle measurement tool from the UC Chemistry Department (Appendix A - Figure A.19) was used in the experiments. Figure 2.18 shows an example of a water drop analysis in the contact angle measurement. A 1.0 μl of DIW droplet was dispensed on a material surface and allowed 15 seconds settling time before the image was manually captured by the system. ImageJ software was used to capture the drop image and a low bond axisymmetric drop shape analysis (LB-ADSA) plugins was used to measure the contact angle.

Figure 2.19 illustrates the contact angle measurements that were carried out on some of materials employed in this research work. As a guideline, a contact angle of above 45^o is considered a strong hydrophobic material surface.

Figure 2.19 shows preliminary results of the comparison between contact angle measurements on various materials such as silicon, Si_3N_4, Quartz, PMMA, tungsten and sputtered titania used in this nanofabrication research work.

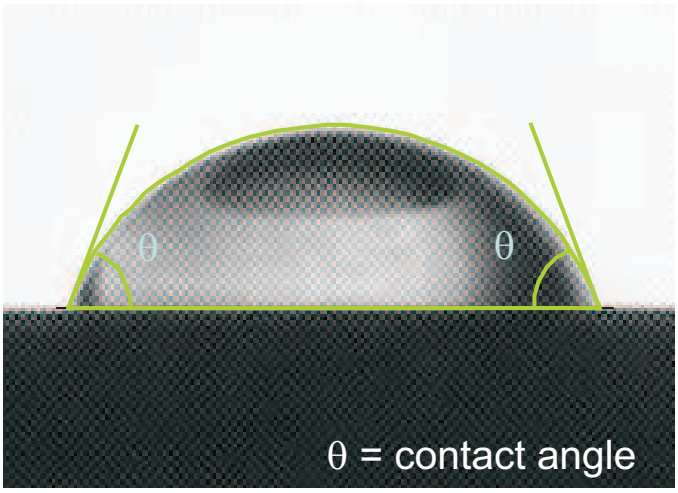

Figure 2.18: The analysis of a water drop in the contact angle measurement method.

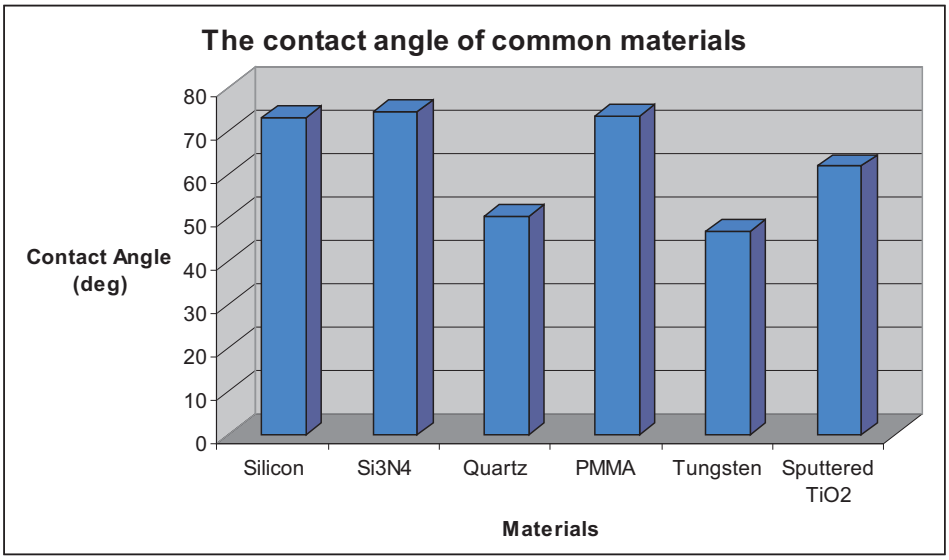

Figure 2.19: The contact angle measurements of some materials used in this work.

2.2 Materials

Materials are at the centre of this research work. The material processing and properties of substrates, resists, and anti adhesive coating were investigated. Substrate materials such as quartz, lithium niobate $(LiNbO_3)$, lead zirconate titanate (PZT) and possibly diamond [77] are transparent materials that have the potential to be a UV-NIL mold substrates. These materials can withstand high temperatures and except for diamond, have unique piezoelectric properties and are highly important in making pressure gauges, oscillators, resonators, watches and many other devices.

Resists are another important materials that investigated in this work. Both positive and negative resists can be used to create 2-D and 3-D structures and since this work utilizes a variable dosage EBL method for patterning 3-D structures, potential negative resists such as Microresist's ma-N2000 series and Hydrogen silsesquioxane (HSQ) were short listed. Imprint resists such as Ormocomp and mr-UVCur06 from Microresist Technology GmbH (MRT) were formulated for UV-NIL purposes and were suitable to be used in the fabrication of optical devices. Anti-sticking layer such as FOTS is an important component in the imprint processes to avoid sticking between the mold surface and the resist. This work also investigates other alternatives to anti-sticking layer such as titania and surface treatments.

The details of all the materials and chemicals used in this research work are listed in Appendix B.

2.2.1 Substrate Material

As compared to the other transparent materials, quartz's optical and thermal properties are the most superior. It has better UV transmission than other transparent materials owing to its purity for which it has been used to make lenses and other optics for the UV systems. It has a low coefficient of thermal expansion which is useful for precision usages. It is highly piezoelectric where it becomes polarized with a negative charge on one end and a positive charge on

the other end when subjected to pressure. It vibrates if an alternating current is applied to it. The piezoelectric properties are important for applications in MEMS and sensors such as surface acoustic wave (SAW) devices.

Silicon dioxide or Silica (SiO_2) is one of the most common and abundant oxide materials on earth. It occurs as quartz, cristobalite, tridymite, silica sands, sand stone and quartzite in nature, and it exists in a variety of crystalline forms or as an amorphous form [78]. Quartz has a unique structure, containing corkscrewing (helix) chains of silicon tetrahedrons which explain many of its physical attributes [79]. Quartz is important as a future substrate material but as yet, there is a huge vacuum of knowledge with regard to its processing at the micro/nano scale. Until recently, most quartz manufacturers have been making large discrete devices.

In this work, quartz samples were supplied by Mark Optics Incorporation, but the material was manufactured by Nippon Silica Glass (now TOSOH SGM USA). A semiconductor quartz grade NSG-N with a dimension of 10 mm x 10 mm and 0.5 mm thick was used as a mold substrate. Table 2.1 shows the material properties of quartz as provided by the TOSOH Quartz Incorporated [80].

Table 2.1: The physical properties of the quartz supplied by TOSOH Quartz Inc.

Thermal Properties		Mechanical Properties	
Strain Point	1090^oC	Density	$2.2g/cm^3$
Annealing Point	1180^oC	Young Modulus	7.3 x $10^5 kg/cm^2$
Softening Point	1720^oC	Vickers Hardness	8.5 x $10^4 kg/cm^2$
Expansion Coefficient	6.5 x $10^{-7}/^oC$	Tensile Strength	5.2 x $10^2 kg/cm^2$

2.2.2 Cleaning in the Mold Making Process

Cleaning is a very important step in the fabrication of quartz molds as well as in the imprint process. There are a few methods used to clean quartz depending on the cleanliness requirements. Generally, most semiconductor materials

including quartz can be cleaned using acetone, methanol and IPA in an ultrasonic bath. Continuing with the cleaning by short oxygen (O_2) plasma is recommended for cleanliness enhancement.

To remove resist from the substrate, especially in the lift-off process, acetone is normally used to attack the resist by soaking the sample in the acetone for two to three hours. For stubborn resist stains, a cleaning process at an elevated temperature is necessary but acetone's boiling point is very low, making it unsuitable for this task. On the other hand, the boiling point of N-Methyl-2-pyrrolidone (NMP) solvent is 95^oC, making it suitable for cleaning stubborn stains at a moderate temperature of below its boiling point. NMP is also suitable to be used in the lift-off process where it keeps the lift-off products floating in the solution resulting in better surface cleanliness.

For an extra cleanliness requirement especially in mold making processes, the quartz samples can be cleaned with a strong degreaser such as nitric acid or hydrogen peroxide to remove the organic and metallic contaminations. For removal of the outer surface layer of the quartz, the sample can be etched in hydrofluoric acid to expose a pristine silica surface [80]. Piranha solution (Appendix B - Table B.3) has also sometimes been used where samples cleaned with piranha were later rinsed in DIW and left to dry in a clean and dust-free environment.

2.2.3 Resists for Mold Fabrication

PMMA is a positive resist, which is a high resolution e-beam sensitive resist suitable for a high resolution patterning. It undergoes main chain scission when exposed to an electron beam irradiation. For 2-D patterning and lift off, normally PMMA bi-layer is used as explained in section 2.1.5.

For 3-D patterning, negative resist such as ma-N2403 from MRT was used in this research work. Previous work [81] has shown some encouraging results for 3-D and multilevel structures. At the same time HSQ has demonstrated its capability as a high resolution electron beam resist [34] and has potential as a 3-D pattern resist.

An experiment was designed to study the relationship between the e-beam dosages and the effects of electrons backscattering and proximity onto the developed ma-N2403 resist height. A single pass line (SPL), double pass lines (DPL) and quadruple pass lines (QPL) schemes with various e-beam dosages range were attempted. For parallel multiple line exposure, the spacing between the lines' exposure was about 20 nm to 30 nm. In a group of uniform dosages for each exposure lines, it was observed that the middle of the developed resist structures received higher exposure dosages because of the electrons' backscattering and proximity effects. Figure 2.20(a) shows AFM traces of resist cross sections for a range of uniform dosages applied to a QPL exposure scheme. It shows that the developed resist height is a factor of the dosages and the top of each developed structure was not flat as it should be. This is caused by the super imposed electrons backscattering and proximity effects as illustrated in Figure 2.20(b).

Figure 2.21(a) illustrates the distribution of resist heights versus the e-beam

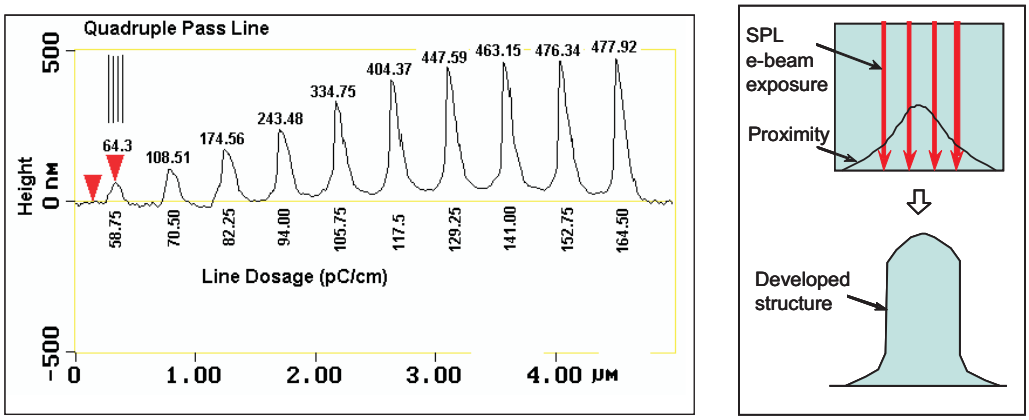

(a) AFM traces of the developed ma-N2403 resist

(b) The electrons backscattering and proximity effects

Figure 2.20: A study of e-beam dosages versus the height of the developed negative resist structure.

dosages for a DPL exposure scheme. Figure 2.21(b) illustrates the distribution of the percentage of resist height as compared to 600 nm initial resist thickness of the QPL exposure scheme. From these data we can observe the huge impact of proximity effects on the parallel exposure lines. The total height of the struc-

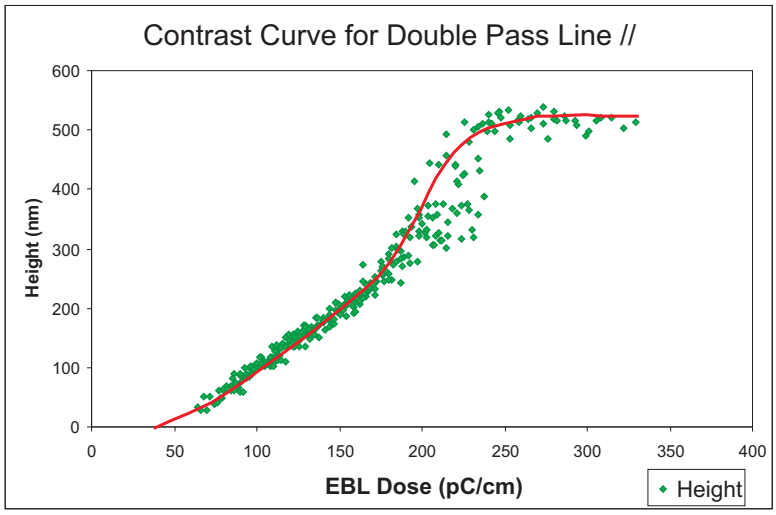

(a) Double Pass Line e-beam exposure

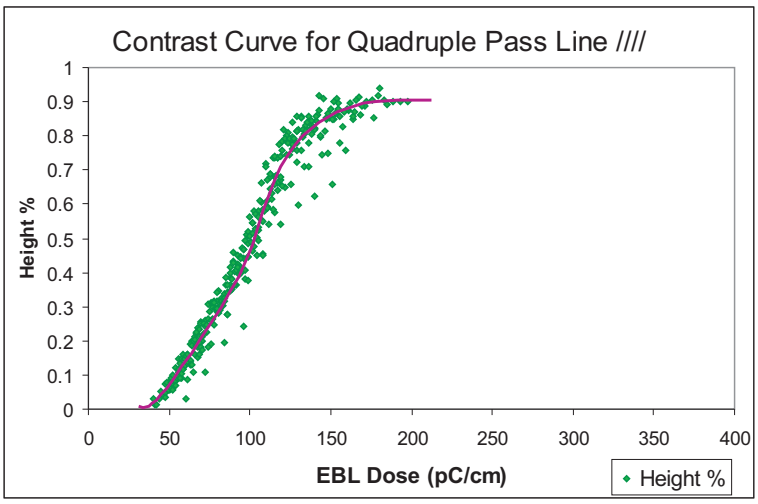

(b) QPL

Figure 2.21: Raw data of e-beam dosages versus the height of the developed structure.

ture is attributed to the combination of the total amount of dosages absorbed in that particular spot and the electrons' backscattering and proximity effects in the middle of the exposed pattern area.

Figure 2.22 illustrates the contrast curve of negative resist ma-N2403 when exposed with SPL, DPL and QPL exposure schemes. The SPL, DPL and QPL curves represent an exposure with zero, medium and high proximity effects respectively. There were huge differences in the structure height between SPL and DPL where without proximity effects in SPL, the structure heights were very low. These data have been used for estimating the dosage factors in designing a 3-D pattern.

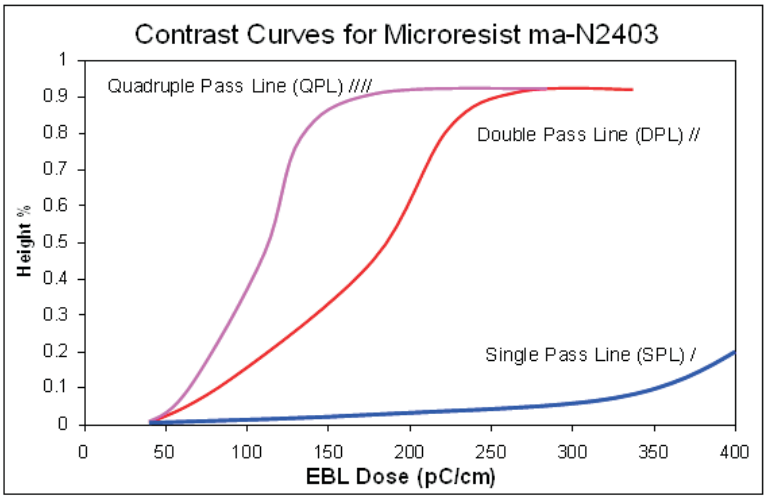

Figure 2.22: The contrast curves of negative resist ma-N2403 for SPL, DPL and QPL exposure schemes.

2.2.4 Resists for Imprint Processes

Resists play a key role in the successful applications of UV-NIL where adhesion between the substrate and resist should be high, but between the resist and mold should be as low as possible [15]. These criteria are crucial in searching for the appropriate resists to be used in this research work.

Acrylate resin ORMOCOMP US-S4 (Ormocomp) from MRT is a UV curable inorganic-organic hybrid polymer designed for UV imprinting or moulding [82]. This transparent material is thermally stable up to 270^oC and it shrinks about 2% to 8% during curing. It requires energy of about 300 mJ/cm^2 for i-line (365 nm wavelength) UV curing and it is suitable to be used as micro optical components produced by molding or imprinting.

Resist thickness is an important parameter in the imprint process and the specification of imprint process should be determined upfront. The required resist thickness relies on the required imprint structure heights, pattern densities and residual layer thicknesses [83].

In this work, Ormocomp has been used as the imprint resist to replicate the inverted shape of the master mold. In 3-D imprinting, the imprinted resist will be further hard-baked to harden the material and improve its solvent resistance in

order to be used as a soft/daughter mold in the subsequent imprint process. The characterization of spin coating of Ormocomp resist was carried out to define a suitable dilution of Ormocomp resist for this work. The undiluted Ormocomp is a honey-like solution which gives a few hundred microns of thickness in normal spin coating, hence it was diluted in an Ormothin thinner to achieve lower resist thicknesses. The samples with spin speeds ranging from 1000 rpm to 6000 rpm were experimented with 30 thicknesses data were recorded for each of the samples at different locations in order to measure the waviness of the coated surface by using the standard deviation of the measured thicknesses. Figure 2.23(a) shows the spin curve of 10% Ormocomp diluted in Ormothin thinner with the standard deviation of the layer thicknesses decreasing from 33.5 down to 9.5 nm when the spin speed is increased from 1000 rpm to 6000 rpm. The standard deviation of the layer thicknesses decreased when the spin speed increased which suggests that the surfaces are more uniform and flat at higher speeds.

Figure 2.23(b) shows the spin curve of 30% Ormocomp diluted in Ormothin thinner. The standard deviation of the layer thicknesses decreased from 82.7 nm to 45.0 nm when the spin speed is increased from 1000 rpm to 6000 rpm. At 4000 rpm, a few data with high thickness make the unusual bump at the maximum line but the average thickness is still in trend. The 30% Ormocomp has a higher standard deviation compared to the 10% Ormocomp. For this work, a 30% Ormocomp was spun coated at 4000 rpm for one minute to achieve a 400 nm resist layer thickness.

Figure 2.24 shows the UV transparency data of Ormocomp resist supplied by the MRT. Ormocomp is suitable for i-line (wavelength 365 nm) UV exposure.

Another UV curable polymer used in this research was mr-UVCur06 from MRT as well. This resist is compatible with various nanoimprint processes either imprinting in a vacuum or under atmospheric pressure. It has fast filling, a very low residual layer $(< 10nm)$ and low imprint pressure owing to its low viscosity $(14mPas)$, as well as a shorter curing time as compared to Ormocomp and high etch resistance in a fluorinated plasma. The 'ready to use' solutions for various film thickness achieved 240 nm thick if spin coated at 3000 rpm in one

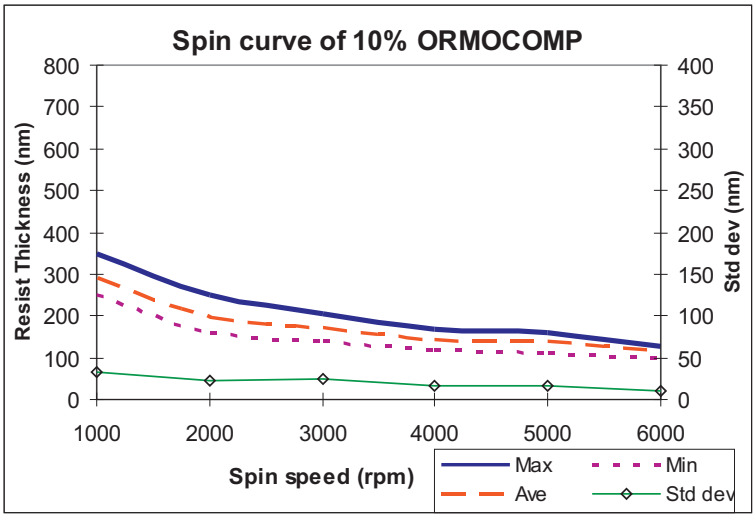

(a) Spin curve of 10% Ormocomp

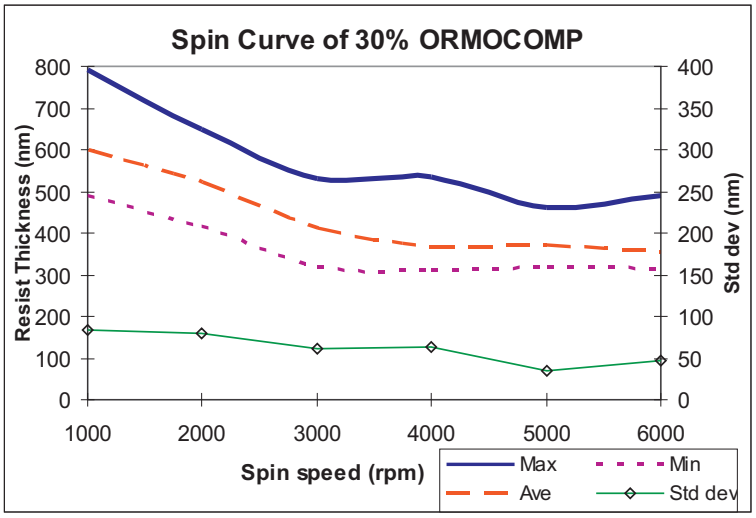

(b) Spin curve of 30% Ormocomp

Figure 2.23: Spin curves of Ormocomp resist that were diluted in an Ormothin solvent

minute. It is suitable for the fabrication of nanopatterns such as nano-optical devices, photonic crystals, and micro/nanofluidics.

2.2.5 Anti-Sticking Layers

Anti-sticking or anti-adhesion materials are important components in imprint processes. There are many methods of achieving a non-stick surface material, either by surface treatment or coating the surface with a non-stick material layer [84].

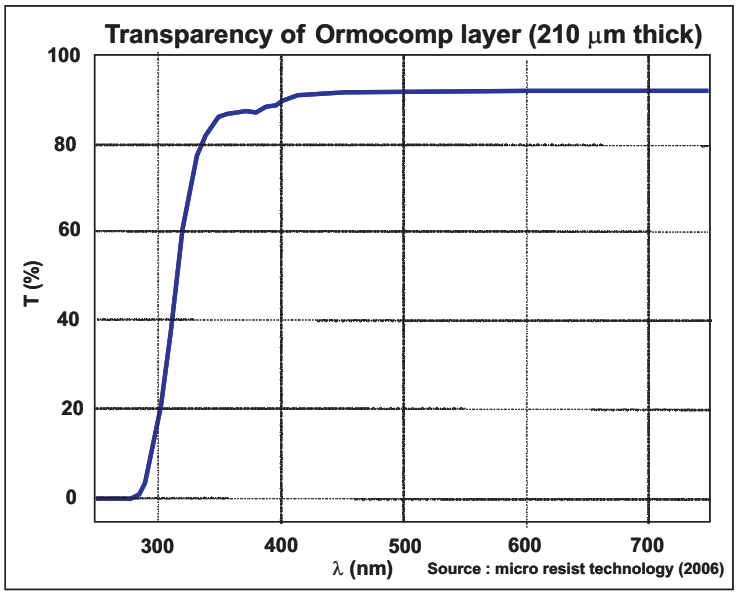

Figure 2.24: The UV transmission data on Ormocer series resist [82].

A 1H,1H,2H,2H-Perfluoroocty-trichlorosilane also known as FOTS solution from Sigma-Aldrich was used as an anti-sticking layer on molds and imprint resists. A self-assembled monolayer (SAM) coating can be achieved on the sample materials by using a slow natural evaporation/convection deposition method at room temperature. In this method, the sample was baked in the oven at a temperature of 90^oC for 30 minutes to fully dry the surface from water moisture and then cooled down to room temperature in a nitrogen desiccator(dry box). A small droplet of the anti-sticking solution (FOTS) was dispensed at the centre of a petri dish and the samples were placed surrounding it as illustrated in Figure 2.25. They were then covered with the petri dish lid and left for 30 minutes at room temperature. The FOTS droplet will evaporate slowly at room temperature and drop on the surrounding cold surfaces. It is similar to the water moisture deposited on the mirror surface in the bathroom after the morning shower.

In the actual manufacturing environment, a liquid anti-sticking material is less preferable because of contamination and evaporation of hazardous substances. Instead a permanent non-stick surface by surface treatment and solid coated materials are most preferable.

Metals such as nickel and tungsten are hard metals that are suitable for the protective layer as well as a potential non-stick material. These metals normally

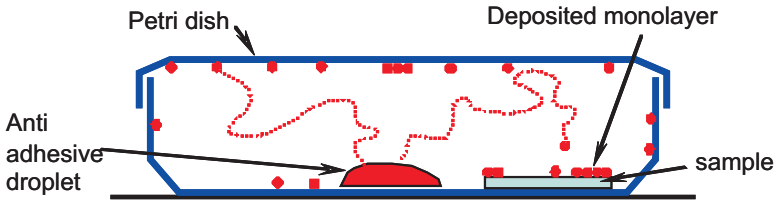

Figure 2.25: The self assembled monolayer (SAM) using a natural convection deposition method of FOTS in a petri dish.

can be coated onto a mold surface using the DC sputtering technique. Titania or titanium dioxide (TiO_2) is a ceramic material that has good non-stick properties. It can be used to coat the mold surface by using the RF sputtering technique. For sputtering an insulating material such as titania, a proper ramp up and ramp down of RF sputtering power is essential to avoid damage to the sputtering target and achieve a desired coating surface as explained in section 2.1.3.3.

2.2.6 Conductive Polymer

Conductive polymers offer a unique combination of properties where their conductivity can be tuned by chemical manipulation of polymer backbone [85, 86]. They are effective discharge layers as well as conducting resists for potential application in electron beam lithography. A water soluble conductive polymer, poly (3,4-Ethylenedioxythiophene)/ poly(styrenesulfonate) (PEDOT/PSS) was used in this work as an e-beam charge dissipation layer. A 30 nm layer thickness of PEDOT/PSS on the ma-N2403 resist layer can be achieved by spin coating at 5000 rpm for one minute. The thin PEDOT/PSS layer can be removed by rinsing with DI water for one minute and blow dry with nitrogen.

2.3 Summary

The UC Nanolab facility hosts a great deal of equipment covering most aspects of semiconductor device fabrication, from materials growth to device charac-

terisation. This research work is divided into two phases: mold making and replication using the imprint technique. Mold making is the major task in this research work, hence most major nanofabrication equipments were utilized in this phase, beginning with substrate preparation/cleaning and resist coating, and then pattern definition using the EBL technique. The patterns were realized after the samples were developed in an appropriate developer and then transferred onto substrate using the RIE technique. In imprinting, a manual UV-NIL tool was employed to replicate the master mold.

Quartz was chosen as the UV-NIL transparent mold because of its optical and thermal properties which are superior to the other transparent materials. A negative resist, ma-N2403 from MRT was used for 3-D patterning because the developed height/thickness is controlled by the e-beam dosages and demonstrated a linear resist contrast curve.

Electron backscattering and proximity effects are an important consideration while designing the 3-D patterns. Ormocomp and mr-UVCur06 are the imprint resists from MRT that were used in the imprint processes. Liquid and solid anti-sticking materials were evaluated in this work, however, solid permanent anti-sticking materials are preferable in the industry to avoid the wet process and evaporation of a hazardous substance. Contact angle measurement is used as a tool to estimate the surface wettability. Coating a conductive polymer of PEDOT/PSS on top of an e-beam resist will suppress the charging effects during an e-beam pattern writing on an insulating substrate.

Chapter 3

MOLD FABRICATION

The main component of NIL technology is the mold or stamp, sometimes called the template. Similar to the 1:1 mask in optical lithography, the feature size of the imprinted pattern is dependent on the mold feature size. The resolution limit is determined by resist molecular weight/size and the smallest mold structures, hence the mold fabrication is the most critical step in this technology.

Lithography is a key technique for making micro/nano structures. Currently the major challenge in lithographic technologies is to find a standard low cost and high resolution with minimum lithography steps. Generally, mold structures can be made by various means such as Electron Beam Lithography (EBL), Focused Ion Beam (FIB), X-Ray Lithography (XRL), Extreme Ultraviolet Lithography (EUVL) and many others.

In this research work, quartz was primarily used as a mold substrate because of its known properties with high UV transmission, ability to withstand high temperatures and high durability which are suitable for UV-NIL. The mold structures were made on the quartz, using an established EBL patterning and RIE pattern transfer techniques. Later these structures can be replicated for mass production using a low cost imprint technique. The EBL technique was chosen because it is a powerful tool for nanoscale fabrication owing to its high resolution pattern writing capabilities. Based on our experience in studying the silicon nitride (SiN) mold fabrication process [83], the established SiN processing was used as a bench mark for the development of the quartz fabrication

process.

The fabrication of 2-D mold structures was studied prior to the investigation of more complex 3-D mold fabrication. The baseline knowledge was developed during the investigation into making the 2-D structure, and a few fabrication methods and materials were investigated for the 2-D structure. The investigation of 3-D structure fabrication was much easier with the assistance of the developed knowledge of 2-D structure fabrication.

This work produced very encouraging results on making micro/nano structure on quartz substrates. The fabrication of 2-D structures with feature sizes below 100 nm and high aspect-ratio of up to 1:10 was demonstrated. The fabrication of 3-D profiles structures with surface roughness below 2 nm had also been demonstrated using simplified fabrication steps.

3.1 The Fabrication of Two-Dimensional Structures

Generally, the basic mold fabrication process was developed for 2-D structures. Since there is a huge vacuum of knowledge of hard-etching materials such as quartz, this work became the learning curve in understanding the underlying science and engineering of quartz processing prior to the investigation of more complicated 3-D mold fabrications.

The main objective of this study was to investigate quartz etching with a vertical profile. The goal was to fabricate 2-D mold structures with a high aspect ratio, anisotropic profile and feature sizes below 100 nm on the quartz substrate. We can find many applications using this type of structure especially in MEMS devices. The etching process was optimized and the relevant reaction mechanism was analyzed and discussed.

2-D patterns were defined using the EBL technique and the developed patterns were then transferred onto the substrate using the dry etching technique. There are two basic methods of pattern transfer: subtractive, where the pattern layer is removed from areas not protected by the mask or unexposed as illustrated in Figure 3.1(a); and additive where the film is deposited over the pattern and the

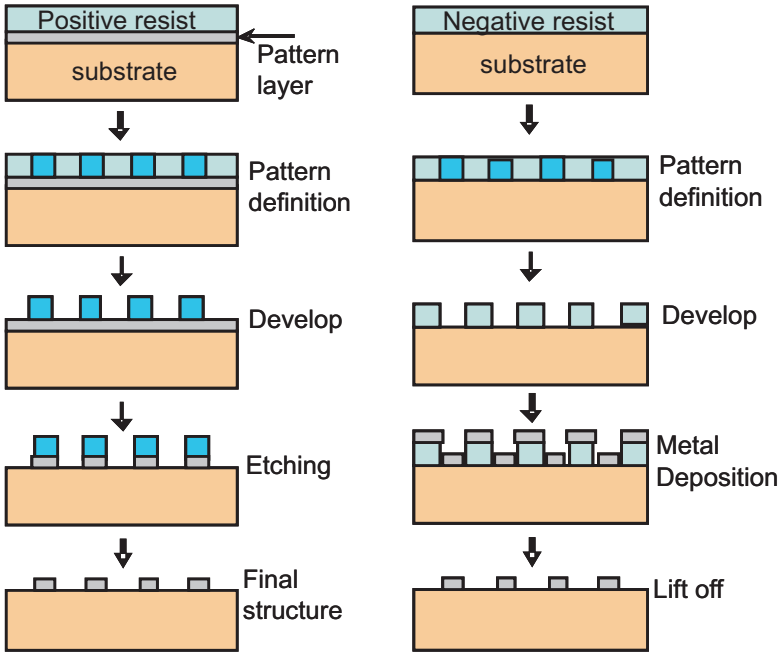

(a) subtractive (b) additive

Figure 3.1: The 2-D pattern transfer methods

resist with undesired film deposits is later removed using the lift-off method as shown in Figure 3.1(b).

For a high aspect-ratio 2-D mold fabrication, the additive pattern transfer method is the most suitable because for etching hard materials such as quartz, it requires mask material that is highly resistant to plasma etch. In this method, a 40 nm of nichrome (NiCr) was deposited as a plasma resistant mask layer using a metal evaporator. The unwanted NiCr layer above the resist was later lifted off by soaking in acetone for at least three hours.

However, the subtractive pattern transfer was suitable for use in 3-D mold fabrication for directly transferring the pattern onto the substrate. The resist and quartz substrate were etched simultaneously with optimized selectivity as described in the next section.

3.1.1 Preparation

For a basic cleaning, quartz substrates were normally cleaned using acetone, methanol and isopropyl alcohol (IPA) in an ultrasonic bath. An additional oxy-

gen plasma step to further clean the substrate surface was carried out when necessary. Figure 3.2 shows the wetting or contact angle measurement on quartz substrate at different cleaning conditions. Figure 3.2(a) shows the contact angle of 56.3^o on uncleaned quartz, meanwhile Figure 3.2(b) shows the the contact angle 50.4^o of cleaned quartz by using solvent. Figure 3.2(c) shows the contact angle of 10.7^o for quartz that was cleaned using oxygen plasma for 4 minutes. Different cleaning processes produced different wettability and the choice of the cleaning process relied on the wettability requirement for a particular application.

For patterning the 2-D structures, a positive PMMA bi-layer e-beam resist was

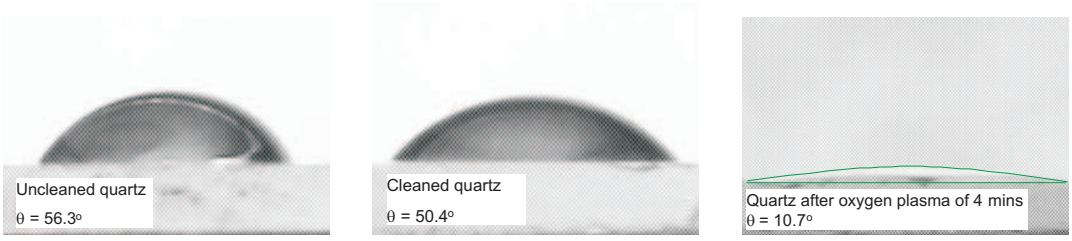

(a) Uncleaned quartz (b) Cleaned quartz with solvents (c) Cleaned quartz with oxygen plasma

Figure 3.2: The contact angle measurements on quartz substrates

used as an imaging layer because the undercut pattern profile that developed at later stage is necessary for metal deposition and lift off processes.

The 2-D patterns were designed using an off line L-Edit pattern layout software and the design files were exported into the Raith-150 EBL system in GDSII file format.

3.1.2 The Fabrication Techniques

Surface charging is the major issue for pattern writing on the insulating substrates using an EBL technique. The trapped charges on the insulating substrates surface may deflect the e-beam and cause undesired effects. A conductive layer is required to ground the trapped charges. There are several ways to reduce the charging and conduct the charge to the ground, such as thin metallic or carbon coating on top or underneath the resist layer [63].

In this work, a number of approaches were attempted for grounding the trapped charges for suppressing the surface charging effects during the 2-D patterning on the quartz substrate. Investigations into the use of the metallic coating on the substrate, the metallic coating on the PMMA resist and top coating using PEDOT/PSS methods have been carried out.

3.1.2.1 Thin Metallic Coating on Quartz Substrate

The fabrication process of the 2-D mold structure using this technique is illustrated in Figure 3.3. A cleaned quartz substrate was sputtered with 5 nm thick tungsten (W) as a charge dissipation layer using the Edward Auto500 Magnetron Sputtering system prior to the PMMA bi-layer resist coating. The thin tungsten layer was chosen because it can be stripped off easily using a short sulfur hexafluoride (SF_6) plasma at a later stage. A positive PMMA bi-layer resist was spun coated as explained in section 3.1.1. The exposed sample was then developed in a MIBK:IPA 1:3 developer at a temperature of 23^oC for 30 seconds. Short O_2 plasma is recommended for descumming the residual resist layers. A 35 nm thick NiCr was then deposited on the developed sample using a metal evaporator system. The lift-off process was carried out to remove the unwanted resist and metal layer by soaking the sample in the acetone for about three hours. A very short (10 seconds) RIE process with SF_6 gas was then utilized to remove the exposed tungsten layer. The RIE parameters of O_2 plasma for resist descumming and the removal of the tungsten layer using SF_6 are tabled in Table 3.1. Finally an RIE process with CHF_3/Ar chemistry was used to etch the quartz anisotropically. By using this technique, two metal layers (NiCr and Tungsten) were left at the top of the 2-D structure. If these structures are to be used as the 2-D imprint mold, both metallic layers might be peeled off during the imprint process, owing to the tungsten surface properties having weak adhesion to the quartz surface. This work proposed another approach to fabricate 2-D structures which will be explained next.

Table 3.1: RIE recipes for descumming the residual layer and removal of the tungsten (W) layer using SF_6 etchant

RIE parameters	Descumming of the residual resist layer	Removal of the tungsten layer
Gas	O_2	SF_6
Flow rate	50 sccm	20 sccm
Pressure	100 mTorr	100 mTorr
Temperature	295 K	313 K
RF Power	100 W	200 W
Duration	5 seconds	10 seconds

3.1.2.2 Thin Metal Coating on Top of Resist

In this method, a thin metal layer is deposited on top of the resist as a charge dissipation layer. Firstly, a cleaned quartz substrate was spun coated with a PMMA bi-layer as described in section 3.1.1. A 20 nm thick aluminium (Al) layer was deposited on top of the PMMA resist using a metal evaporator or sputtering system. Aluminium was chosen because this light material is easy to remove using an acidic solution of aluminium etcher (Appendix B) at a later stage. A thickness range from 20 nm to 30 nm is the optimum thickness because the e-beam can easily penetrate the aluminium layer without significant backscattering. However, very low to no conductivity was observed on the thin aluminium layer of less than 20 nm thickness and an aluminium layer thickness of more than 30 nm may affect the e-beam penetration through the layer and could be more difficult to fully remove at a later stage.

The fabrication process of the 2-D mold structure using a conductive top coating method is illustrated in Figure 3.4. After an e-beam exposure, the sample was soaked in aluminium etcher for at least 30 seconds or until the metal layer was etched away completely. The sample was then cleaned with deionised water (DIW) rinsing and blown dry with nitrogen. The sample was then developed in MIBK:IPA 1:3 which was used as a developer for the PMMA bi-layer to realize the exposed 2-D pattern.

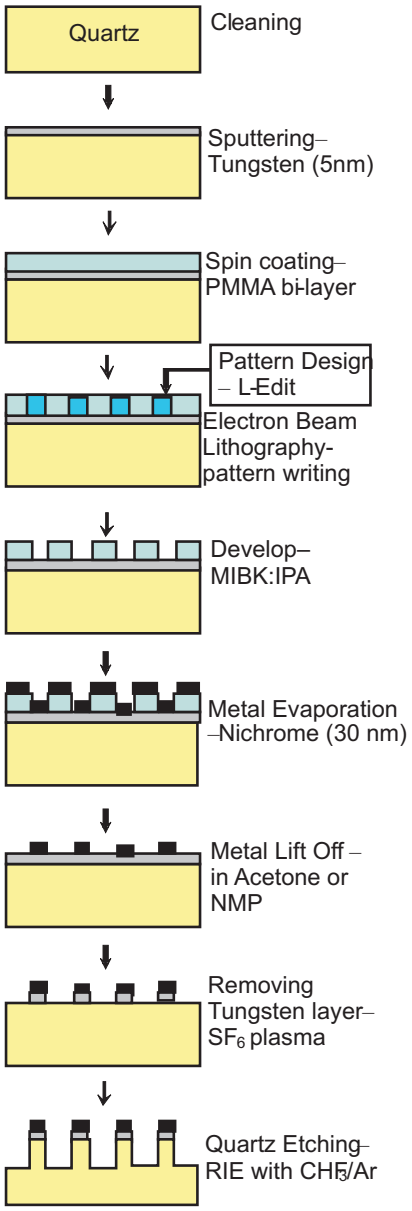

Figure 3.3: The fabrication of 2-D structures on quartz substrate using a common method of depositing a thin metal layer on the substrate

Short O_2 plasma is recommended for descumming the residual resist layers. A 35 nm thick NiCr was then deposited on the developed sample using a metal evaporator system. The lift-off process was carried out to remove the unwanted resist and metal layer by soaking the sample in the acetone for about three hours. Finally a RIE process with CHF_3/Ar chemistry was used to etch the quartz anisotropically.

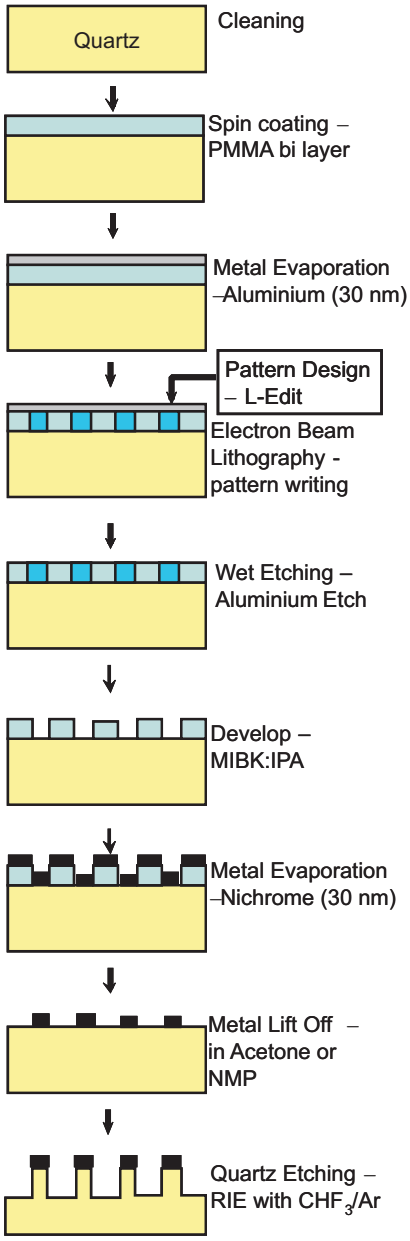

Figure 3.4: The fabrication of 2-D structures on quartz substrate using metal coating on top of the resist layer

3.1.2.3 Conductive Polymer Coating on Top of Resist

Removing a metal layer completely from a resist surface is quite a difficult task especially a thick metal layer. Incomplete removal of the metal layer may prevent the developer from dissolving the patterned resist. One attractive option is for the charge dissipation metal layer to be replaced by a water soluble conductive polymer [86] such as Poly(3,4-ethylenedioxythiophene) poly(styrenesulfonate) (PEDOT/PSS). The fabrication method by applying a conductive polymer layer as a charge dissipation layer is illustrated in Figure 3.5.

In this work, PEDOT/PSS was spun coated on the top of PMMA bi-layer resist at a spinning speed of 5000 rpm for one minute to achieve a 30 nm layer thickness. The only issue with PMMA bi-layer resist was that its hydrophobic surface caused great difficulties for the watery solution to adhere to its surface. An average contact/wetting angle of 70.3^o was measured on the PMMA bi-layer surface as shown in Figure 3.6(a). One well-known method of reducing the hydrophobicity or in other words, increasing the wettability of the PMMA surface is by O_2 plasma surface treatment. Table 3.2 shows the recipe used for O_2 plasma surface treatment.

A very short oxygen plasma was needed to improve the wettability of the PMMA surface. Too long oxygen plasma may harden the PMMA surface causing great difficulties in developing the exposed pattern at a later stage. Too high wettability may prevent the removal of the PEDOT/PSS layer from the PMMA surface at a later stage.

Figure 3.6(b) shows a contact angle measurement on the PMMA bi-layer surface that was treated using oxygen plasma. An average contact angle of 39.9^o was measured showing that the treated PMMA surface has improved its surface wettability as compared to the untreated PMMA surface.

The unexposed PEDOT/PSS layer can be removed by rinsing with DIW at room temperatures for about a minute. But removing the e-beam exposed PEDOT/PSS layer, especially for feature sizes of more than 500 nm was quite difficult. The electron bombardment especially by high energy e-beam, high dosage and large pattern area, diffused part of the PEDOT/PSS molecules into the PMMA surface which made its removal quite troublesome. Figure 3.7 shows

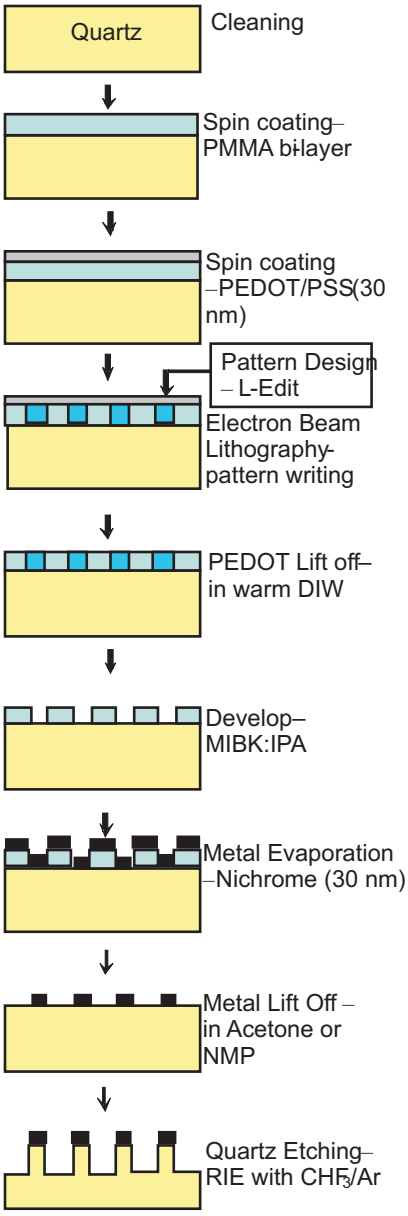

Figure 3.5: The fabrication of 2-D structures on quartz substrate using conductive polymer (PEDOT/PSS) coating on top of the resist.

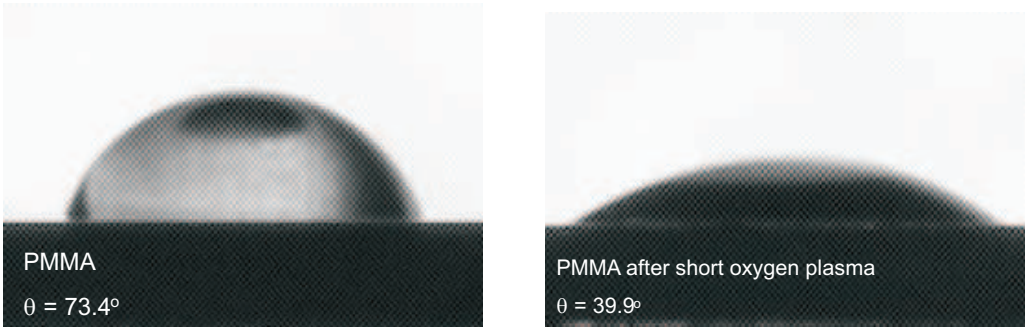

(a) wetting on untreated PMMA (b) wetting on treated PMMA

Figure 3.6: Optical images of the contact angle measurement on PMMA surfaces

Table 3.2: The recipe of O_2 plasma surface treatment on the PMMA surface

RIE parameters	Surface treatment
Gas	O_2
Flow rate	50 sccm
Pressure	100 mTorr
Temperature	295 K
RF Power	100 W
Duration	2 seconds

two optical images of an exposed PEDOT/PSS pattern of one micron feature size that was not removed completely after soaking in a warm DIW for five minutes. The larger the feature size or exposed area, the harder it was to remove them. If this happened, we adopted a method to remove the e-beam exposed PEDOT/PSS layer by using a combination of 45^oC warm DIW with a periodic ultrasonic bath of two seconds every two minutes until clear. However, a long and continuous ultrasonic bath in a warm DIW may ruin the PMMA pattern.

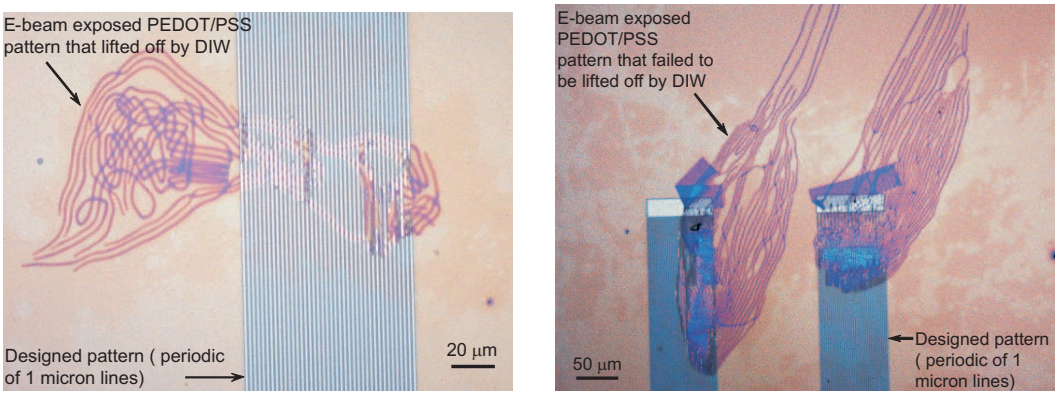

(a) (b)

Figure 3.7: Optical images of incomplete removal of an e-beam exposed PEDOT/PSS layer using DIW on PMMA resist with a feature size of about 1 micron

3.1.3 Pattern Definition using EBL

2-D patterns were designed in off line L-Edit software and the design files were exported to a Raith-150 EBL system in a GDSII file format. L-Edit is an electronic circuit pattern layout software that is only capable of handling rectangle shapes for its layout design. Other shapes such as circles and curvature designs were created using other drawing software or by using Raith software itself.
For exposing an e-beam on a generic 2-D pattern with feature sizes more than 100 nm, voltage acceleration of 10 keV, an aperture of 30 microns and e-beam dosage of 110 $\mu C/cm^2$ are normally used for patterning on the PMMA bi-layer resist. To achieve a finer pattern, higher voltage acceleration and a smaller aperture were used in order to minimize the proximity and back scattering effects. Table 3.3 shows the EBL parameters used in this work for a fine 2-D pattern of feature sizes below 100 nm.

The exposed sample was then developed in MIBK:IPA 1:3 at a temperature

Table 3.3: EBL parameters for defining a fine 2-D pattern on PMMA resist

EBL parameters	setting
Voltage acceleration	20 keV
Aperture	20 microns
Area Dosage	140 $\mu C/cm^2$
Area step size	24 nm

of 23^oC for 30 seconds. A short oxygen plasma was normally performed to remove the residual resist. A 15 seconds of 100 W oxygen plasma should be enough to clear the residual resist of 10 to 20 nm thick for 100 nm features, however, longer oxygen plasma may enlarge the feature sizes. Figure 3.8 shows an AFM image of the developed pattern on a PMMA bi-layer resist with a feature size of 60 nm.

For minimizing the proximity effects on the exposed 2-D patterns, the proximity correction features in the Raith-150 EBL system have been activated. In this software patch, the exposures are simulated and the proximity effects are estimated. The 2-D patterns are reconstructed based on the proximity correction

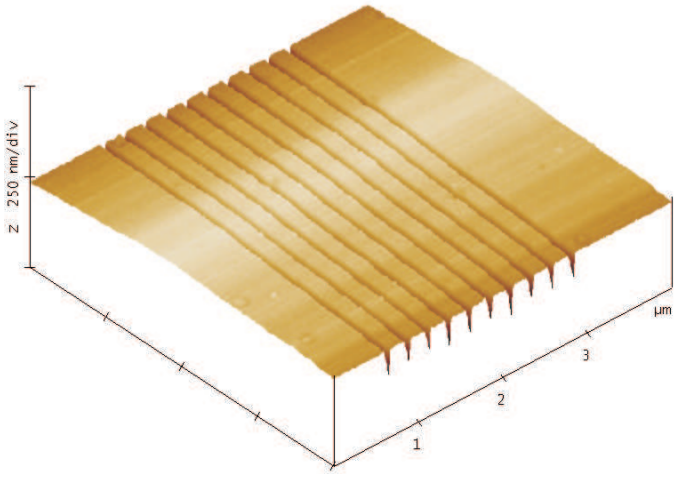

Figure 3.8: AFM image of the developed 2-D pattern of 60 nm lines on PMMA bilayer resist.

estimation as explained in section 2.1.1. In conjunction with charge suppression techniques, the successful 2-D profiles were obtained.

3.1.4 The 2-D Pattern Transfer

In this work, we investigated the pattern transfer process using the RIE technique for making vertical profiles and high aspect ratio structures on a quartz substrate. The etching process parameters such as pressure, temperature, and RF power were optimized and the relevant reaction mechanism in plasma etching such as etching chemistry was analyzed. RIE was carried out using a Plasmalab 80^{plus} of Oxford Instruments RIE system, and a 100 mm diameter silicon wafer with a thick NiCr coated layer was clamped physically onto the power electrode as a sacrificial electrode masking layer. The electrical power was supplied to the electrode at a radio frequency (RF) of 13.56 MHz to produce plasma discharge. Plasma is a gas which contains equal numbers of positive and negative charges; neutral atoms, radicals, or molecules; and a gas of emitted photons [87].

There are only a few etchant gases that can be used for quartz etching [88] and generally the fluorinated gases such as CF_4 and SF_6 based chemistries are used because of their high F content. Other fluorohydrocarbons such as CH_2F_2 and

CHF_3 have lower etch rates owing to a lower F/C ratio. In this work, a trifluoromethane (CHF_3 or Freon 23, sometimes called Halocarbon 23) was used as the main processing gas owing to its moderate F/C ratio resulting in a moderate etch rate which is essential in controlling the etched profiles. It is a popular etchant gas in semiconductor industries and extensive studies have been carried out previously on the RIE of silicon nitride [81].

Table 3.4 shows the optimized RIE parameters used in 2-D deep quartz etching. For etching the narrow high aspect-ratio structures, there were limited ions and neutral transport present within the trench which limited the chemical reaction, hence, large aspect ratio and dense structures were etched more slowly than low aspect ratio structures [75].

Oxide such as silicon dioxide (quartz) etching using CHF_3 etchant can only take place for RF bias values above 55 V at 1 mTorr etching pressure [89]. A higher RF bias values are required for quartz etching if operating at a higher etching pressure.

An additive inert gas argon (Ar) was added to stabilize plasmas and also to add

Table 3.4: RIE recipe for etching 2-D structures on quartz substrate

RIE parameters	2-D Quartz Etching
Gases	CHF_3/Ar
Flow rate	50/30 sccm
Pressure	$<$ 30 mTorr
Temperature	295 K
RF Power	200 W
RF Bias voltage	-330 V
Etching rate	10 to 15 nm/min

inert ion bombardment of a surface, resulting in more directional or anisotropic etching [88] for a steep sidewall profile. There were two steps involved in the CHF_3/Ar RIE plasma process. Firstly the bombardment of heavy inert ions of argon mechanically breaks the bond of the substrate elements (Si-O). Si-O bonds are very strong and could only be dissociated by high energy plasma bombardment using heavy inert ions such as Argon. Then ion-induced chemi-

cal reaction at horizontal surface created the etching products. The combination of these actions resulted in highly selective anisotropic etching of the substrate material. To achieve a vertical sidewall of the 2-D structures, an anisotropic etching process condition was essential.

As the etching pressures used in this work are very low $(< 30mTorr)$, physical bombardment reactions are expected to dominate and less chemical reactions are involved in the etching process. At very low process pressure (refer to Figure 2.13), to the right, at the border of ion milling process, the reactions are no longer an ideal RIE process. The majority of erosion processes are carried out by physical bombardments and the erosion products react with plasma species to create volatile and other etching products. We discuss the chemical reactions next.

3.1.4.1 Etching Chemistry

Plasma discharges are very complex entities and can be very difficult to understand. In a fluorine-containing plasma, surface reactions, etching, and polymerization can occur at the same time. The domination of certain reactions is dependent on the gas feed, the operating parameters and the chemical nature of the polymer/substrate and electrode [90]. In a quartz etching process using CHF_3 etchant, the free fluorine radicals, F^* are created by the plasma discharge and the etching chemistries could be described as follows;

$$e^- + CHF_3 \rightarrow CHF_2^+ + F^* + radicals(e.g. CF_x) + 2e^- \tag{3.1}$$

$$SiO_2 + xF^* \rightarrow SiF_x + O_2 \tag{3.2}$$

$$CF_x radicals + 2O_2 \rightarrow CO + CO_2 + COF_2 \tag{3.3}$$

F^* is the reactive fluorine atom and SiO_2 is the quartz.

Figure 3.9(a) shows the etching mechanism for etching quartz using the CHF_3/Ar chemistry. RIE plasma generates the reactive fluorine atom F^* from the supplied CHF_3 gas (Eqn 3.1). The bombardment of Argon ions break the the Si-O bonds and then the dissociated silicon ions react with F free radicals to form a SiF_x (Eqn 3.2).

The CF_x radicals tend to deposit polymer films on all surfaces, but the oxygen liberated in the etching of quartz reacts with CF_x radicals to form volatile CO, CO_2, and COF_2 (Eqn 3.3). Thus, both F and C are consumed but the polymer deposition releases the F atom which enriches the fluorine content hence, increasing the F/C ratio [91].

The surface model for SiO_2 etching in fluorocarbon which developed by Gogolides and co-workers [92] has demonstrated that the polymer deposition of CF_x is a strong function of ion energy, ion type, F flux and carbonaceous neutrals flux. The polymer deposition regime can be shifted to etching regime with the change of these combinations [93].

When the F concentration in the plasma is high, the CF_x radicals are destroyed by recombination at the various surface of the plasma reactor and probably leads to re-creation of volatile CF_4. When the F concentration is low, surface production mechanism dominates the production of CF_2 which leads to the formation of a polymer layer at the surface (polymerization) [94]. For etching purpose, the F content in the plasma should be increased.

It is worth noting that during the plasma etching where polymer deposition enriched the fluorine content of the gas phase species of F/C and continuous ion bombardment of the surface in contact with a plasma has resulted in increasing the sample surface temperature with the process time.

In anisotropic etching, vertical sidewalls are the location where chemical reaction less occur and are not exposed to ion bombardment, hence polymerization will build up on these locations. This process is called sidewall passivation which undercut etchings are prevented and steep sidewall profiles are realized. Figure 3.9(b) shows the schematic of CF_x sidewall passivation formation during the etching process.

Figure 3.10 shows an SEM image of a pillar structure that was accidently constructed when a hard particle of etching product dropped on the substrate and acted as a nanomask in the 2-D etching process. The sidewall passivation layer where the CF_x was deposited on the vertical wall can be observed. The concentration of plasma near the sidewall formation caused the formation of a deep trench at the bottom of the structure. This occurred at operating pressure below

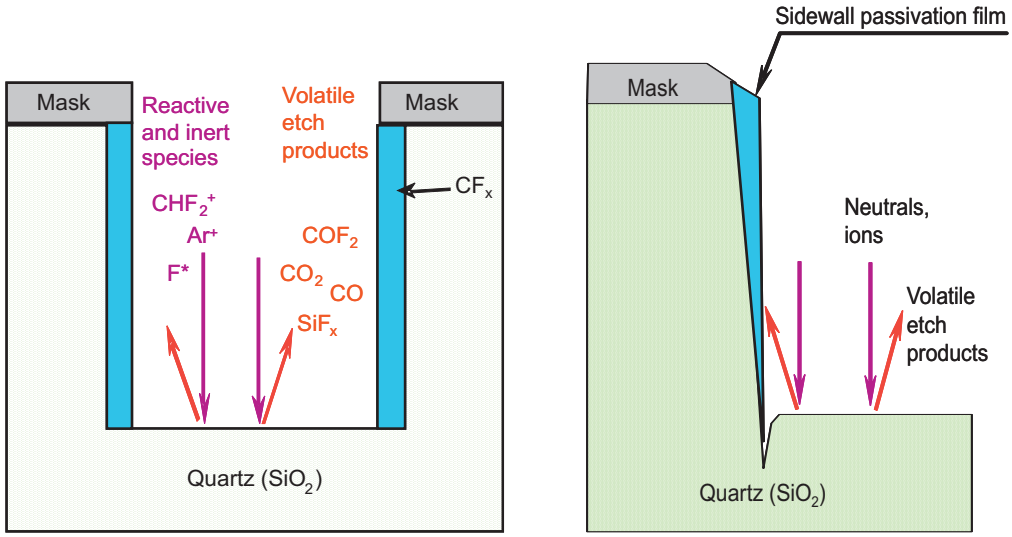

(a) The CHF_3/Ar etching mechanism

(b) Side wall passivation during anisotropic etching

Figure 3.9: Schematic of RIE mechanism for a 2-D structure

30 mTorr. Further explanation will be presented in section 3.2.3.1.

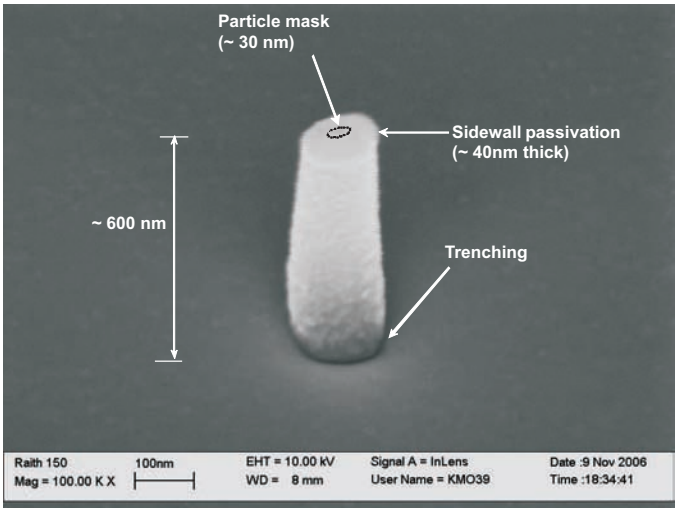

Figure 3.10: SEM image of a pillar showing sidewall passivation and trenching effects at the bottom of the structure when operating pressures are below 30 mTorr.

3.1.4.2 Etching Analysis

It is well known that polymer deposition rates decrease as the surface temperature is increased [91] also the temperature of surfaces in contact with plasma increases with process time. When the surfaces heat up, the F/C ratio could

decrease to the point where the quartz etching actually stops [95].

Figure 3.11(a) shows an SEM image of a 2-D lines structure on a quartz substrate with dimensions of 70 nm in width, 210 nm spacing and 160 nm in height, which represents a large trench structure (trenches with small aspect-ratios). This structure was fabricated using the initial RIE recipe as tabled in Table 3.4. The sample was etched for a continuous one hour until the etching had reached the 'stop etching' conditions caused by the depleting fluorine atoms (so called loading effects) and heated up surfaces. The etching rate as well as the sidewall passivation decreased over time. As a result, an 80 to 85 degree angle of sidewall was formed instead of a vertical sidewall.

Figure 3.11(b) shows an SEM image of 2-D 150 nm line structures on a quartz substrate where the dimensions of the lines were 70 nm in width, 70 nm spacing and 160 nm in height. This represents a narrow trenches structure (trenches with high aspect-ratios). This structure was on a similar substrate as in the previous figure which had gone through a similar etching process. The narrow trenches were not uniformly etched where it shows a huge variation in trenches depth and width.

Aspect ratio dependent etching (i.e. variation in etch rate with aspect ratio) is

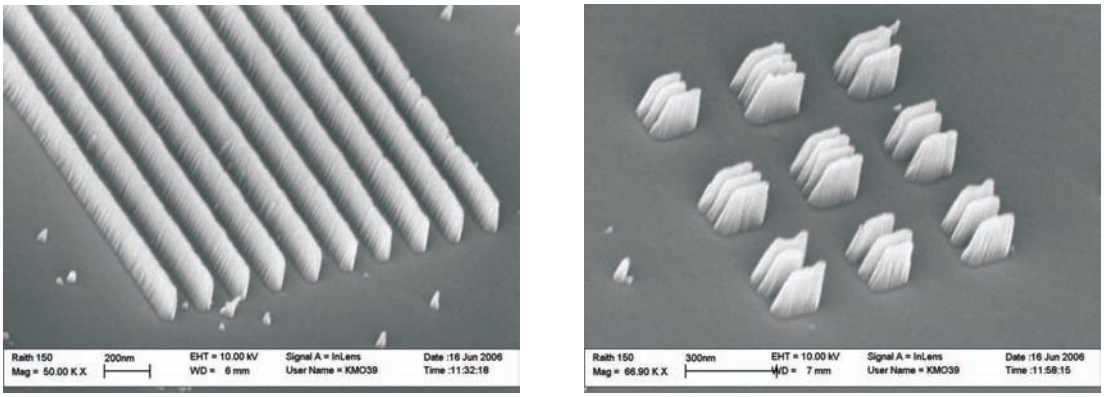

(a) Deep RIE on a 2-D line structure with large trenches

(b) Deep RIE on a 2-D structure with narrow trenches

Figure 3.11: SEM images of a few results of continuous deep RIE on quartz substrate. Structure heights are about 150 nm and about 80 to 85 degrees of vertical angle.

often observed in deep silicon trench etching [75]. A similar observation applies to quartz etching. Trenches with large aspect ratios are etched more slowly than

trenches with a small aspect ratio as expected/mentioned before.

To achieve high aspect ratio structures and close to 90^o profile, a number of actions have been followed/implemented. These include reducing the process pressure to increase the anisotropic etching as well as to improve the transport of etching products away from the trenches by the enlarged voltage-bias. The decrease in F/C ratio which leads to the 'stop etch' conditions can be avoided or minimized by etching in a short interval of time and repeating the cycle after the samples have cooled down.

In this experiment, the process pressure was reduced to 20 mTorr and etching cycles of 15 minutes plasma etching with 5 minutes cooling interval have improved the results as displayed in Figure 3.12. Figure 3.12(a) shows the SEM image of 60 nm lines structure with 600 nm height and 120 nm spacing and Figure 3.12(b) shows the SEM image of 90 nm lines structure with 600 nm in height and 180 nm spacing. This etching method of quartz substrate has achieved a 2-D high aspect-ratio structure of about 10:1 and a vertical sidewall angle of almost 90^o.

Figure 3.13 shows SEM image of 2-D structure on quartz substrate. Figure

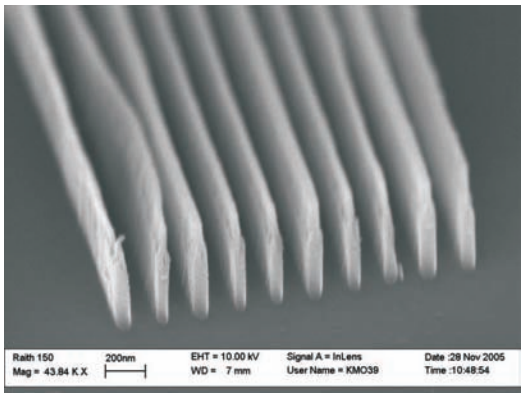

(a) 60 nm lines structure with 600 nm height and 120 nm spacing

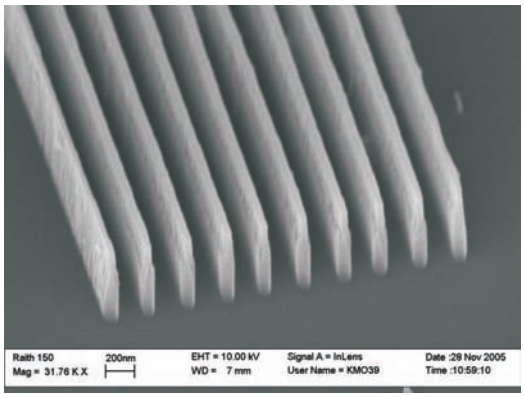

(b) 90 nm lines structure with 600 nm in height and 180 nm spacing

Figure 3.12: SEM images of the fabricated 2-D high aspect-ratio structures on quartz substrate.

3.13(a) shows the comparison of 50 nm and 70 nm line widths after the etching process. Features of 50 nm and below failed to preserve the flat top surface compared to 70 nm features because of an uneven and thin NiCr mask layer. Figure 3.13(b) shows other 60 nm structures such as parallel lines, corner lines

and transistor-like structures that are able to preserve the flat top profile after heavy deep etching process.

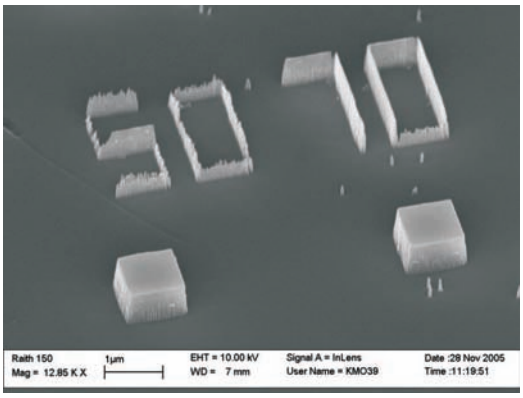

(a) 50 nm and 70 nm features on quartz substrate

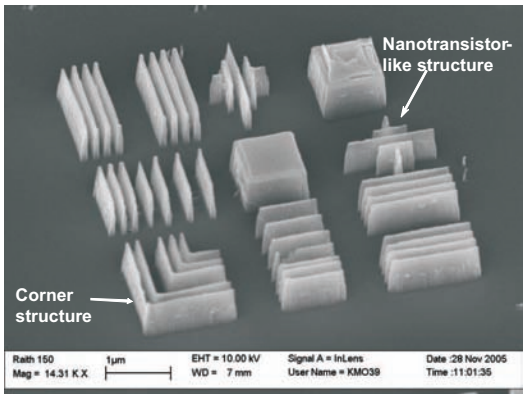

(b) Other 60 nm features on quartz substrate

Figure 3.13: SEM images of the fabricated 2-D structures on quartz substrate

The etching selectivity of Chromium (Cr) or NiCr to quartz is about 18:1 [96]. Hence, the samples require a NiCr masking layer of at least 35 nm thick to mask the 2-D pattern structures to achieve a 600 nm structure height. However, it was difficult to deposit a NiCr layer of more than 30 nm for feature sizes below 50 nm on the PMMA bi-layer resist for lift-off as illustrated in Figure 3.14(a). The metal deposition directed to the substrate surface was blocked by the deposition on the edge of the pattern trench (shadowing effects). Figure 3.14(b) shows the SEM image of NiCr deposition on 20 nm lines. Features at below 50 nm can be achieved but metal deposition is unable to achieve the required layer thickness of more than 35 nm as expected. It could be improved by using a thinner resits layer and special developer designed for less than 50 nm feature sizes.

Figure 3.15 shows another result of the smallest feature of a 40 nm line when etched with similar RIE parameters. The 40 nm line feature failed to preserve the flat top surface as compared to 60 nm features because of an uneven and insufficient thickness of NiCr mask layer as explained earlier.
All SEM images were captured when using accelerating voltage of 10keV and

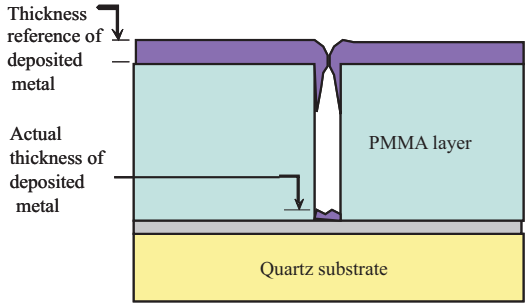

(a) schematic of metal deposition on PMMA bi-layer resist pattern

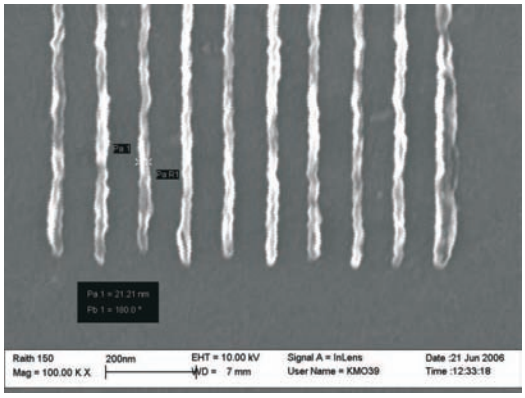

(b) SEM image of an uneven layer thickness of deposited NiCr on quartz substrate

Figure 3.14: Issue of metal deposition on a feature size below 50 nm using PMMA bi-layer resist

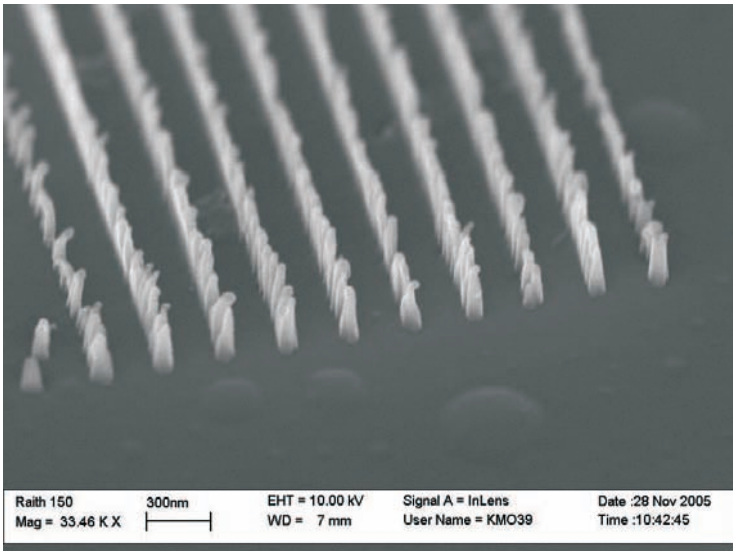

Figure 3.15: SEM image of the etched 40 nm feature on quartz substrate which failed to preserve the flat top profile.

30 μm aperture size causing some blurred background image. To improve the sharpness of the SEM image background, a smaller aperture size should be used in order to increase the depth of focus [65].

3.2 The Fabrication of Three-Dimensional Structures

The 3-D mold fabrication was the actual aim of this research work. The 2-D mold fabrication was used as a platform in understanding the basic science and engineering of mold fabrication. The focus of this work was to develop a 3-D profile on negative photoresist and then directly transfer the pattern using a single-step RIE plasma. The 3-D geometrical shapes such as pyramid, hemisphere, cone and other complex shapes were investigated. These 3-D structures can be found in many applications especially in optical devices.

For a 3-D structure, a subtractive pattern transfer method was employed because the 3-D patterns have to be directly transferred onto the mold substrate in a single-step RIE process to simplify the mold making process. A negative photoresist was employed as a 3-D imaging and masking layer.

Since the 3-D mold fabrication requires direct pattern transfer from mask to substrate, depositing a thin metal coating on the substrate-resist interface as a charge dissipation/grounding layer was not possible. Depositing a thin metal layer on top of the negative resist surface as a charge dissipation/grounding layer was also ruled out. Acidic solution used to remove the thin metal layer prior to pattern development process caused crosslinking with negative resist surface [97, 98]. Hence, no development process would be possible. New fabrication methods have been used by the present work in order to suppress the surface charging during the 3-D pattern writing on insulating substrates using the EBL.

3.2.1 Preparation

The 3-D pattern layout was designed using EBL Raith-150 pattern layout software where the single pass line (SPL) writing scheme was used as explained in section 2.3.2. Figure 3.16(a) shows an example of a writing scheme for a hemispherical shape. Every SPL path/route was assigned with an individual dosage which was defined through the optimisation process. The spacing between lines is about 20 nm to 30 nm. The developed profile is a result of the combi-

nation of proximity effects, back scattering and e-beam dosages. To achieve the desired profile, a trial and error method was employed to change the e-beam dosages and it took a number experimental cycles to satisfy the profiles. Figure 3.16(b) shows another example of a writing scheme for a pyramid profile with a similar method.

The negative tone photoresist from Microresist technology, ma-N2403 was

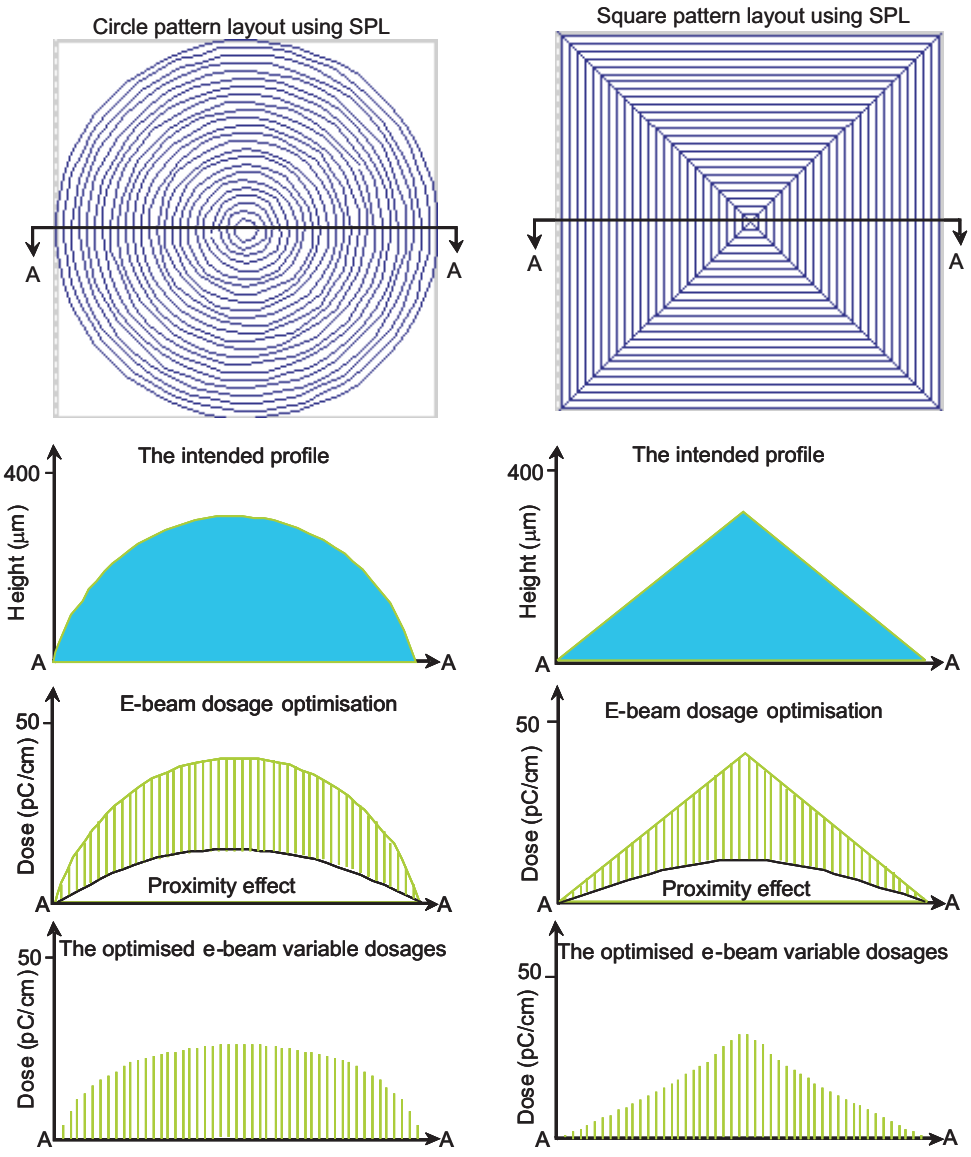

(a) The 3-D hemispherical shape (b) The 3-D pyramid shape

Figure 3.16: The SPL writing scheme for 3-D patterns

spun coated on a cleaned quartz substrate at 3000 rpm for 30 seconds and pre-baked in an oven at a temperature of 95^oC for 30 minutes to achieve a 600 nm layer thickness.

3.2.2 Fabrication Techniques

As mentioned earlier, surface charging is the major challenge in patterning on insulating substrate such as quartz and it is even more difficult for 3-D patterning. Surface charging trapped near the insulating surfaces causes great difficulties in focusing the e-beam onto the resist surface and the unbalanced surface potential of the resist deflects the beam and causes severe pattern distortion [99].

Two fabrication approaches were developed. The first approach is an application of e-beam at low accelerating voltages (low keV). The use of low keV leads to reduced beam interaction volume as illustrated in Figure 3.17. The penetration depth of the electrons into insulating materials/substrates is much less than higher keV electrons. Based on this approach a 3-D fabrication method called called Critical Energy (CE) or Accelerating Voltage method was developed and followed. In the CE method as illustrated in Figure 3.18(a), a variable controlled e-beam dosages at an optimised low accelerating voltage is employed in 3-D pattern writing on a negative resist using EBL. The developed pattern is then used as a masking layer in a single-step RIE pattern transfer onto quartz substrate.

The second approach is an application of high accelerating voltages (high en-

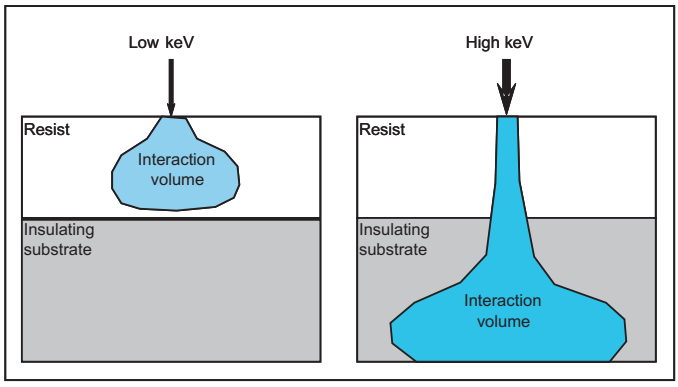

Figure 3.17: Schematic diagram of e-beam interaction volumes of low keV as compared to high keV

ergy/keV) in conjunction with top conductive coatings. The use of high keV will produce a greater penetration depth and reduce the number of back scattered electrons which will result in a more confined beam size. Based on this

approach, a Top Conductive layer method (TC) was developed and followed in this work. In the TC method as illustrated in Figure 3.18(b), a water soluble conductive polymer, PEDOT/PSS is spun coated on the negative resist as a charge dissipation layer prior to the 3-D pattern writing. A high accelerating voltage that provides a more confined e-beam and less backscattering and proximity effects is used in exposing the 3-D pattern on a negative resist using EBL. Finally the developed pattern is used as a masking layer in a single-step RIE pattern transfer process.

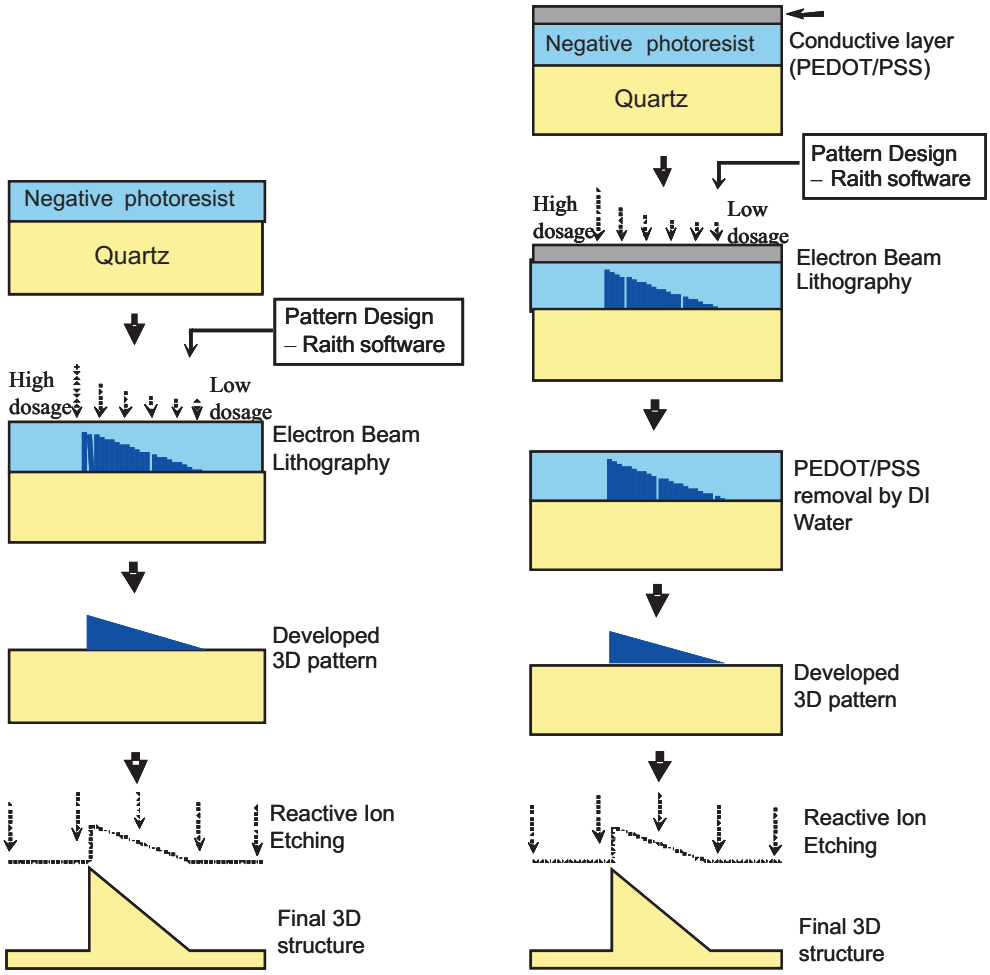

(a) The critical energy method (b) The conductive polymer method

Figure 3.18: The fabrication process flow options for fabricating the 3-D structures on insulating substrates

3.2.2.1 The Critical Energy or Critical Accelerating Voltage

Many insulating materials often have points where they reach equilibrium. This equilibrium is the point where the charge into the sample material equals to the charge out of the sample. The charge out of the sample will be from secondary electrons (SE), backscattering electrons (BSE), Auger electrons, x-ray and whatever current is absorbed and then transmitted through the sample to the ground. This is referred to as a state of unity [100]. It can be described as in Figure 3.19 where the critical energy assumes a neutral charge at points E1 and E2 as suggested by Jaebum Joo and co-workers [99]. At high accelerating voltages (energy), an e-beam negatively charges the insulating substrates but at very low accelerating voltages the surface can actually charged positive when more electrons are scattered or ejected from the surface than are stored in the insulating substrates itself. Polarity of charging is dependent on the e-beam configuration.

To estimate the range of suitable low energy for writing a 3-D pattern on non-

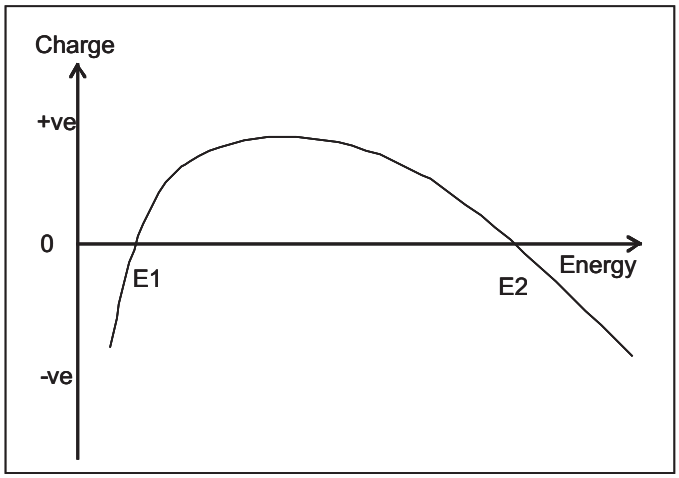

Figure 3.19: Schematic diagram of critical energy [99]

conductive substrates, Monte Carlo simulation using CASINO software [101] was employed. Figure 3.20 illustrates the 200-electron trajectories simulation of electron beams with accelerating voltages of 4.5, 5.5, 6.5 and 20 keV. In these simulations the e-beams were exposed onto 600 nm thickness of ma-N2403 resist layer coated on quartz substrate.

The volume of electrons interaction increases when the e-beam accelerating

voltage increases. At accelerating voltage of 4.5 keV as illustrated in Figure 3.20(a), the penetration depth of electron trajectories is far from reaching the quartz substrate surface. The volume of crosslinked negative resist after the e-beam exposure is not attached/linked to the quartz surface and will be washed away in the developing process at a later stage.

Further simulations were carried out to find a suitable/critical accelerating voltage that will crosslink resist down to the quartz surface and neutrally charge the resist. The observation from simulation shows that most of the electron trajectories settled at about 85 % of the longest vertical distance. For example, as illustrated in Figure 3.20(b), the penetration depth of 5.5 keV accelerating voltage was estimated at approximately 550 nm which is less than the resist thickness (600 nm). At this condition, the resist surface could be positively charged.

After further simulation at an accelerating voltage of 6.5 keV as illustrated in Figure 3.20(c), the penetration depth is estimated at approximately 660 nm which is larger than the resist thickness of 600nm. At this condition, the resist surface could be negatively charged. Based on this analysis, the critical e-beam accelerating voltage for a 600 nm thickness of ma-N2403 resist on quartz substrate is in the range of 5.5 to 6.5 keV. This is the method used as an estimation in finding the critical e-beam accelerating voltage that assumes a neutral charge for certain resist thicknesses. An accelerating voltage of 6.25 keV is estimated for a 600 nm resist thickness.

Figure 3.20(d) shows the simulation of electrons trajectories when a high accelerating voltage of 20 keV is exposed on the sample. A very deep penetration, more confined trajectories, less electrons backscattering and less proximity effects are observed. Electron trajectories are dependent on the medium properties such as density and elements composition. This is a useful guide for patterning smaller and higher density patterns which will be discussed in the next section.

Charging comes in several species often exhibiting several characteristics, either positive or negative charging. When the sample is charged positively, the image will appear dark and when there is a negative charge, the image will appear bright [100].

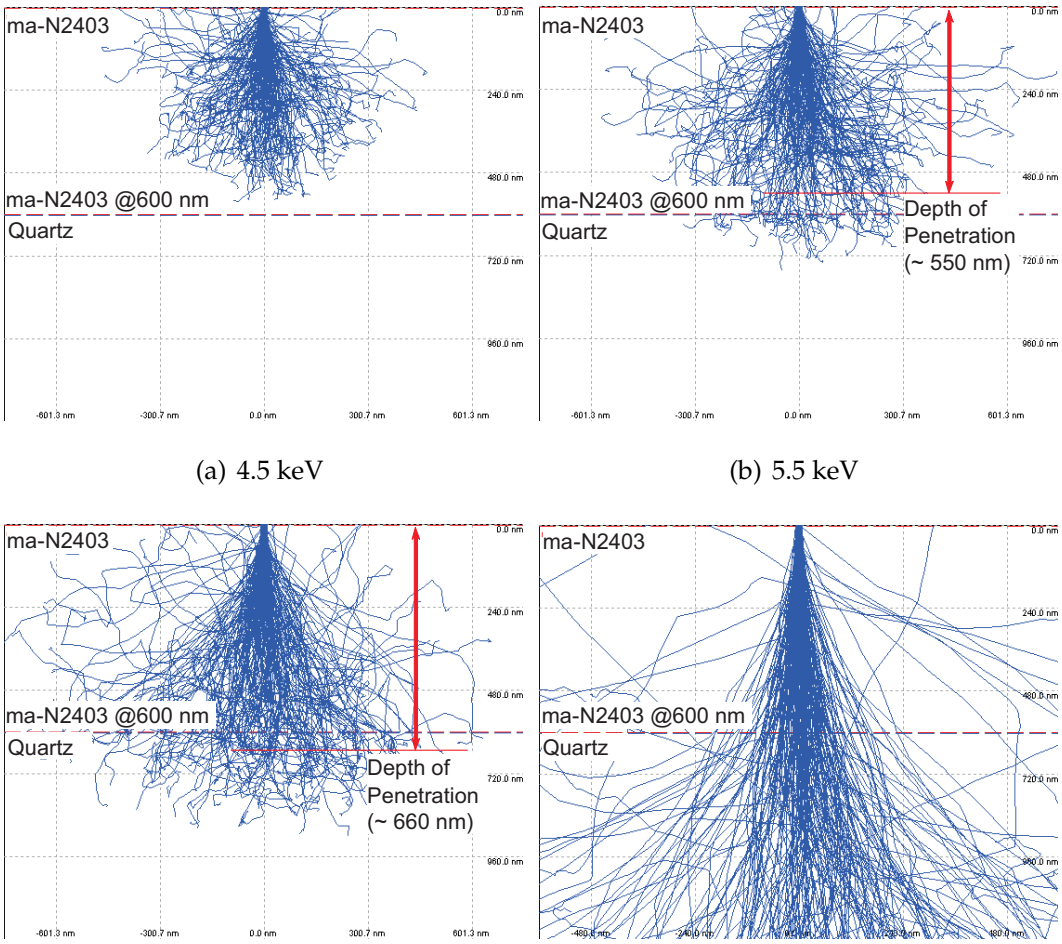

(a) 4.5 keV (b) 5.5 keV

(c) 6.5 keV (d) 20.0 keV

Figure 3.20: Electron trajectories of various e-beam acceleration voltages across a 600 nm thick ma-N2403 resist layer and quartz substrate by employing Monte Carlo simulation using CASINO software.

Further experiments were carried out on a range of ma-N2403 resist layer thicknesses (350 nm to 800 nm) using a Raith-150 EBL tool. The actual critical energy values were determined by gradually increasing the accelerating voltage from the lowest values as estimated by Monte Carlo simulation. To find an optimized or critical accelerating voltage that leaves no charging marks on the zoomed SEM image, magnification images of between 200X and 500X magnifications were then zoomed in and out for each accelerating voltage increments.
Figure 3.21 shows the critical energy with respect to the resist thicknesses that was estimated by the Monte Carlo simulations as compared to the experimental results. There were no significant differences between them and they could be used as a guideline for e-beam exposure at any resist thickness.

As discussed earlier, in this work, the e-beam voltage acceleration of 6.25 keV

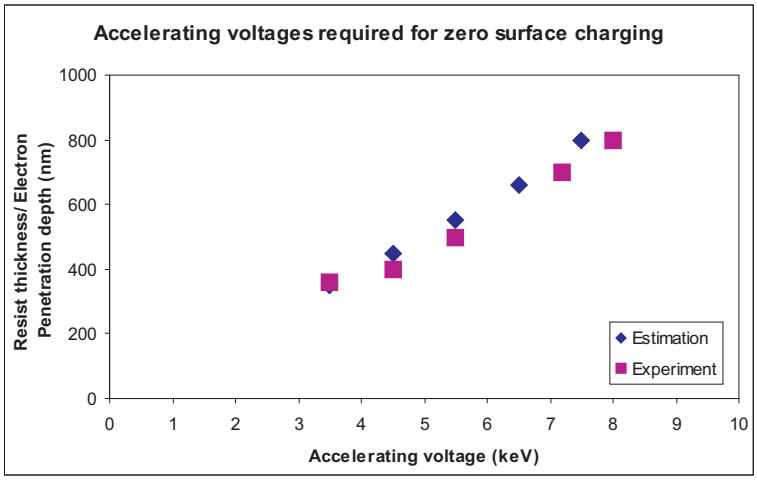

Figure 3.21: Accelerating voltages required for zero surface charging in various resist thickness compared to the estimated penetration depth at those voltages.

has been used for the 3-D patterning on the 600 nm thick ma-N2403 resist. The SPL pattern writing scheme was utilized for 3-D patterning with a line dosage ranging from 0.6 to 42.0 pC/cm. The examples of SPL pattern writing scheme for 3-D structures have been explained in section 3.2.1. After the e-beam exposure, the samples were developed in Microresist ma-D532 developer for 15 seconds at a temperature of 20^oC.

Figure 3.22(a) shows the AFM image of the developed 3-D rings test pattern on a ma-N2403 resist. This test pattern has three 3-D shaped structures. The first is the centre lens shape of 3 microns in diameter and 300 nm on its highest point. The second is the middle 3-D ring, which is 5 microns in inner diameter and 9 microns in outer diameter with a ramp down profile from the highest point of 300 nm at its inner diameter and zero at its outer diameter. The third(outmost) 3-D ring structure which is 11 microns in inner diameter and 13 microns in outer diameter with a ramp down profile from the highest point of 300 nm at its inner diameter and zero at its outer diameter. The study of this test pattern has the potential application for micro Fresnel lens fabrication.

Figure 3.22(b) shows another AFM image of the developed 3-D pyramid with a multilevel array test pattern on a ma-N2403 resist. Each outer pyramid has a one micron square base and is 300 nm in height. There are four similar pyra-

mids in the center but at an elevated level of 300 nm.

No proximity correction feature is available for writing 3-D patterns using

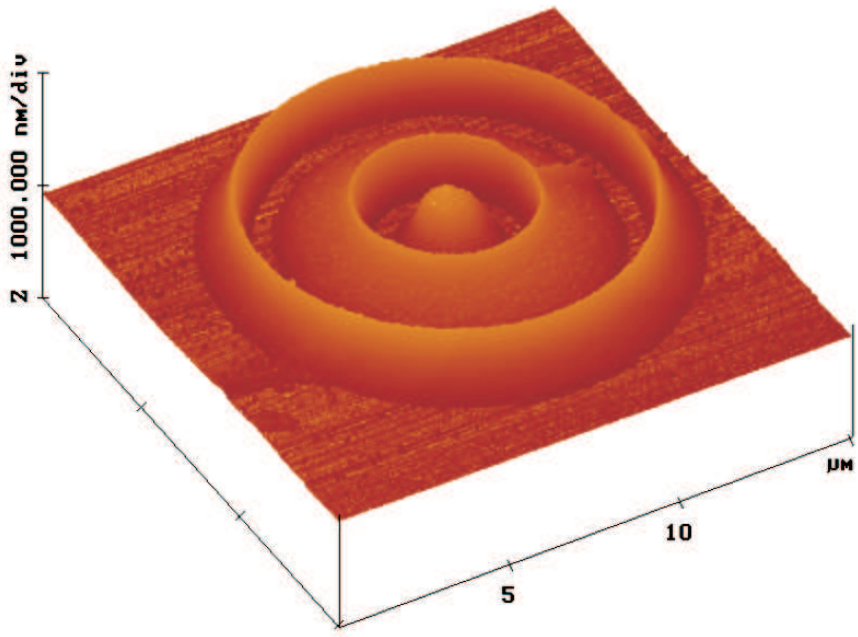

(a) 3-D ring structure

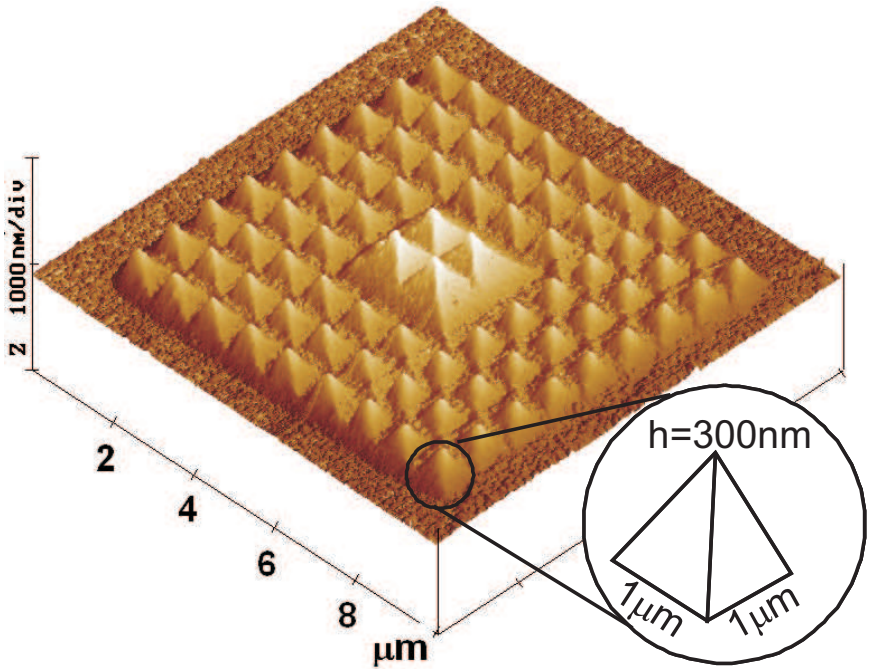

(b) 3-D multilevel pyramid array

Figure 3.22: AFM images of the developed 3-D structures on the negative resist

Raith-150 software. Owing to the electrons backscattering and proximity effects, the line dosage was defined using a trial and error method. This method

took a long iteration process to arrive at a suitable dosage for each line. Further developments on this process application are being worked out by the Raith manufacturer in terms of software application to address the 3-D issues.

3.2.2.2 Top Conductive Dissipation Layer using PEDOT/PSS

Conducting polymers, particularly the soluble derivatives, are other potential alternatives as a charge dissipator layer for EBL pattern writing on insulating materials. This work proposed using a water soluble conductive polymer, PEDOT/PSS as the top conductive coating on the negative resist layer.

The PEDOT/PSS was spun coated on top of the ma-N2403 resist at 5000 rpm for one minute, and baked on a hot plate at a temperature of 90^oC for two minutes to achieve a thickness of about 30 nm.

The effectiveness of this material was verified through the exposure experiments. Figure 3.23 shows SEM images of quartz substrates exposed with an e-beam at a higher acceleration voltage of 20 keV and with 20 μm aperture. Figure 3.23(a) shows an SEM image of quartz substrate coated with negative photoresist only, without the conductive polymer layer; these display the characteristic bright area of built up negative charges. No objects can be resolved for imaging or writing under the influence of surface charging. Figure 3.23(b) shows an SEM image of a substrate coated with negative photoresist and the proposed top conductive coating PEDOT/PSS after it has been exposed with e-beam. No charging effects were observed at the resist surface as is evidently shown by the confined 20 nm dot where surface charging is significantly suppressed.

The surface charging build up phenomena could be explained as illustrated in Figure 3.24(a), which illustrates the schematic diagram of the electron path that leads to secondary electron emission and built up charges. In comparison, Figure 3.24(b) illustrates the schematic diagram of the electron path with the existence of a PEDOT/PSS conductive layer. Most trapped and built up electron charges are grounded through the PEDOT/PSS layer.

This 3-D fabrication method was developed to overcome the limitation of the

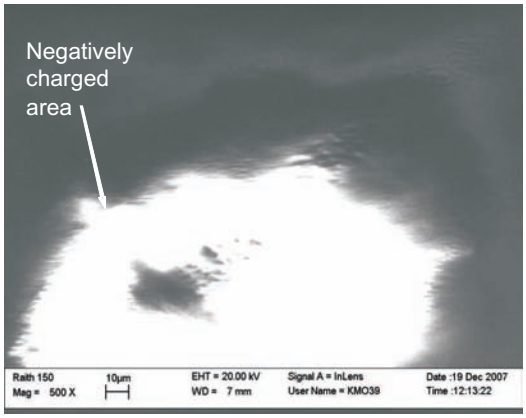

(a) Resist surface without dissipator layer a showing bright area (negatively charged)

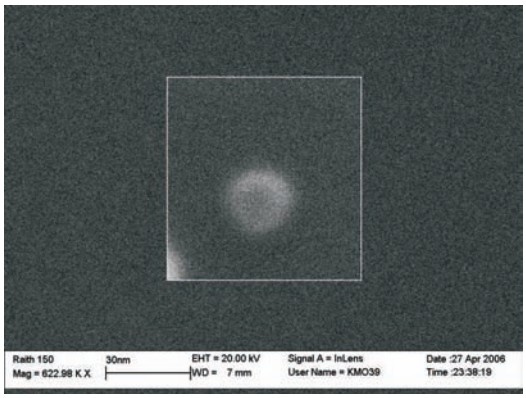

(b) Resist surface with dissipator layer

Figure 3.23: A comparison of the appearance SEM images of the resist surface without and with a PEDOT/PSS conductive polymer layer

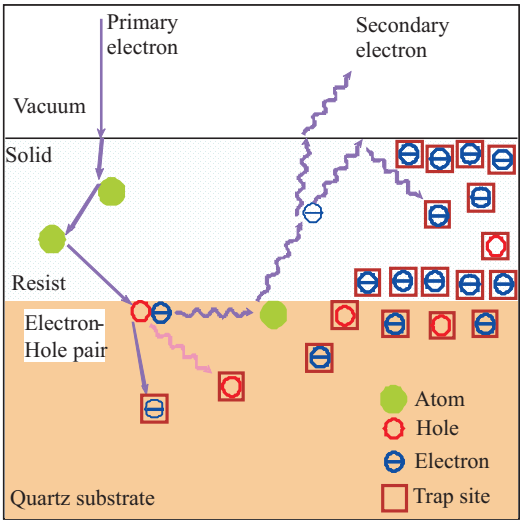

(a) schematic without dissipator

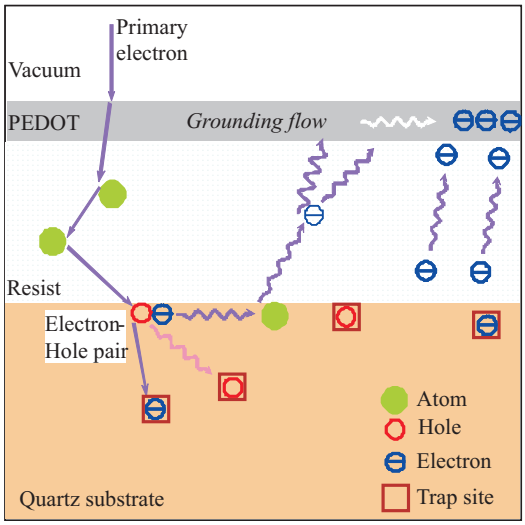

(b) schematic with dissipator

Figure 3.24: Schematic diagram showing electron trajectories when the e-beam was exposed on the resist

previous CE method where the creation of smaller feature sizes below 500 nm have been hindered by proximity effects. In 3-D patterning on negative resist, the developed resist height at a particular spot is determined by the magnitude of resist crosslinking at that location due to direct e-beam exposure plus the proximity effects from adjacent exposures. At lower acceleration voltages of 10 keV and below, the spread of the e-beam is quite large (up to 3 μm) as referred to Figure 3.20. Hence, the developed resist height at a particular spot is heav-

ily affected by multiple electrons' backscattering and proximity effects caused by line exposures near to the spot. Exposing a line with low dosage does not necessarily produce a low remaining resist height if the surrounding lines are exposed with high dosages. Manual optimisation of line dosages in order to achieve certain resist height in 3-D patterning requires a long iteration experiment process owing to multiple electrons' scattering and proximity effects from surrounding exposures.

In this method, a higher voltage acceleration of 20 keV has been employed as compared to 6.5 keV used in previous method that followed the critical energy method. The single pass line (SPL) pattern writing scheme was utilized for 3-D patterning with line dosages starting at 0.6 pC/cm up to 42.0 pC/cm. Figure 3.25(a) shows an example of a 3-D pattern writing scheme for a 300 x 300 nm^2 base pyramid. It was created using e-beam writing on a 600 nm negative resist layer by routing the multiple SPL parallel paths with various dosages assigned for each SPL (path 1 to path 6). The spaces between each SPL route ranged from 20 nm to 30 nm.

Figure 3.25(b) shows an AFM image of the developed 3-D pyramid test pattern on a ma-N2403 resist. Each pyramid has a 300 x 300 nm^2 base and is 300 nm in height.

The advantage of exposing an e-beam at a higher acceleration voltage is that it

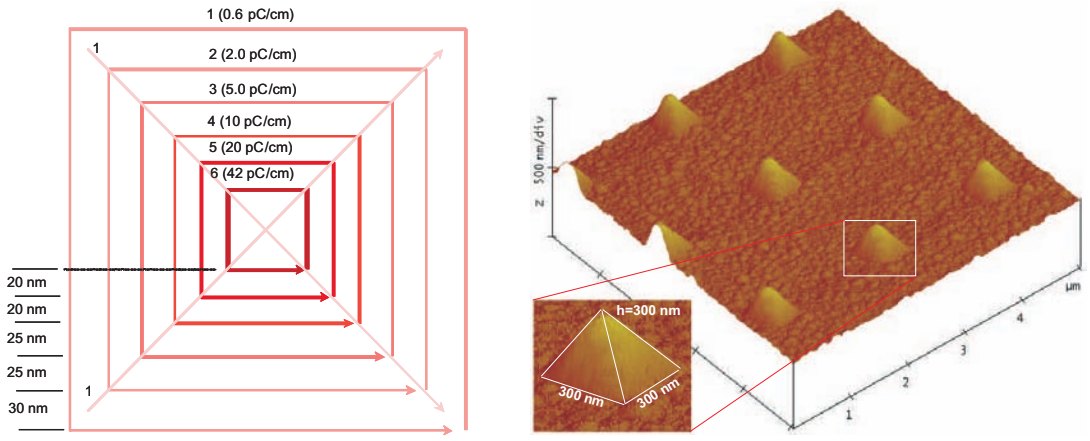

(a) A SPL routing for writing a 300 x 300 nm^2 base pyramid

(b) AFM images of the developed 300 x 300 nm^2 pyramid array

Figure 3.25: The EBL writing scheme for 3-D patterns and the associated results

will suppress the electrons' scattering and proximity effects on the surrounding

exposure region as illustrated by confined electron trajectories in Figure 3.20(d) of previous section. This results in a better control over the developed profiles, less time required for the dosage optimization process, and higher pattern density of 3-D patterns is possible. Figure 3.26(a) shows an AFM image of an array of a 500 x 500 nm^2 pyramid structure with 800 nm pitches.
These are the closest pitches achieved using the previous pattern writing method where low accelerating voltage of 6.25 keV is used. The electrons backscattering and proximity effects have hindered the high density 3-D structures. Figure 3.26(b) shows an AFM image of an array of cone structure (300 nm base diameter) with 400 nm pitches which were achieved using a conductive layer pattern writing method. A much higher density 3-D pattern is possible with the proximity effects suppression using a combination of higher accelerating voltages and conductive coating. This high accelerating voltage allows deeper penetration, more confined beam, and less electrons backscattering and proximity effects.

3.2.3 Three-Dimensional Pattern Transfer

The developed 3-D patterns on ma-N2403 resist have been directly transferred into the quartz substrate by a single-step RIE with suitable selectivity of resist-to-substrate by optimising the process gases. CHF_3/Ar gases were chosen for quartz etching based on their moderate F/C ratio which is important in the 3-D pattern transfer.
The aim of this work is to achieve a smooth linear gradient or curved 3-D surfaces of the fabricated mold with a surface roughness of less than 5 nm after the RIE pattern transfer process. This is an essential requirement for micro optical devices where the general guidelines required the surface roughness have an upper limit of 5 nm.
It was quite difficult to create a relatively tall 3-D structure using the EBL 3-D patterning technique owing to the electrons back scattering and proximity effects. Hence, an upper limit of 600 nm has been achieved in our 3-D structures through appropriate resist to substrate selectivity. In this work, the RIE pattern

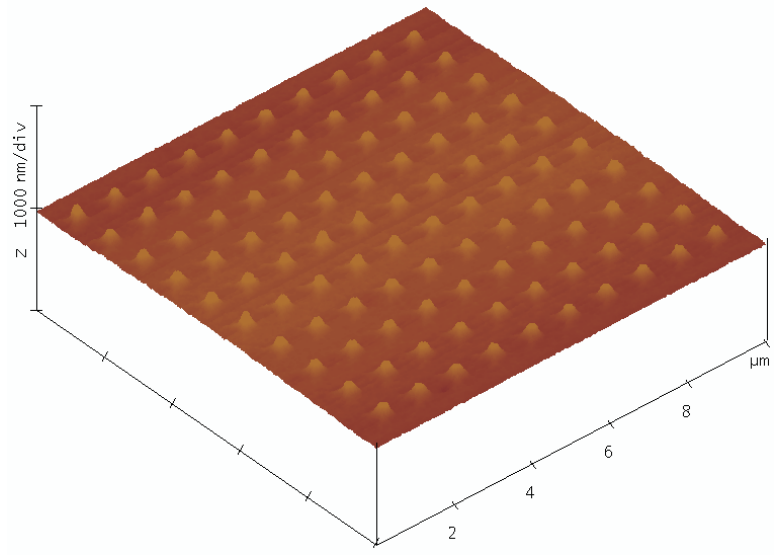

(a) AFM image of an array of 500 x 500 nm^2 pyramid structure with 800 nm pitches using CE method.

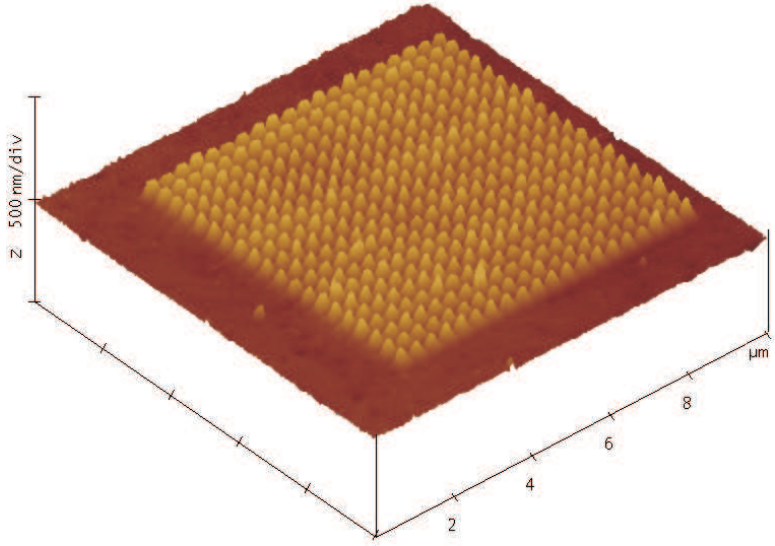

(b) AFM images of an array cone structure with 400 nm pitches using TC method.

Figure 3.26: The comparison of the highest pattern density of two pattern writing methods.

transfer parameters were optimised to yield 1:2 resist-to-substrate selectivity ratio. This selectivity ratio was found to achieve double the height of the final mold structure as well as minimise the trenching effect profiles.

RIE parameters for a 2-D pattern transfer were used as a baseline process and gradual adjustments were carried out till the aimed at criteria were achieved. As explained earlier in section 3.1.4, a very low etching pressure causes physi-

cal etching by Ar ions bombardment dominating the erosion process.
Table 4.2 shows the final optimized RIE parameter employed to achieve a smooth surface finish with surface roughness of less than 5 nm and 1:2 selectivity.

Table 3.5: The optimized CHF_3/Ar RIE parameter for 3-D pattern transfer onto quartz substrate

RIE parameters	3-D pattern transfer
Gas	CHF_3/Ar
Flow rate	9.0 sccm/6.25 sccm
Pressure	$<$ 6 mTorr
Temperature	295 K
RF Power	125 W
Bias voltage	-344 V
Selectivity (Resist:substrate)	1.0 : 2.0
Etch rate	10 nm/min on quartz

3.2.3.1 Etching Chemistry

In 3-D pattern transfer, the presence of resist polymer with 3-D profiles as the 3-D masking layer became the major difference in etching chemistry as compared to the 2-D pattern transfer. The novolak based negative resist (ma-N2403) polymer which consists of $C_xH_yO_z$ elements backbone reacts with the fluorinated plasma, enhances its crosslinking and harden the polymer [102]. The resultant polymer could be harder than even quartz. This might be the reason for the 1:2 etching selectivity. The bombardments of heavy Argon ions break the C-H-O bonds of the resist backbone, creating the volatiles of these elements. The dissociated resist elements increased the C ions increased, hence decreases the F/C ratio and causing domination of polymerization reactions.
Figure 3.27 illustrates the 3-D etching chemistry analysis. Similar to the 2-D pattern transfer, reactive ions bombarded the 3-D surface in a vertical downwards direction, irrespective of the resist pattern shape of profile.

Let us consider a plasma etching on an inclined quartz surface at angle θ

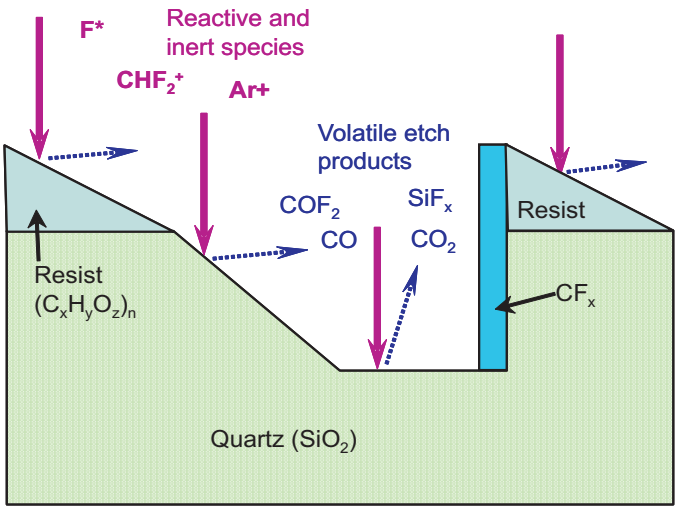

Figure 3.27: The 3-D etching chemistry

where the plasma bombardments are presumably in a vertical downwards direction as illustrated in Figure 3.28(a). Ion bombardments on the angled surface bounced/backscattered in a downhill direction and bounced ions from the inclined substrate surface collided with another incoming ion plasma from the top causing another bouncing down hill. Cumulatively, the plasma concentration increased towards the downhill direction.

On resist etching by heavy Ar ions bombardments, the ion/resist ratio at the thin resist caused a higher etching rate on the thin resist layer as compared to the thick resist layer. As for the 3-D masking layer, various resist masking thicknesses caused a varied etching rate on every location.

Higher plasma concentration induced a higher etch rate as illustrated in Figure 3.28(b). The steeper the surface slope, the higher and the narrower the plasma concentration at the bottom of the slope at location D.

Backscattered/bounced ions towards the vertical or angled walls collided with vertically downwards plasma ions creating a higher concentration of ion bombardment at the bottom of the vertical or angled sidewalls, thus causing a trenching effect as illustrated in Figure 3.28(c). At location C, the trenching effects are wider as compared to the narrow trenching effects at location D. Location D is the representation of the trenching effect of an inclined surface when the inclined angle θ is approaching 90^o.

These observations are based on our study and by no means are complete. This

subject need further indepth treatment as it is still controversial.

Figure 3.29(a) shows an SEM image of the centre of the 3-D ring shape after

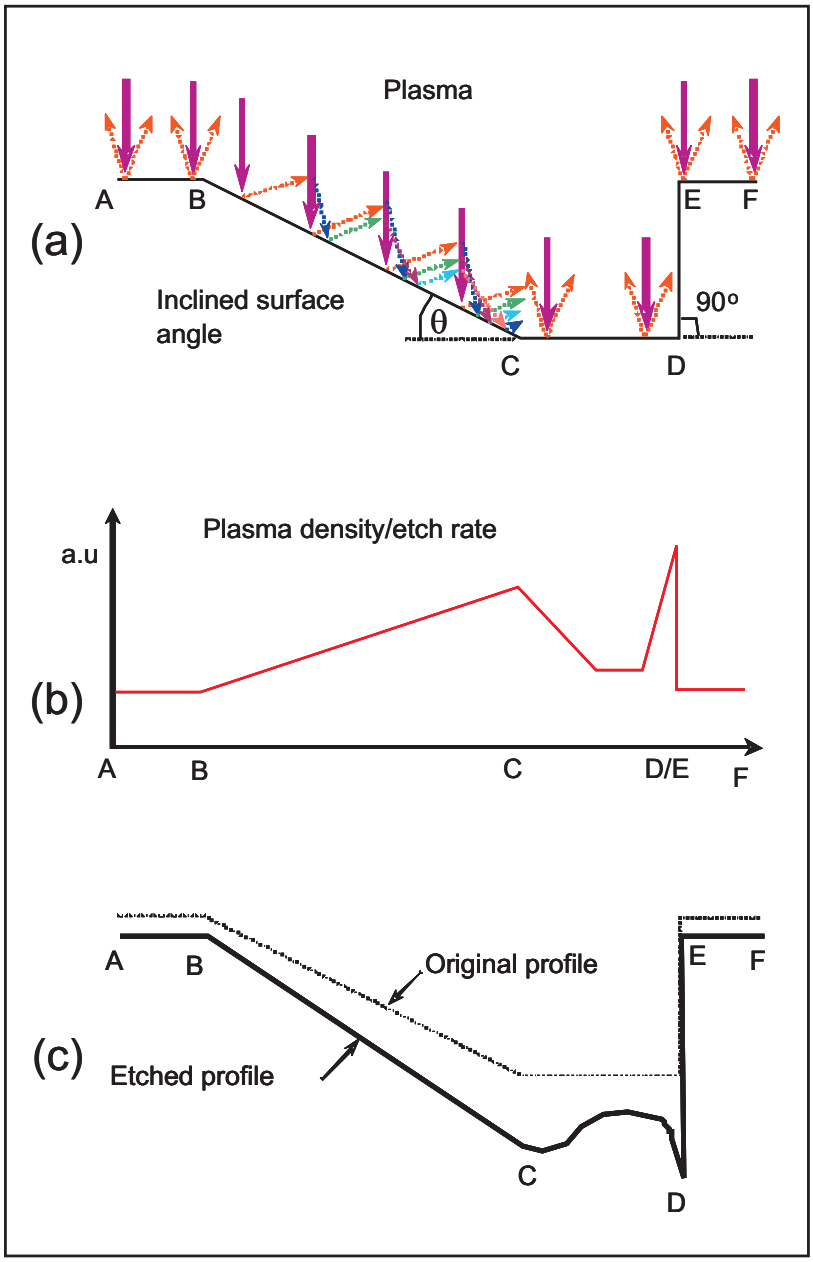

Figure 3.28: The 3-D etching mechanism

the CHF_3/Ar RIE process. It shows the final 3-D ring etched profiles with the lens shape and a vertical sidewall for the middle 3-D ring. The trenching effect formed around the 3-D lens and at the bottom of the middle 3-D ring structure are observed. Figure 3.29(b) shows the AFM cross sectional traces of the 3-D ring mold structure with trenching effects. The deep trench profiles were unable to be traced perfectly owing to the limitation of the AFM tip artifact itself.

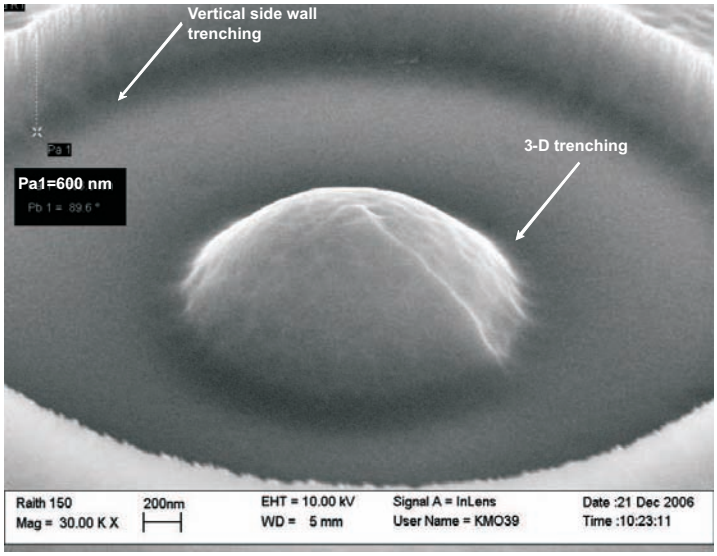

(a) The SEM of the 3-D ring etched profiles showing the trenching effects.

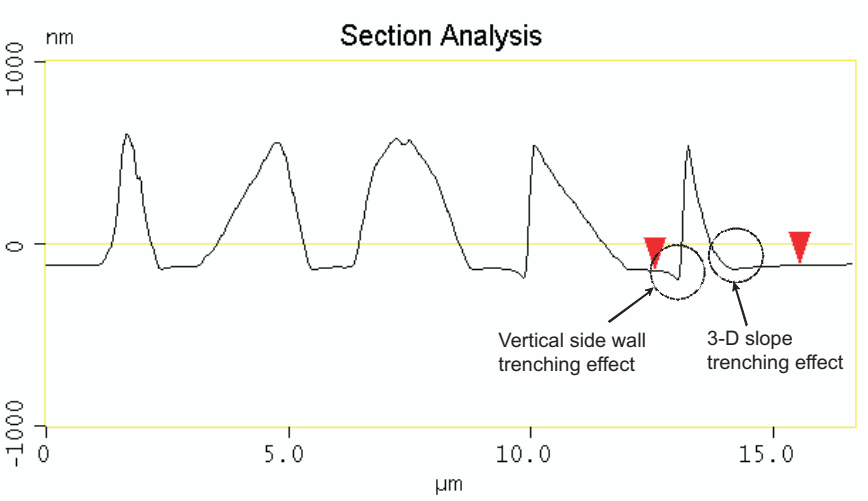

(b) The AFM cross sectional traces on 3-D ring mold structure.

Figure 3.29: The SEM and AFM cross sectional view of trenching effects on 3-D ring mold structure.

3.2.3.2 Etching Analysis

In etching hard materials such as quartz where polymerization reactions dominate, high plasma density is essential to increase the etching rate, especially for a deep etching in a 3-D pattern transfer process. High power density can be achieved by increasing the RF power and/or reducing the electrode surface

area (loading effect). The maximum RF power that can be set on an Oxford Plasma 80plus RIE is 200 Watts. In this experiment, a NiCr coated electrode was clamped with a two-inch (50 mm diameter) PTFE electrode holder. Hence, the maximum power density is set to the highest setting of 10.2 W/cm^2 with this arrangement.

The experiment began with the RIE process using parameters that are similar to the 2-D etching as tabled in Table 3.3. In this high density etching process where polymerization reactions dominate, some of the etched materials may dropped back on the sample forming a nanomasking island. This will form nanopillars as illustrated in Figure 3.31(a) and will be discussed later.

The highly dense nanopillar structures that formed from the plasma etching process were finally collapsed after long high density plasma bombardment over a long period of time. Figure 3.30(a) shows an SEM image of a 3-D ring structure when etched with the high power density plasma setting for 40 minutes. The result shows a very rough surface and only a vertical sidewall passivation is clearly observed. It can be concluded that increasing the plasma and/or power densities could not achieve a smooth etched surface as a requirement for the 3-D pattern transfer process.

In the next experiment, the plasma density was reduced to a normal condition by changing the electrode clamp to the four inch (100 mm diameter) electrode holder which gives a power density of 2.5 W/cm^2 with RF power of 200 W. The surface roughness was found to be improved by lowering the RF power density as shown in Figure 3.30(b).

Since this etching process was dominated by polymerization reactions, CF_x radicals tended to be deposited anywhere on the etched surface. At an operating pressure of 20 to 30 mTorr, the mean free path of the plasma species was very short and etching products were close to each other causing continuous collisions. In this saturated condition, the species produced as a result of ion bombardment of the resist mask and substrate surface will reach a level at which the vacuum pump is unable to extract away these by-products. The lack of vacuum pumping capacity had let the etching products and particles drop onto the substrate surface causing nanomasking effects as illustrated in Figure

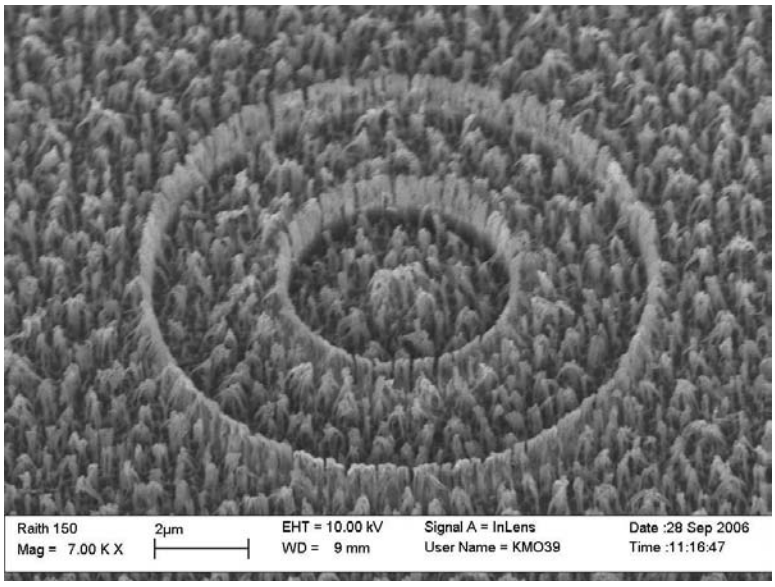

(a) 3-D ring etched using 10.2 W/cm^2 power density

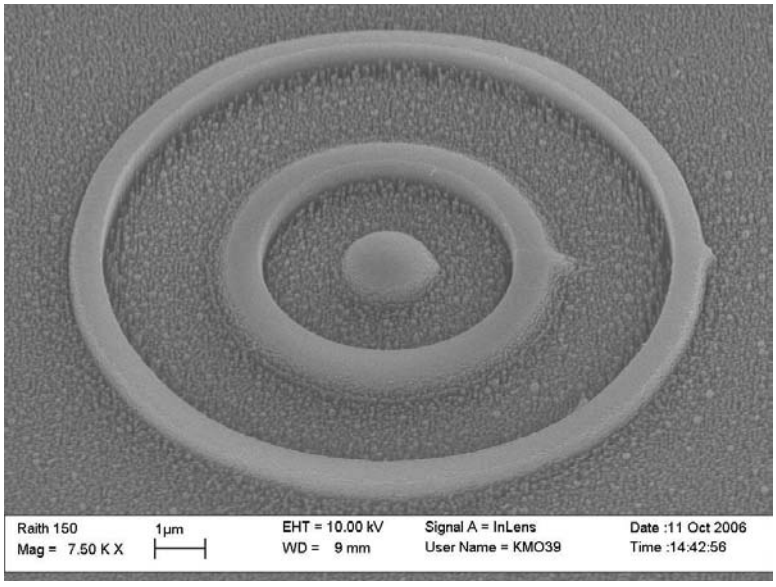

(b) 3-D ring etched using 2.5 $Watts/cm^2$ power density

Figure 3.30: SEM images of the 3-D structures on quartz substrate after etching with different plasma power densities.

3.31(a). From the above experiments, it was found that the etching process was limited by the vacuum pumping capacity in extracting the etching by-products during the etching process at this condition.

The CHF_3 plasma made the polymer resist used for the 3-D masking layer very hard, as demonstrated by the 1:2 selectivity. During the etching process, the dropped nanoparticles of the resist became the nanomasks on the etched substrate. In addition, in very long etching process, the NiCr electrode was also

etched by the plasma physical bombardment. The etched NiCr particles may also be dropped on the substrate surface. It can be summarised that nanomasking effects in the 3-D etching process are the combination of plasma bombardment products, etched electrode particles and ongoing polymerization reactions at high operating pressure. Figure 3.31(b) shows an SEM image of the example of a nanopillars surface. A thick sidewall passivation layer of about 50 nm can also be seen clearly.

The size of each nanopillar was about 30 nm in diameter and about 200 nm in height. This is a very dense nanopillar structure where the nanopillars are about 30 to 50 nm apart.

To achieve a smooth surface finish, an etching process with a moderate plasma

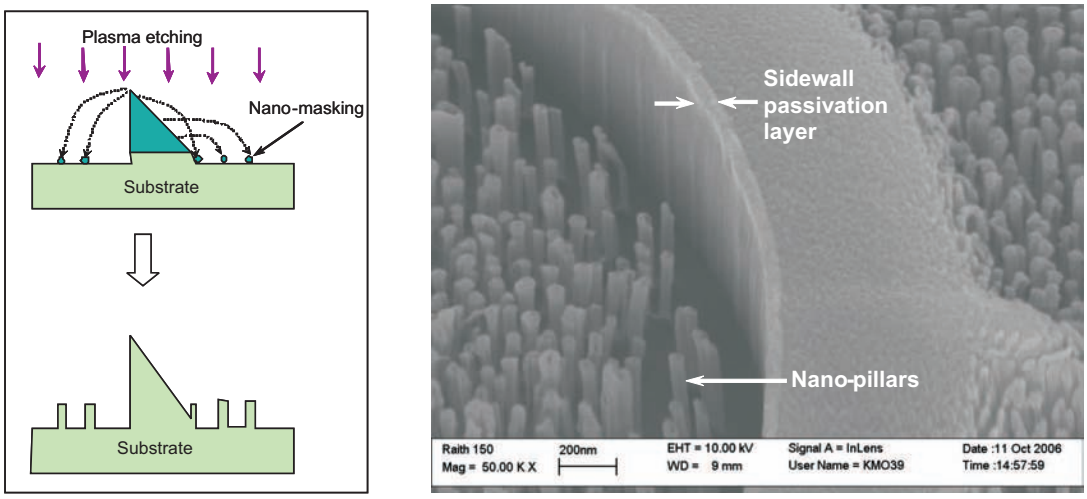

(a) nanomasking effects (b) nanopillars

Figure 3.31: The etching product that created a nanomasking effects resulting in a nanopillar surface finish

density and a higher physical than chemical reaction should be adopted/followed. The optimum etching process should be then set at below the maximum vacuum pumping out capacity. In that sense, a very low operating pressure was required so that the etching products are extracted immediately before they are allowed to drop on the sample surface. This process is similar to the physical etching mechanism. In a very low operating pressure condition below 20 mTorr, the mean free path is increased, which minimizes the collision between atoms and ions. To achieve low operating pressure, the gas feeds have to be re-

duced. As a result, the products of the chemical reaction are hugely minimized and the etching is mostly carried out by the physical bombardment. This condition was achieved by reducing the incoming flow rates of the etching gases which results in a lower operating pressure but lower etching rate.

From the above experimental analysis, it was found that the operating pressure has a direct effect on the surface roughness. Further experiment has demonstrated the relationship between the surface roughness and etching pressure as illustrated in Figure 3.32. AFM was used to measure the surface roughness of the etched samples. A surface roughness of about 85 nm is measured when the etching pressure is 30 mTorr and surface roughness below 2 nm measured at etching pressure is below 6 mTorr. At 25 mTorr pressure, the measured surface roughness was much lower than actual because of the limitation of the AFM in tracing the nanopillars effectively.

Figure 3.33 shows the surface roughness analysis on the quartz mold substrate

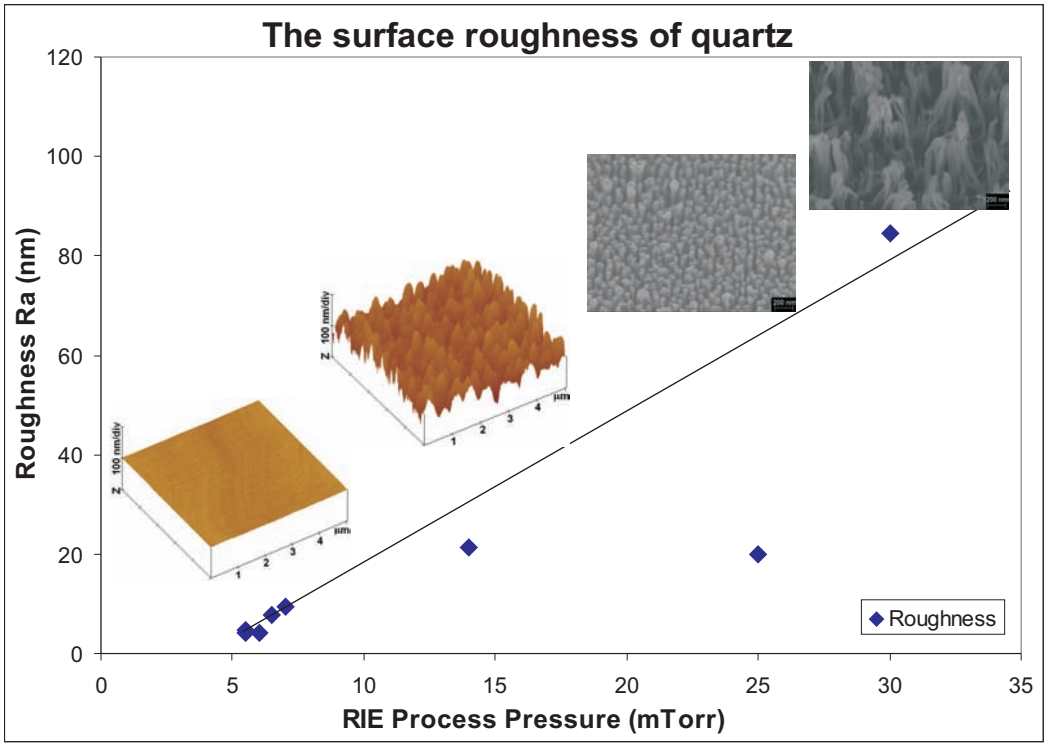

Figure 3.32: The surface roughness versus RIE operating pressure

using the AFM roughness analysis after the etching process. It shows that the surface roughness $R_{q(rms)}$ of 1.429 nm is achieved on the surface beside the 3-D structure.

Figure 3.34 shows the results of 3-D pattern etching with the optimized RIE

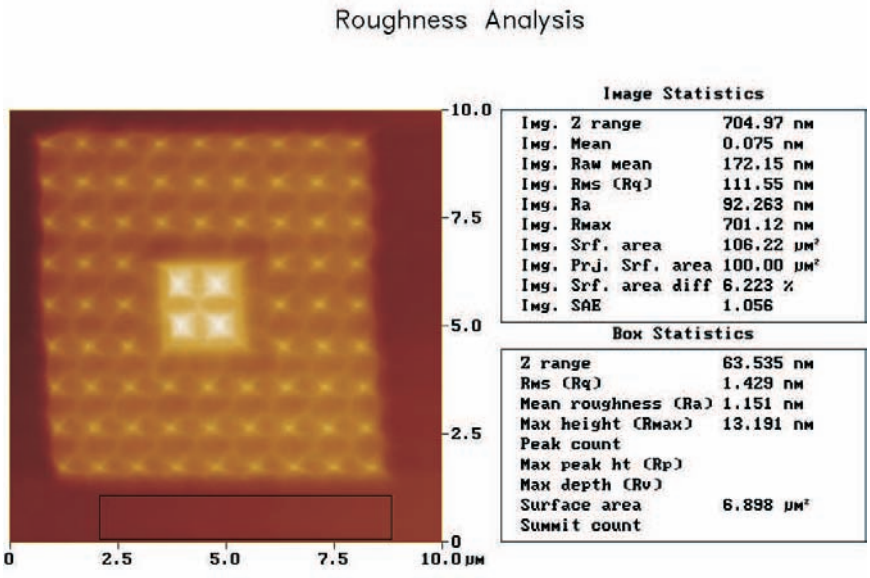

Figure 3.33: The surface roughness analysis using AFM

recipe where Figure 3.34(a) shows the SEM image of the 3-D ring structure on a quartz master mold substrate with the highest point of 600nm. Figure 3.34(b) shows another SEM image of 3-D pyramid structures with multilevel features on quartz substrate. These structures were used as the test pattern of the master mold in the 3-D imprint.

Profile analysis was carried out using AFM technique on some of the results for the optimization process as illustrated in Figure 3.35. Figure 3.35(a) shows the ma-N2403 resist 3-D ring profile before the RIE process, while Figure 3.35(b) illustrated the etched 3-D ring profiles on quartz substrate after the pattern transfer process. In both figures, the dotted lines represent the intended profiles and the solid lines are the achieved profiles, while the bottom trace shows the differences between them. Based on these results, iterations were followed to optimize the resist and etching structures accordingly. This was the process adopted until the intended profiles were achieved.

The vertical sidewall profiles were not traced efficiently which is attributed to the AFM STING tip profile used in this work. This has caused the high differences between the intended as compared to the achieved profiles on the vertical sidewall. In addition, the trenching effects also contributed to the high differences between them.

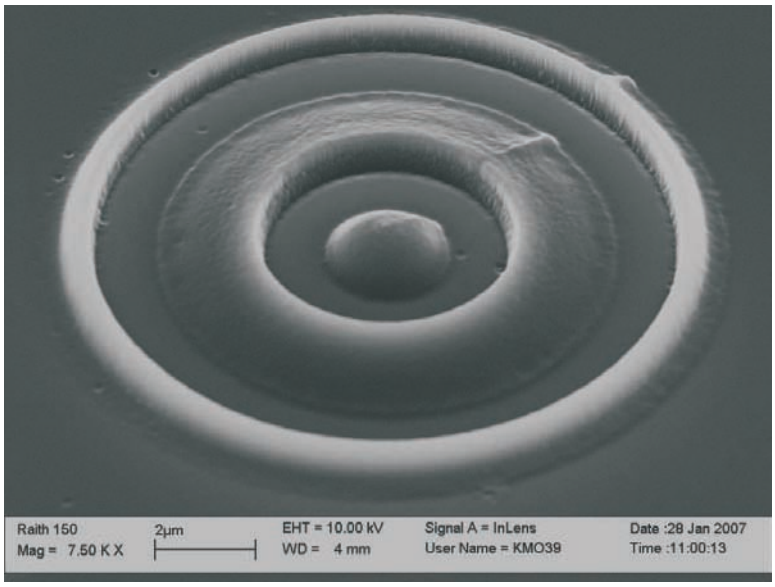

(a) 3-D ring structure

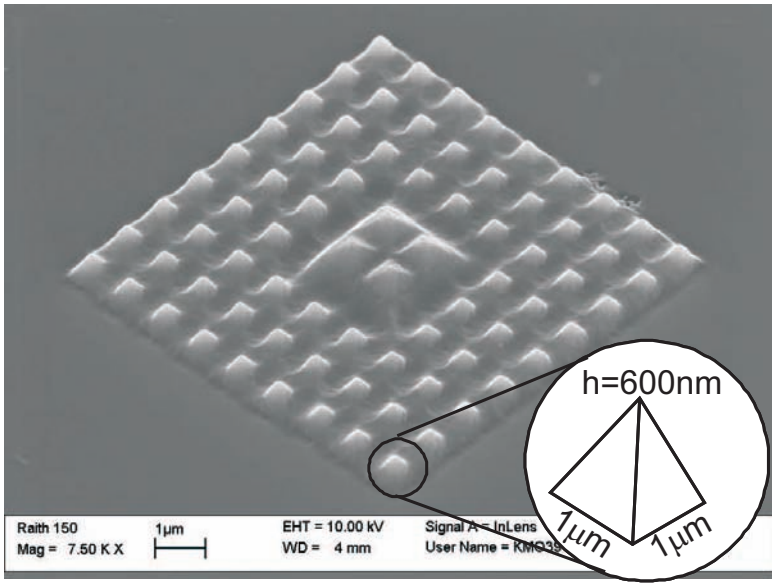

(b) 3-D multilevel pyramid array

Figure 3.34: SEM images of the 3-D structures on quartz substrate.

Other geometrical shapes have also been attempted. Figure 3.36 shows some of the SEM images of various 3-D geometrical shapes fabricated in this work so as to demonstrate the capability and reproducibility of this technique. Left centre is the SEM images of a group of 3-D geometrical shapes on quartz substrate and surrounding that image are the enlarged SEM images of particular shapes, (a)3-D triangle, (b) saw tooth, (c) hemisphere, (d) square base pyramid and (e) vertical angle saw tooth. The highest structure was about 700 nm and

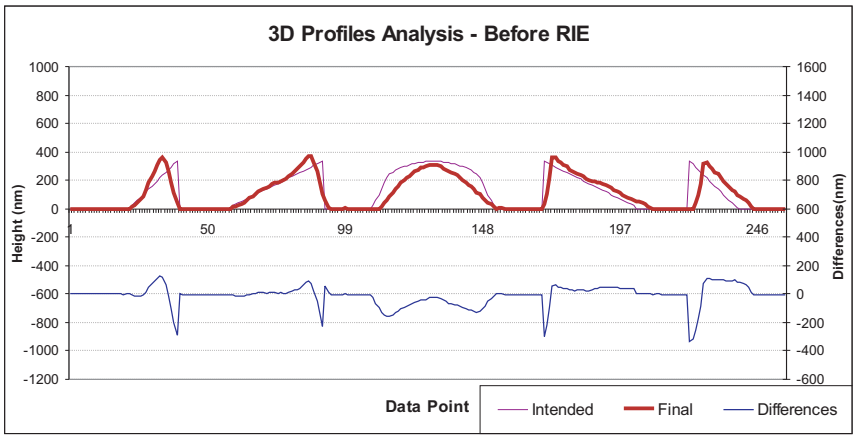

(a) before RIE

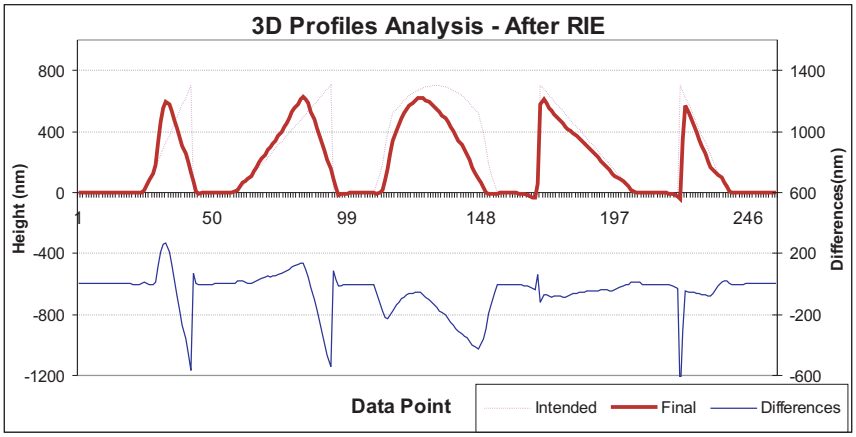

(b) after RIE

Figure 3.35: The profile analysis for 3-D ring profiles before and after the RIE process.

the smallest feature size was about 500 nm. The trenching effects can be observed at every corner of the structures. Some of other related SEM images produced by this research work are shown in Appendix C.

3.3 Summary

2-D and 3-D structures have been fabricated on quartz substrate using EBL and dry etching techniques with simplified process steps. The 2-D structures were fabricated using an additive pattern transfer method while the 3-D structures were fabricated using a subtractive pattern transfer method.

The 3-D mold profiles were created on the ma-N2403 negative tone photoresist

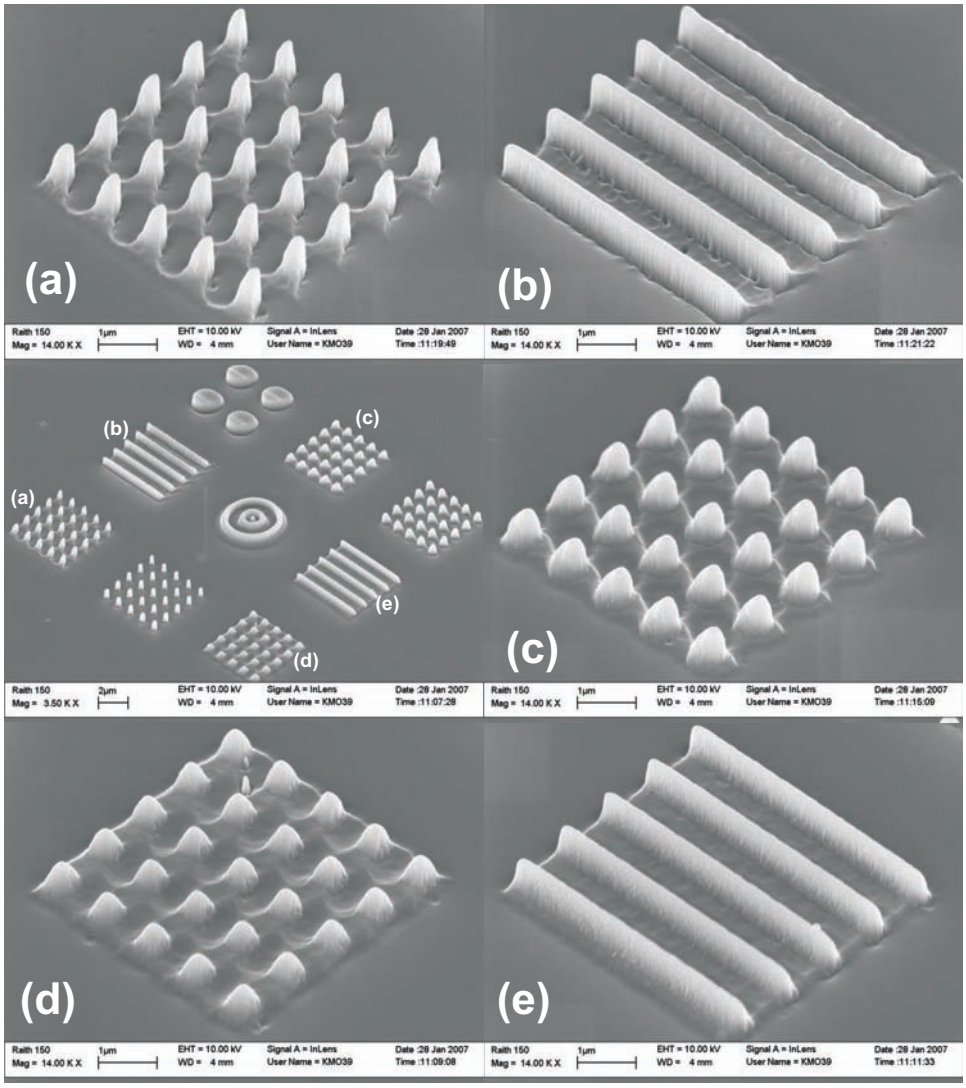

Figure 3.36: The left center is the SEM image of various 3-D shaped structures on the quartz substrate after the 3-D pattern transfer and the surrounding are the enlarged SEM image of (a) 3-D triangle, (b)saw tooth, (c) hemisphere, (d) square base pyramid and (e) vertical angle sawtooth.

using the Raith-150 EBL tool with variable dose controlled exposure. Variable e-beam dose was used to obtain resist contrast curve to determine the gradient of various 3-D structures. For a 600 nm layer thickness of ma-N2403 resist, the e-beam critical energy was set at 6.25 keV. A higher acceleration voltage of 20 keV was used for the conductive polymer (PEDOT/PSS) top coating method. EBL exposure with line dosages ranging from 0.6 pC/cm to 42.0 pC/cm were used for 3-D resist contrast approach. A linear resist contrast profile was obtained with a negative tone photoresist and subsequently was utilized as the

3-D masking layer. The 3-D pattern was transferred onto the quartz mold substrate by an optimized single-step reactive ion etching (RIE) process with selectivity resist-to-substrate of 1:2 using fluorinated plasma CHF_3/Ar.

The main issues in EBL are surface charging, electrons backscattering and proximity effects. In the fabrication of 2-D structures, this was solved by using thin metallic coatings and conductive polymer PEDOT/PSS as a charge dissipation layer. 2-D structures with feature sizes below 100 nm and a high aspect-ratio of up to 1:10 had been demonstrated. The use of critical acceleration voltage and high accelerating voltage in conjunction with conductive polymer PEDOT/PSS have suppressed the surface charging effects in the fabrication of 3-D structures, where feature size down to 300 nm had been demonstrated. The high surface roughness caused by nanomasking effects in the 3-D etching is the result of the combination of plasma bombardment products, etched electrode particles and dominating polymerization reactions at a high operating pressure. A very low RIE operating pressure was found to produce a smooth etched quartz surface. A surface roughness of below 2 nm was achieved when the RIE process pressure was lower than 6 mTorr.

Chapter 4

IMPRINTS

Imprint is primarily a physical deformation process where a mold with micro/nanostructures on its surface is utilized to deform a thin resist film (or an active material) deposited on a substrate [103]. The resist can be either a thermal plastic or UV curable material. After the de-molding process, an etching pattern transfer process takes place by utilizing the imprinted structures as the masking layer. This is a promising low cost technique for mico/nanostructure fabrication. Another unique feature of NIL technology is that it is a direct 3-D patterning technology, not found in other lithography technologies.

There has been a worldwide demand for an innovative lithography technique, where nano-scale resolution, high throughput and cost-effectiveness are fused together, and the NIL technologies fall within these criteria. A low imprint pressure, minimization of residual resist layers thickness after the de-molding process and the avoidance of thermal cycles are the main factors that have to be overcome to apply NIL for mainstream semiconductor manufacturing technology.

In this chapter, the imprint press and results will be presented for 2-D and 3-D structures using UV-NIL and UV curable resists. For the 2-D structures, imprint is used for defining the resist pattern on the imaging layer, followed by the final pattern transfer onto the substrate using a dry etching technique. The imprinting capability of the imprint resist materials and the process tool employed were explored in 2-D imprinting, while 3-D replication explores the advanced imprinting capability of the UV-NIL technique. The 3-D replication is an en-

hancement of advanced fabrication where two imprint steps are involved.
To carry out the imprint experiments, the vacuum operated manual imprint tool was attached onto the UV illumination source of the Karl Suss Mask Aligner (MA-6) system. A UV illumination of 365 nm wavelength with an intensity of about 0.6 W/cm^2 was utilized for resist curing while imprinting.
In imprinting, achieving the thinnest possible residual resist layer is an essential requirement to ensure a successful pattern transfer. This requires optimization of pattern density, resist viscosity, resist thickness and imprint pressure. Hence, the study of the behaviour of resist reflow during and after imprint is important in NIL technologies [104].
In this imprint experimental work, imprint problems such as sticking, bubbles, and the uniformity of the residual resist layer have been investigated. For sticking issues, a number of options were followed in order to modify the mold substrate surface properties where surface chemistry for each material used was considered to minimize the sticking problems. Surface treatment of polymer using plasma to modify the surface energy has been studied extensively with wide range of suggestions and solutions [90]. Minimization of defect density and contamination are also important aspect in imprinting processes.
De-molding is the process by which the mold is separated from the imprinted polymer structure by a vertical movement of the mold. This is a crucial step in the imprint process and extra care must be taken to minimize failures at this point. Distortion or damaging of the imprinted structure during this movement can happen as a result of different effects such as adhesion at the surface, friction due to surface roughness of sidewalls and trapping of the polymer due to negative slope of cavity sidewalls. De-molding without resist damage is one of the key elements for successful nanopatterning using NIL technology. De-molding method by separating the mold and substrate using an air knife has been demonstrated by S. Merino and co-workers[105].
Final pattern transfer using the CHF_3/O_2 RIE process was attempted and investigated. The results were unsatisfactory owing to the equipment and process limitations. Suggestions for improvement will be discussed in section 4.2.4 and 5.4.1.

4.1 The Imprint of Two-Dimensional Structures

A number of resist materials could be used for imprinting the 2-D structures using an UV-NIL technique. UV curable resist such as polydimethylsiloxane (PDMS) and perfluoropolyether (PFPE) were among a few popular resists normally used by many researchers [106, 107]. In this work, Ormocomp was selected as UV-NIL resist because of its excellent UV transmission properties and being a very hard material that is suitable for use as a soft mold in the 3-D imprint process.
The aim of this 2-D imprinting section is to study pattern replication on Ormocomp resist using 2-D mold structures including the high aspect ratio structure. Imprint experiments were carried out using two types of molds: transparent molds and transparent molds with a NiCr absorber that will be explained in section 4.1.2.

4.1.1 Preparation

In the imprint process, the UV curable resist must have strong adhesive properties to the substrate surface on one hand but not stick to the mold surface [108]. To achieve a strong adhesion between resist and quartz substrate, an extra cleaning process combined with appropriate surface treatment were performed on the quartz surface. Substrate cleaning was normally carried out with acetone, methanol and IPA solvents in an ultrasonic bath but for recycled substrate, cleaning with NMP solvents was found to give better results. An oxygen plasma step was appropriate to enhance the surface cleanliness as it removes organic residual resist materials.
Ormocomp resist is a honey-like polymer liquid which could achieve a few microns of thickness when spun coated on a substrate. To achieve a thinner Ormocomp layer, a 30% of Ormocomp resist diluted in an Ormothin thinner was spun coated on a quartz substrate at a spinning speed of 3000 rpm for one minute to achieve a 400 nm layer thickness. Ormodev was the developer used for Ormocomp resist.

Prior to the imprint process, a surface wetting experiment was carried out to quantify the surface properties of each material. The contact angle measurements of quartz, resist and metal surfaces were performed using a contact angle measurement system as detailed in section 2.1.8. The contact angles were measured on the surfaces before and after the surface treatments to determine the changes of the surface energies.

Figure 4.1(a) shows the contact angle of a spun coated Ormocomp surface. An Ormocomp contact angle θ of 73.6^o was measured which is considered a hydrophobic surface. Figure 4.1(b) shows the contact angle of the Ormocomp surface when coated with anti adhesive monolayer of FOTS. The contact angle θ was increased to 98.3^o which is highly hydrophobic. This shows that the FOTS monolayer has enhanced the non-sticking properties on the Ormocomp surface which is essential for the imprinting process.

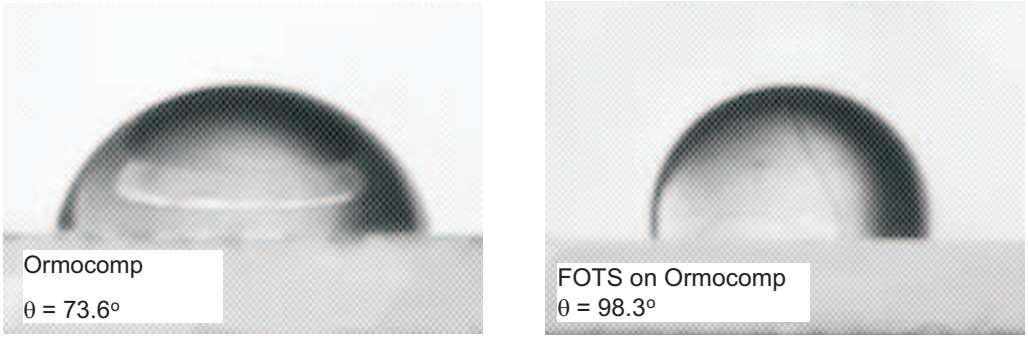

(a) Ormocomp (b) Ormocomp coated with FOTS

Figure 4.1: The contact angles on the surface of Ormocomp resist at normal conditions and after being coated with an anti adhesive monolayer

4.1.2 Imprint Process

The 2-D structures that fabricated on the quartz substrates using techniques as described in section 3.1.2 have NiCr layers left on top of the patterned structure. The NiCr layer is normally removed by soaking in the chrome etcher solution at a room temperature for 30 seconds to achieve a transparent mold. When this mold is used in the imprint as illustrated in Figure 4.2(a), the UV light transmitted through the transparent mold will polymerize/harden the whole exposed

resist underneath the transparent imprint mold. This followed by an oxygen plasma that is required to remove the residual resist layer to achieve a pattern that ready for the subsequent pattern transfer process.

However, if the NiCr layer is not removed from the fabricated transparent mold, it can be used as an UV light absorber during UV exposure as illustrated in Figure 4.2(b). The unexposed resist layer can be removed using the developer to achieve a pattern that is ready for the subsequent pattern transfer process.

The details of imprinting using both procedures will be explained in the next sections.

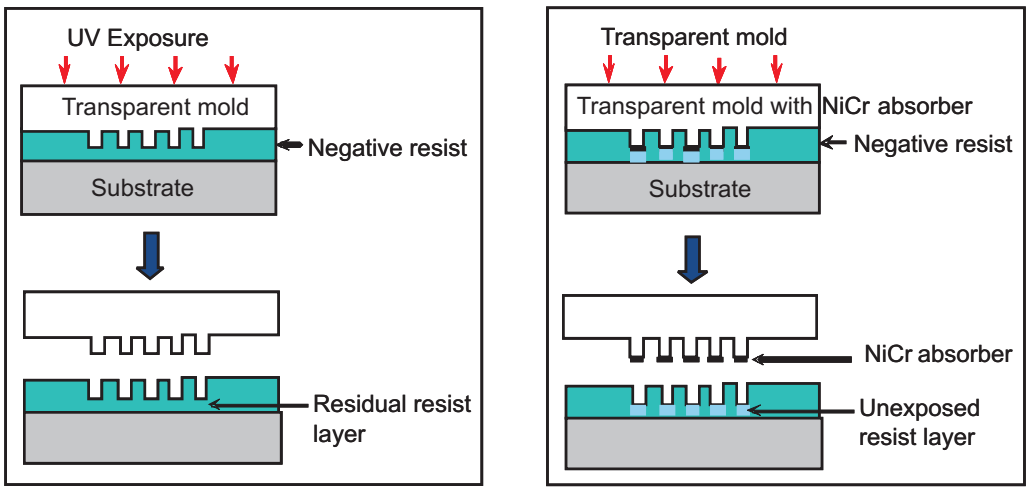

(a) transparent mold (b) transparent mold with NiCr absorber

Figure 4.2: Two types of transparent molds used for 2-D imprints.

Separating the mold from the resist layer or de-molding is a critical step in the imprint process as failures normally occur at this point. The difficulty levels depend on the surface area and the amount of friction existing on the vertical sidewalls. The surface area, pattern density and the imprint depth of penetration contribute to the amount of friction between mold and imprinted resist during the de-molding process [109].

Many de-molding methods have been investigated, but the ideal de-molding process is found by gradually moving the mold and imprint resist in an opposite outwards direction perpendicular to the surface contact. However, holding the transparent mold and/or substrate from their backside was quite difficult in order to minimise the blockage of UV exposure through the mold/substrate

surface area. In this work, a manual de-molding process was employed by applying gradual force using a scalpel at one corner of the mold in order to de-laminate between two material surfaces as illustrated in Figure 4.3. It should be carried out gently by starting at one corner and avoiding any twist movements. A fast de-molding movement always causes resist breakage/tear out problems.

Figure 4.4 shows the AFM images of some imprint and de-molding results

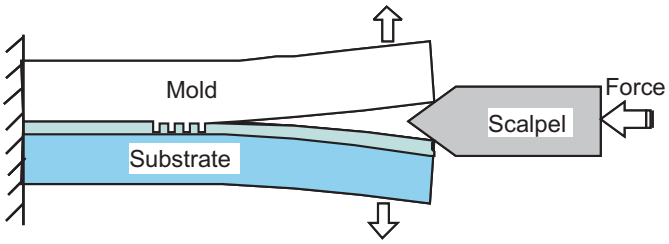

Figure 4.3: The schematic of the manual de-molding process.

on Ormocomp resist using manual imprint and de-molding methods. Figure 4.4 shows AFM images of a 2-D imprint on an Ormocomp resist layer. Figure 4.4(a) shows the imprinted resist with a feature size of a 500 nm mold. It was imprinted smoothly without any sticking issues. Meanwhile Figure 4.4(b) shows the imprinted resist of a 90 nm feature. For a smaller feature size mold, the contact surface between mold and resist is larger than the contact surface of large mold features which causes increased sticking and potential breakage failure especially for high aspect-ratio structures.

4.1.2.1 Imprint using Transparent Molds

The first imprint method is illustrated in Figure 4.5(a). The transparent mold was coated with FOTS layer as an anti-sticking layer as explained in section 2.2.5. In this imprint procedure, a normal 2-D transparent mold was imprinted on an Ormocomp resist layer by applying a constant vacuum pressure of below 100 bar on the manual imprint tool. The sample was then cured under a UV exposure for 8 minutes. This followed by the de-molding process and descumming of the residual resist layer using oxygen plasma as explained in

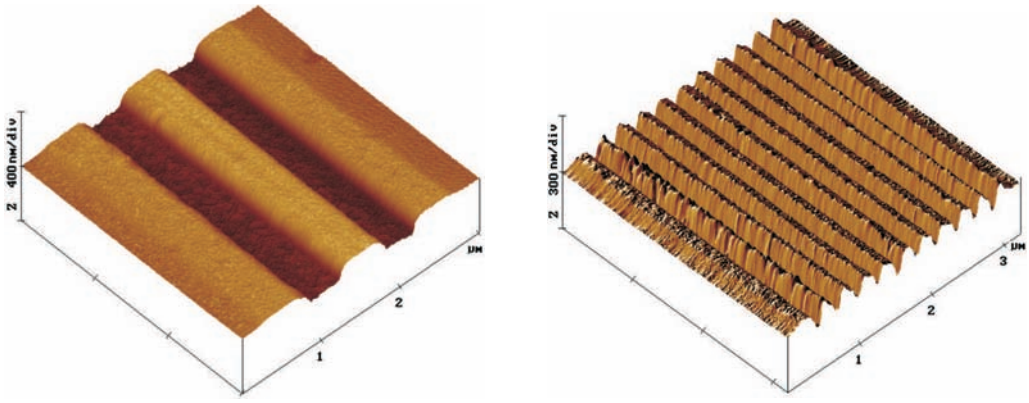

(a) An imprint of a 500 nm feature (b) An imprint of a 90 nm feature

Figure 4.4: The 2-D imprint of two types of feature sizes on Ormocomp resist

section 3.1.2.1. The pattern was transferred onto quartz substrate using an additive pattern transfer method where a 40 nm NiCr layer was deposited on the imprinted pattern using a metal evaporator and later lifted off in the acetone. Finally the CHF_3/Ar RIE process was carried out to etch the replica of the master mold.

The lift off process for the Ormocomp resist layer together with the metal layer using acetone were quite difficult because UV cured Ormocomp is very hard material (glass like hardness). As an alternative, a lift off process by soaking in warm NMP solvent at a temperature of 45^oC was found to give better results.

4.1.2.2 Imprint using Transparent Molds with a NiCr Absorber

The second imprint method is illustrated in Figure 4.5(b). The NiCr layer functioned as a mask/absorber preventing the UV light passing through and created an exposed and unexposed pattern. Since Ormocomp is a negative resist, the unexposed regions were washed away by Ormodev developer. The sample was developed in Ormodev for 20 to 30 seconds at a temperature of 20^oC to remove the unexposed residual resist layer.

This was followed by metal deposition, lift off, and a pattern transfer process similar to first imprint method.

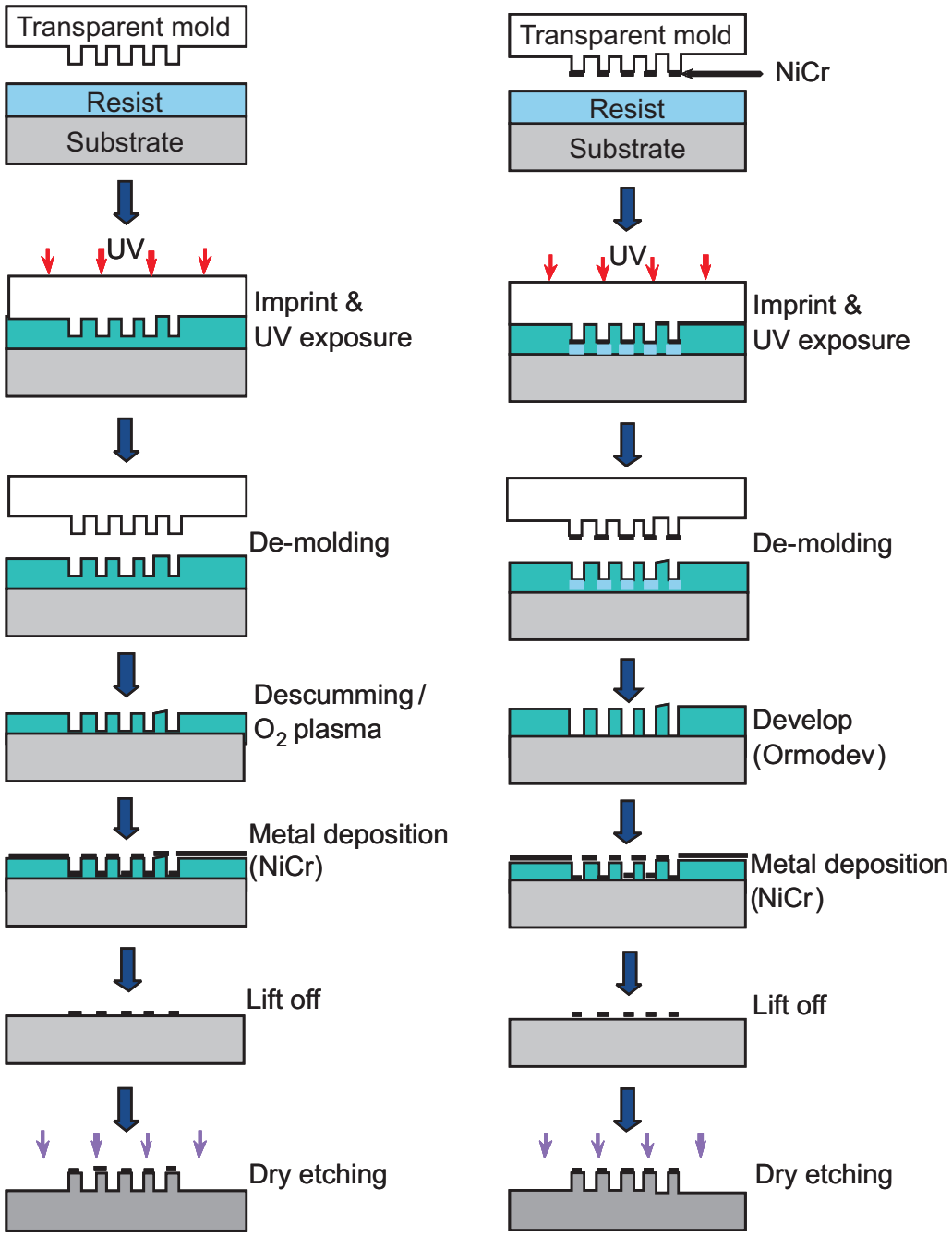

(a) using normal 2-D transparent mold

(b) using 2-D transparent mold with NiCr absorber

Figure 4.5: The 2-D imprint procedures using a transparent mold and a transparent mold with a NiCr absorber.

4.1.3 Final Pattern Transfer

Following imprint, an RIE etching process using a CHF_3/Ar recipe similar to the 2-D mold making process was employed for the 2-D pattern transfer. The RIE process for a 2-D structure on a quartz substrate was explained in section

3.1.4 of previous chapter.

The examples of the pattern transfer results are shown in Figure 4.6. Figure 4.6(a) shows an AFM image of periodic line structures of 90 nm in width and 250 nm in height. Figure 4.6(b) shows another AFM non-periodic image of a corner shape structure on a replicated quartz substrate with a dimension of 150 nm in width and 400nm in height. The sharp profiles at the bottom of the structure were unable to be traced properly and this was attributed to the AFM tip profile used in this work.

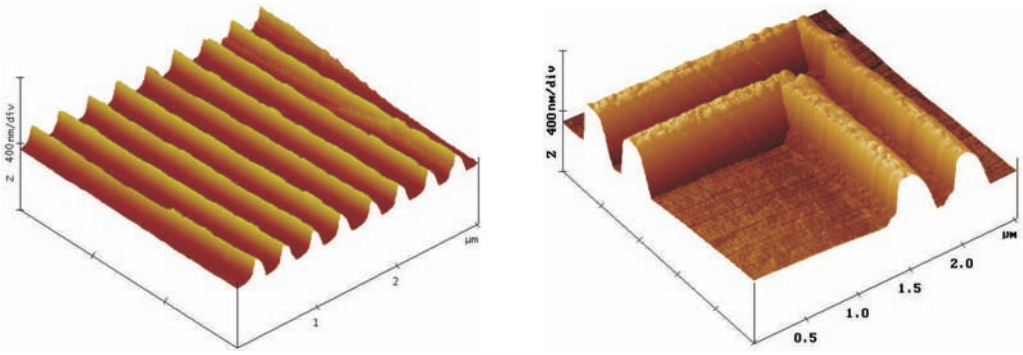

(a) A line structure of 90 nm in width and 250 nm in height

(b) A corner line structure with dimension of 150 nm width and 400nm in height.

Figure 4.6: The AFM images of the examples of the final 2-D structures on quartz substrate.

4.1.4 2-D Imprint Analysis

In 2-D imprinting, resist sticking on the mold cavity and the residual resist were the two major concerns. Figure 4.7 shows an AFM image of the missing imprinted structure that stuck on the mold cavity and the breakage of mold structures of feature sizes below 200 nm. Besides high friction, the twist movement during the de-molding process and rapid de-molding movement were suspected to cause these problems.

Figure 4.8 illustrates the de-molding analysis of a high aspect ratio structure below 200 nm feature size. Figure 4.8(a) shows the condition of resist reflow during imprinting and UV exposure. The notch formed at the mouth of the

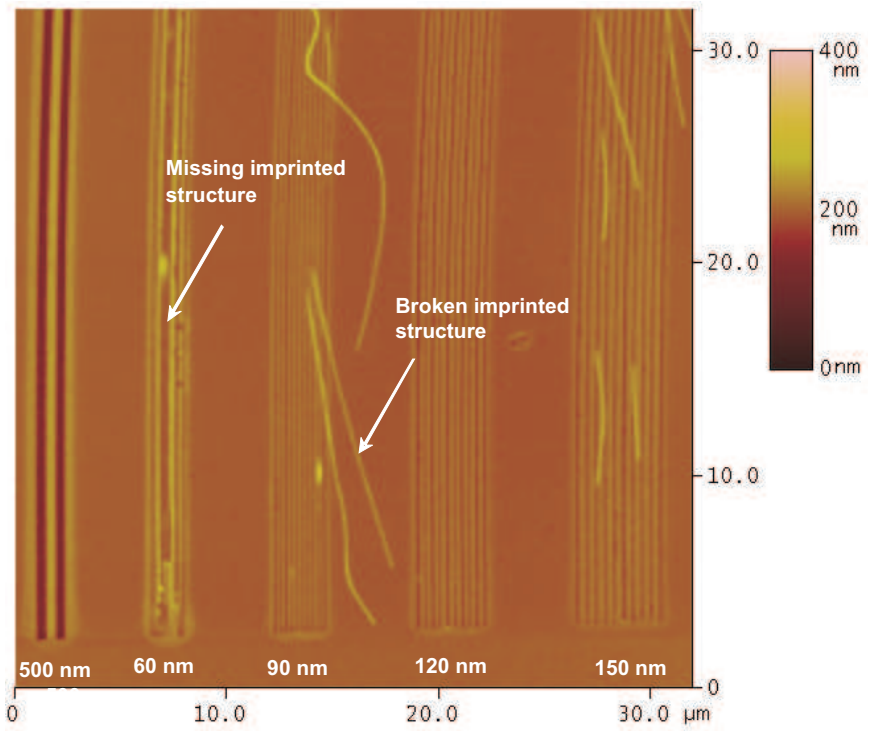

Figure 4.7: The AFM image showing the missing and broken imprinted structures after de-molding process.

mold cavities became the weakest point during the de-molding process. Figure 4.8(b) illustrates the condition during de-molding process. The large contact area on the vertical sidewall and the adhesion of resist/sidewall passivation layer interface induced high friction force between resist and mold. The imprinted resist structure will experience high stress and possibly break if the friction forces are above the yield strength of the resist material at that particular cross sectional dimension. The weakest points that might break are located at the edge mold structure. This presents a situation where adhesion between resist and substrate is working against the de-molding force. The residual resist layer opposite the mold cavity will delaminate and eventually break if the de-molding pulling force is higher than the adhesion strength.

Simulations using ABAQUS finite element analysis software [110] were carried out to simulate the imprinting process that led to the sticking problem. Figure 4.9 shows the result of the simulation. The simulation shows that during resist filling into the mold cavity, pressure was built up on the vertical sidewalls. The vertical sidewall of mold structure consists of CF_x polymer layer deposited

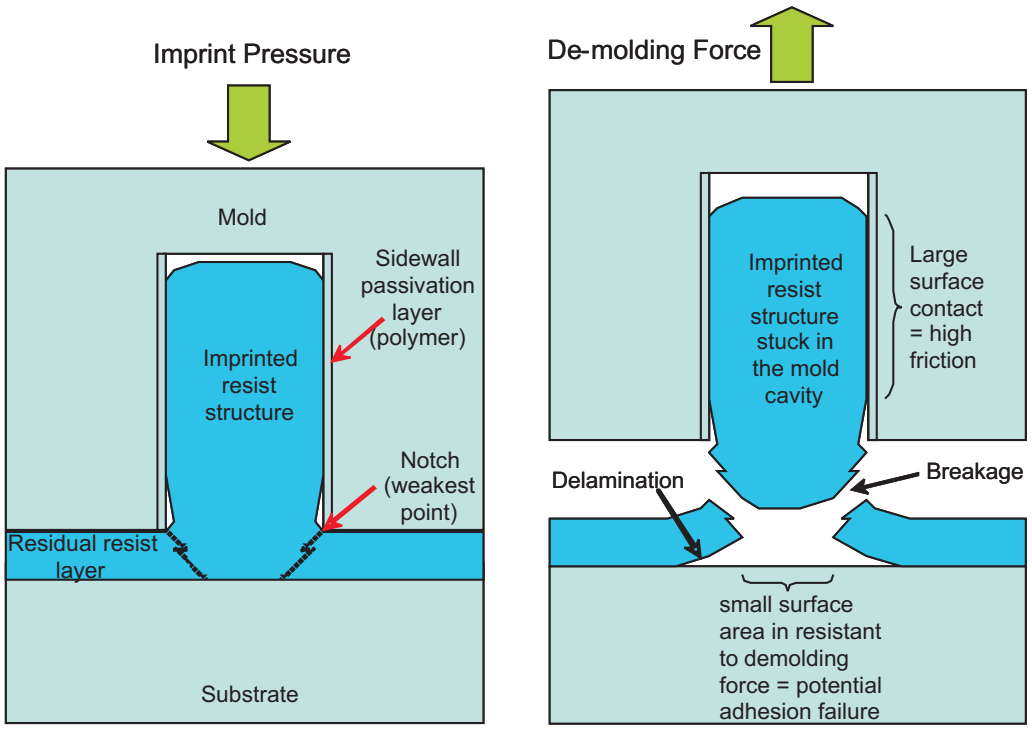

(a) Imprint (b) De-molding.

Figure 4.8: The schematic diagram showing an analysis of de-molding failures.

during the CHF_3/Ar plasma etching process. It has good adhesion when in contact with other polymer surface such as the Ormocomp resist used in this work. The combination of these factors causes a high friction between the vertical sidewalls and the imprinted resist structure which leads to sticking and breakage problems during the de-molding process.

The effects of imprint conditions such as initial resist thickness, temperatures, mold feature sizes and friction coefficient values between mold and resist surfaces have been investigated by using experiments and simulations in author's M.E thesis titled "Resist Deformation in NIL" [83]. In 2-D imprint, the residual resist thicknesses are a function of initial resist thickness. A larger imprinted resist height for periodic structures as compared to non-periodic structures owing to the difference in space available for resist reflow. The largest imprint height of periodic structures is achieved when the ratio of the initial resist thickness t_o over the mold cavity width W approaches unity. For the effects of mold feature sizes, less overall resistance caused a larger imprint height to be formed with $S/W = 1.0$ as compared to a mold with larger S/W (refer to Figure 1.8(a), sec-

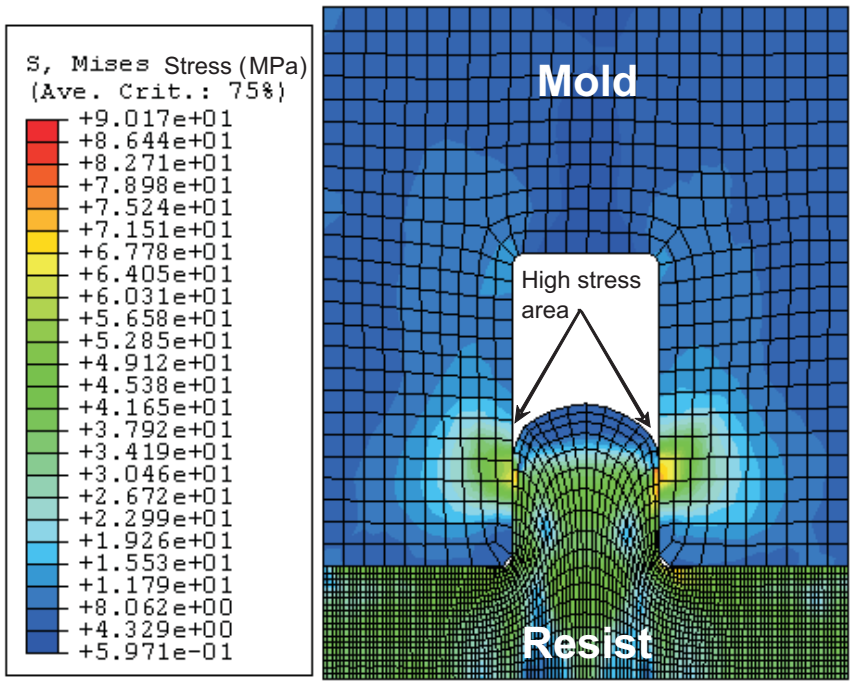

Figure 4.9: The simulation of resist reflow into a 2-D cavity using ABAQUS finite element software showing a high stress area on the vertical sidewall contact area which causes a sticking problem.

tion 1.4). Lower friction coefficient values resulted in lower residual resist thickness and would allow formation of a larger imprint height of periodic structures if compared to higher friction values [111].

The information of the above study applies to 2-D imprint in UV-NIL technique especially imprinting using high aspect ratio molds. As aimed for in every imprint process, in order to achieve a lowest possible residual resist layer, the process parameter such as initial resist thickness was optimized. For smaller feature size, the lower initial resist thicknesses are required for imprinting process. Since in this work, transparent molds with periodic line structures ranging from 60 nm to 500 nm were used, an initial resist thickness ranging 300 nm to 400 nm was found appropriate.

4.2 The Imprint of Three-Dimensional Structures

In 3-D imprinting, the pattern on the mold has to be the inverted shape of the intended 3-D structure. The mold making process of the inverted shape of the intended 3-D structure can be quite difficult. Hence, an imprint technique was used to fabricate the inverse shape of the mold from the master mold. This process is similar to a casting or moulding process widely used by the industry. It means that the master mold structures can be fabricated on any material and later replicated on the intended materials.
In this work, the master mold of quartz was impressed into Ormocomp, a transparent UV curable resist, which could then be used as a soft/daughter mold for the subsequent imprint step.
The pattern transfer onto the final substrate after the imprint process was the final task of this work. This was a little different compared to the pattern transfer in the mold making process. The existence of the residual resist layer of about 100 nm thick presented a great final challenge in completing the whole process.

4.2.1 Preparation

In the 3-D imprint, an Ormocomp resist from Microresist was used as the imaging layer for the first imprint step and a mr-UVCur06 resist from Microresist was used in the second imprint step. Ormocomp has excellent properties for UV transmission which was crucial as a transparent mold, while mr-UVCur06 has low viscosity which was essential to achieve a minimum and uniform residual resist thickness in Imprint 2.
The required resist thickness for Imprint 1 is dependent on the height of the master mold structure and the pattern density. It should not be too thick to avoid the shrinkage stress during the UV curing where a high stress is normally present at the edge region of the 3-D patterns. For this work, a 400 nm layer thickness was found appropriate in replicating the 3-D master mold. To achieve this thin layer, a 30% Ormocomp was spun coated on a quartz substrate at a spin speed of 3000 rpm for one minute and pre baked on a hot plate at 80^oC

for two minutes.

For imprint 2, the required initial resist thickness is more critical achieving a minimum residual resist thickness. In this work, a trial and error method was used to determine the right resist thickness guided by our previous modelling [83]. Another approach is by dispensing the resist using the drop-on-demand method as in $S-FIL^{TM}$ technology. A 400 nm of mr-UVCur06 resist thickness was found to be appropriate for this work to yield a residual resist thickness of below 100 nm. The resist was spun coated at 2800 rpm for 45 seconds and pre baked on a hot plate at a temperature of 80^oC for two minutes to achieve a 400 nm thickness.

Prior to the coating, quartz substrate was cleaned and surface treated using oxygen plasma to promote better adhesion at the interface between quartz and resist interface.

It was important to ensure that surfaces in contact during the imprint process had low surface energies to minimize the sticking problems. A surface wetting experiment was carried out to measure the wettability of the quartz surface versus other metal surfaces such as tungsten and NiCr or ceramic surfaces such as titania (TiO_2). As the objective of this work is to find alternatives for the chemical anti-adhesive layer, these materials have the potential to be a permanent anti-adhesive layer on the mold surface.

Surface wetting experiments were carried out to identify the wettability of the surfaces involved in the UV-NIL imprint process. Figure 4.10 shows the contact angle of different materials in a normal condition and after being coated with a FOTS anti-adhesive monolayer. In normal conditions, resists such as PMMA, Ormocomp and mr-UVCur06 have higher contact angles as compared to cleaned quartz and sputtered coated tungsten and titania.

Another method of minimising the sticking problem is by surface treatment using plasma. A contact angle up to 80^o can be achieved on quartz or silicon substrates when exposed to $SF_6 : CHF_3$ 1:1 plasma [112]. The resist surface can also be treated using fluoride containing plasma such as CHF_3 [90] in order to increase the contact angle. Table 4.1 shows the RIE recipes for the surface treatments of quartz and resist.

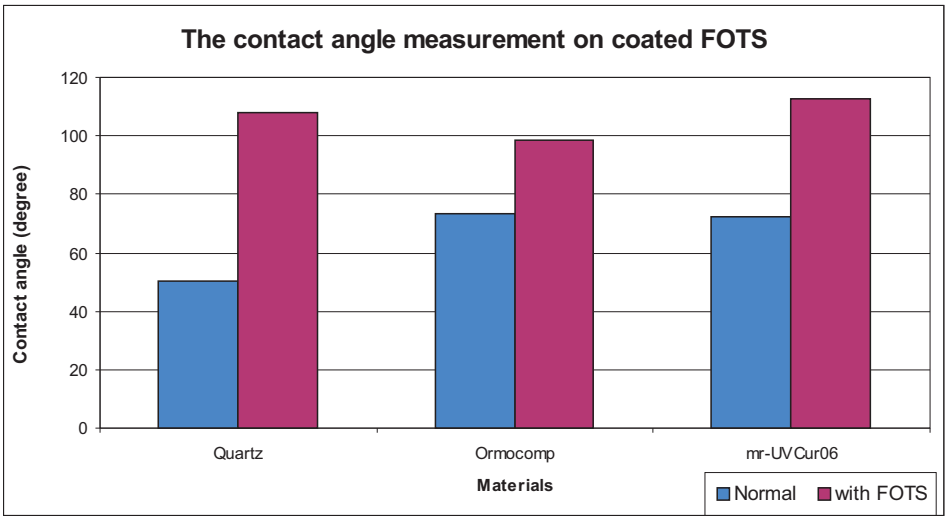

Figure 4.10: The contact angle measurement of the materials in normal conditions and after being coated with a FOTS anti adhesive monolayer

Table 4.1: The RIE parameter for surface treatment

	Quartz Surface	Resist Surface
Gases	SF_6/CHF_3	CHF_3
Flow rate	15.0 sccm/15.0 sccm	30 sccm
Pressure	28 mTorr	30 mTorr
Temperature	295 K	295 K
RF Power	50 W	100 W
Time	2.0 min	30 seconds
Contact angle	up to 80^o	up to 85^o

4.2.2 Imprint Process

The manual vacuum operated imprint tool was used in this imprint experiment to create a vacuum environment in order to reduce the air bubbles trapped in between the mold and the resist during the imprint process.

Replicating the 3-D structure of the master mold involved two imprint steps. The first imprint (Imprint 1) produces the inverted shape of the master mold while the second imprint (Imprint 2) produces the inverted shape of the first

imprint (Imprint 1) which became the replica of the original master mold.
Two 3-D test master molds were used in this work, the first was the 3-D rings structures and the other was the 3-D multilevel structures. Figure 4.11(a) shows the optical image of the 3-D ring mold structures in a 5 x 5 matrix with a 50 microns pitch and Figure 4.11(b) shows the enlarged SEM image of a single 3-D ring mold structure.

Figure 4.12(a) shows the optical image of the second 3-D master mold structure

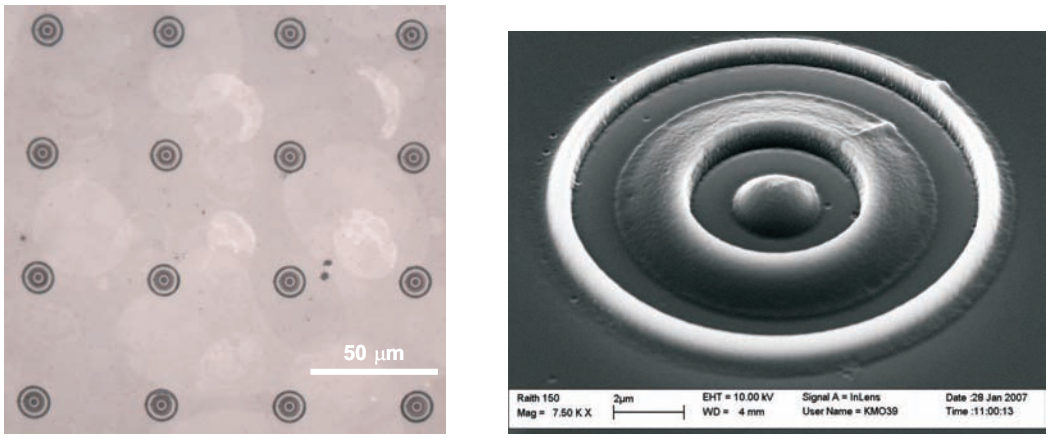

(a) An optical image (b) An enlarged SEM image

Figure 4.11: The master mold of a 3-D ring structure

which is the 3-D pyramid array with multilevel features in a matrix of 5 x 5 and a 50 microns pitch. Figure 4.12(b) shows the enlarged SEM image of a single 3-D multilevel master mold structure.

Imprint cycles with repetitive imprint pressures and UV exposure made resist

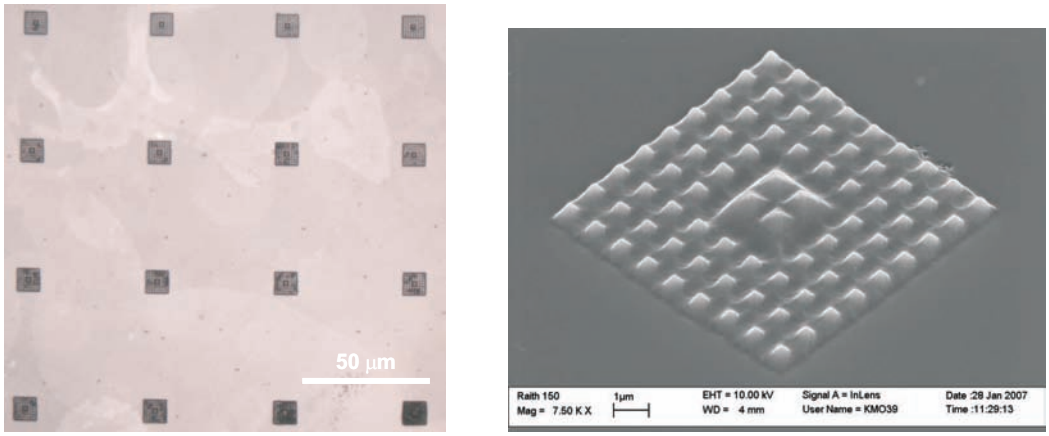

(a) An optical image (b) An enlarged SEM image

Figure 4.12: The master mold of a multilevel pyramid structure

stain and contamination particles stick hard to the quartz mold surface. Cleaning the stubborn resist stains and particles on quartz mold using normal solvents and ultrasonic baths was quite difficult. It could only be cleaned slowly by an oxygen plasma or burnt in a high temperature furnace. However, this type of cleaning will not guarantee the quartz mold surface will keep the original profiles and properties. It normally changed the quartz surface properties to have more adhesion to resist materials.

It was found that to have a thin layer of low surface energy material could prevent a direct contact of the stains with the quartz mold surface. In this work, the mold was coated with a 4 nm tungsten layer using a DC sputtering technique. The thin tungsten layer can be easily removed by a short SF_6 plasma for 10 seconds at a later stage if required. This was found to be useful for protecting the master mold surface from damage.

In this work, the filling of the 3-D cavities with the resist and the required initial resist thickness were investigated by a trial and error method. The 100 % cavity filling in the 3-D mold, the required imprint pressure and minimum residual resist thickness were optimized.

4.2.2.1 Imprint 1

The purpose of the first imprint was to mold the inverted shape of the master mold into a UV curable resist. Figure 4.13 illustrates the schematic diagram of the Imprint 1 process step.

A very thin monolayer of FOTS was used as an anti sticking layer on the

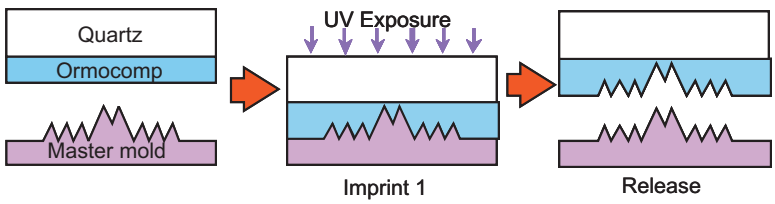

Figure 4.13: The schematic of the first imprint of the 3-D imprint step (Imprint 1)

quartz mold surface. It was deposited on a mold surface by a natural convection method in a petri dish at room temperature as explained in Section 2.2.5,

Chapter 2.

The 3-D mold was placed face up at the bottom of the imprint tool to ease the release of trapped air bubbles from the mold structures. The 400 nm thick Ormocomp resist coated on the quartz substrate with the face down was manually aligned on top of the 3-D master mold. The vacuum pressure of the mask aligner MA-6 which was set at 4 mbar was then activated and followed by UV flood exposure at a room temperature. Under 365 nm UV illumination, Ormocomp resist requires $300mJ/cm^2$ energy for curing, which is about an 8 minute exposure time using $0.6mW/cm^2$ illumination intensity.

The Imprint 1 results were imaged using an optical microscope and AFM. In AFM, a STING tip from Mikromash as described in section 2.1.4.2 was used to trace the profiles of the 3-D imprint cavities.

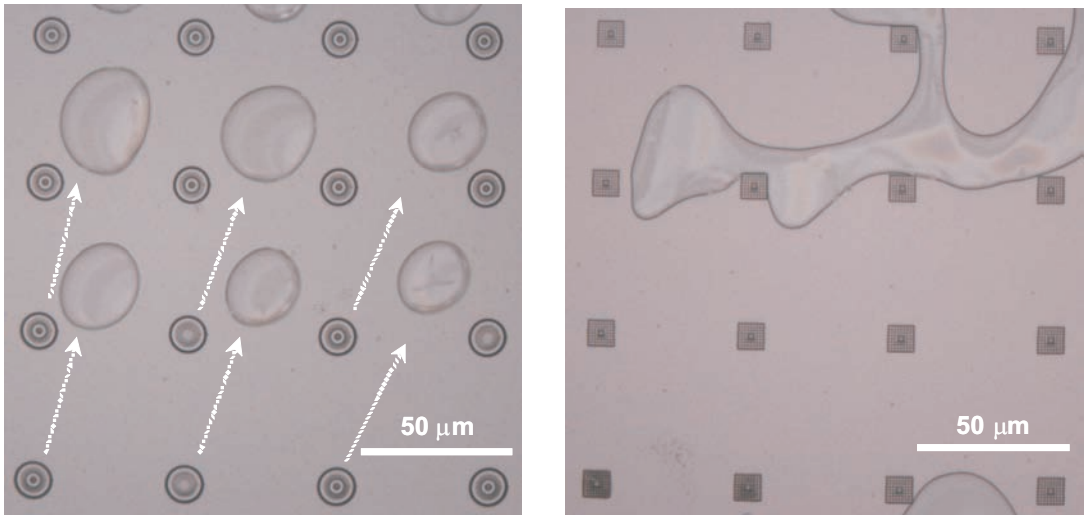

(a) 3-D ring structure (b) multilevel pyramid structure

Figure 4.14: The optical image of the inverted shapes of the master mold on Ormocomp resist after the Imprint 1 process.

Figure 4.14(a) shows an optical image of the imprinted 3-D ring structures on an Ormocomp resist layer. The 3-D ring mold profile is a confined structure which allows the air bubbles to be trapped in between the structures. When the mold further penetrated the resist layer, the resist reflow pushed the trapped air bubbles away in an outward direction from the center of the mold as shown in the optical image. The arrows show the direction of the resist reflow during

imprinting.

Figure 4.14(b) shows an optical image of the imprinted 3-D multilevel structure on an Ormocomp resist layer. The marks of the trapped air bubbles flowing in an outward direction can also be observed.

Figure 4.15(a) shows a close-up AFM image of the associated imprint results

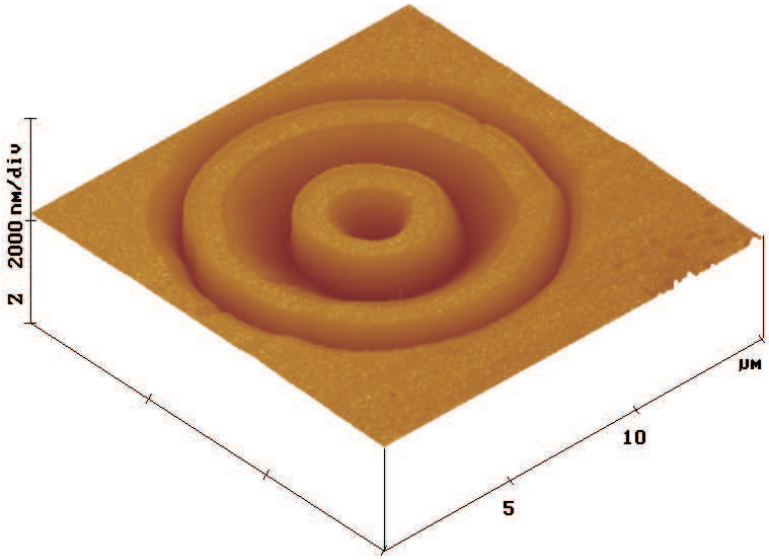

(a) An AFM close up image

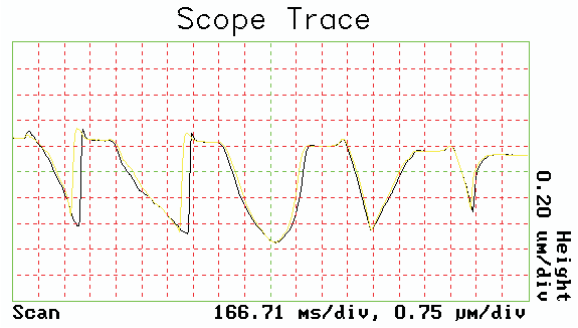

(b) cross sectional traces

Figure 4.15: The replication of of a 3-D ring structure on Ormocomp resist after the Imprint 1 process which will be used as the soft/daughter mold in the subsequent imprint step.

of the 3-D ring mold that was used in this work. The master mold profile was faithfully replicated. Figure 4.15(b) shows the AFM cross sectional traces of the imprint profile.

Figure 4.16(a) shows the AFM image of the associated imprint results of the 3-D multilevel molds used. Figure 4.16(b) shows the AFM cross sectional traces

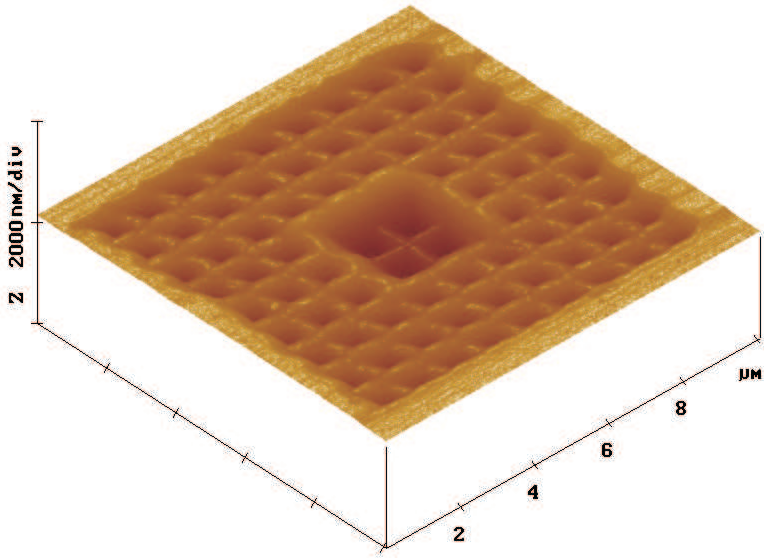

(a) An AFM close up image

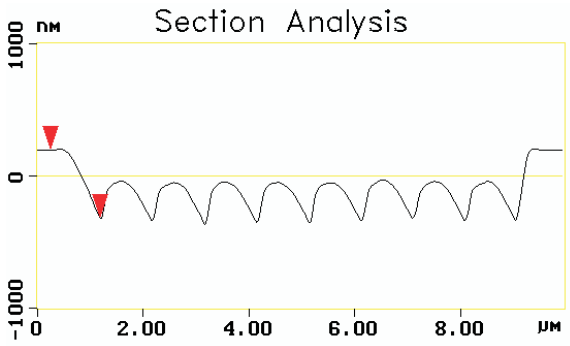

(b) cross sectional traces

Figure 4.16: The replication of a multilevel pyramid structure on Ormocomp resist after the Imprint 1 process which will be used as the soft mold in the subsequent imprint step.

of the imprint profile at lower pyramid level.

The soft mold for a repetitive imprint requires a material which is hard, solvent resistant and can withstand a long UV exposure. In order to use the imprinted Ormocomp resist as a soft mold in the subsequent imprint step, the soft mold was hard baked at 185^oC for 2 hours to improve its hardness and enhance its solvent resistance properties.

4.2.2.2 Imprint 2

The purpose of the second imprint is to replicate the inverted shape of the master mold onto another UV curable resist layer in order to create the positive original 3-D structure. Figure 4.17 shows the schematic diagram of Imprint 2 process steps.

The relationship between the resist reflow and cavity filling versus the initial

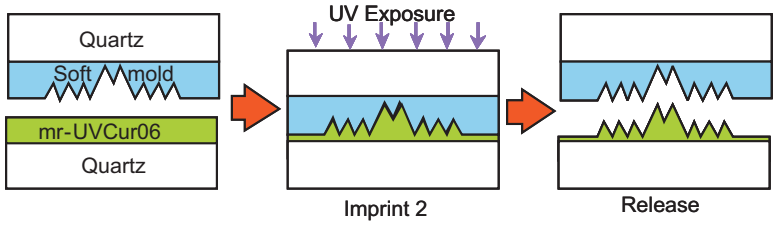

Figure 4.17: The schematic of the second imprint of the 3-D imprint step (Imprint 2)

resist thickness was investigated. To achieve a minimum residual resist thickness, a specially formulated mr-UVCur06 resist which has low viscosity was used. With proper optimisation, a 10 nm thick residual resist layer could be achieved.

For Imprint 2 process, the 365 nm UV source was used to expose the samples for 2 minutes at room temperature. A post imprint bake at a temperature of 120^oC on a hot plate for 5 minutes to make it harder as masking layer against RIE was carried out after the sample was released from the soft mold.

Imprint 2 results were imaged using optical microscopes and the AFM technique. Figure 4.18(a) shows the optical image of the imprinted 3-D ring structure on the mr-UVCur06 resist using the 3-D ring soft mold. Figure 4.18(b) shows the close-up AFM image of the imprinted 3-D ring structure.

Figure 4.19(a) shows the optical image of the associated imprint results of the multilevel soft mold used. Figure 4.19(b) shows the close-up AFM image of the imprinted 3-D multilevel structure on the mr-UVCur06 resist.

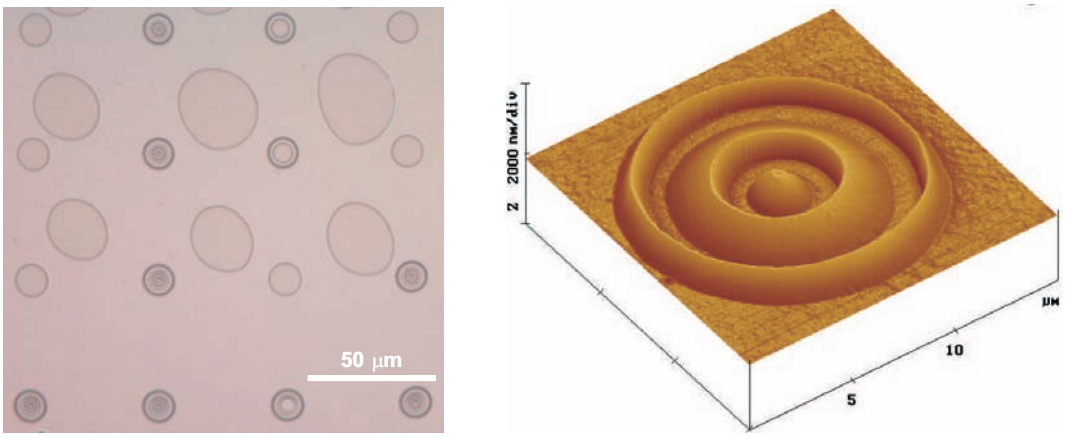

(a) An optical image (b) An AFM image

Figure 4.18: The molding of the 3-D ring soft mold structure on the mr-UVCur06 resist.

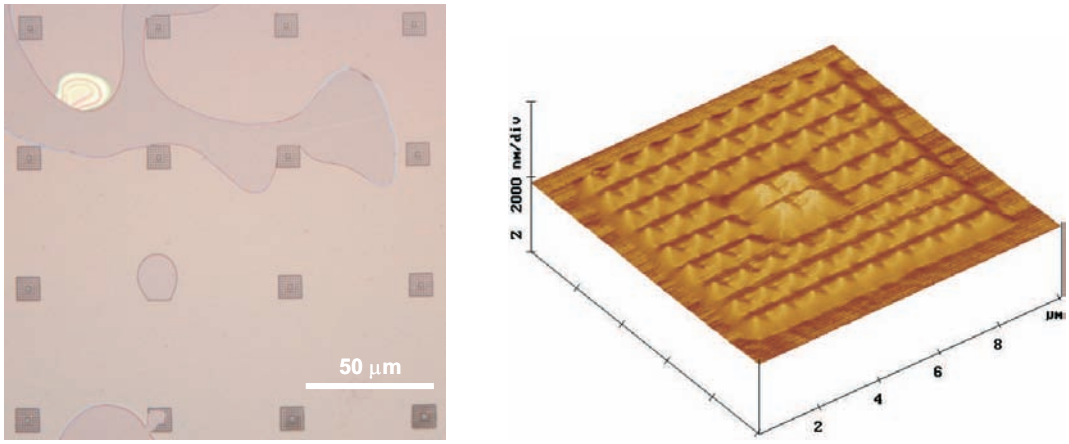

(a) An optical image (b) An AFM image

Figure 4.19: The molding of multilevel pyramids soft mold structure on the mr-UVCur06 resist

4.2.3 Final Pattern Transfer

The final challenge of this work was on the optimization of the final pattern transfer onto the final substrate as illustrated in Figure 4.20. A single-step RIE process by simultaneous descumming residual resist layer and 3-D pattern transfer onto quartz substrate was attempted. This dual process approach minimized the etching time and avoided the multiple etching steps. CHF_3 plasma makes the resist harder to etch than the quartz substrate but the introduction of an optimized small volume of oxygen mixed with the CHF_3 equalizes the etching rate between the resist and quartz substrate. An optimized 97%/3% of CHF_3/O_2 gases in RIE plasma was used in achieving the 1:1 selectivity of resist

to the quartz substrate.

As discussed earlier, this pattern transfer process is dominated by the poly-

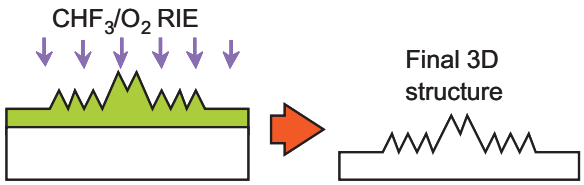

Figure 4.20: The schematic of the 3-D final pattern transfer)

merization reactions because the presence of polymer resist decreased the F/C ratio. This etching process requires very low operating pressure to increase the mean free path. An optimised RIE parameter used in this experiment is tabled in Table 4.2. An etching rate of 10 nm/min was achieved in this experiment.

Figure 4.21(a) shows an AFM image of the final result of the 3-D ring shape on

Table 4.2: The optimized CHF_3/O_2 RIE parameter for final 3-D pattern transfer onto quartz substrate

RIE parameters	final 3-D pattern transfer
Gas	CHF_3/O_2
Flow rate	16.5 sccm/0.5 sccm
Pressure	6 mTorr
Temperature	295 K
RF Power	130 W
Selectivity (resist:substrate)	1.0 : 1.0
Etch rate	10 nm/min

quartz substrate. The domination of polymerization reactions has resulted in CF_x deposited on the highest points of the 3-D structure.

Figure 4.21(b) shows an AFM image of the final result of the 3-D multilevel structure on quartz substrate. The CF_x was deposited on the highest point of the pyramid peaks forming pillar like structures. These pillars were formed by the CF_x passivation process when lack of oxygen content in the gas mixture during the plasma etching process as explained in section 3.1.4.1.

It was very difficult to achieve a consistent flow rate of oxygen gas supply at 0.5

sccm during a long etching process of about 2 hours. The controllable range of the micro flow controller (MFC) used in the RIE system (Plasma OxfordPlus80) is from 0 to 50 sccm. A 0.5 sccm oxygen flow rate which is at the lower end of the MFC range might not accurately controlled. A better results could be achieved if the oxygen content in the gas mixture is maintained. Increasing to a higher flow rate but with similar gases mixture percentage (97%/3% of CHF_3/O_2 gases) increases the etching pressure which leads to a higher surface roughness. This is one of the limitations of the process and equipment used in this work.

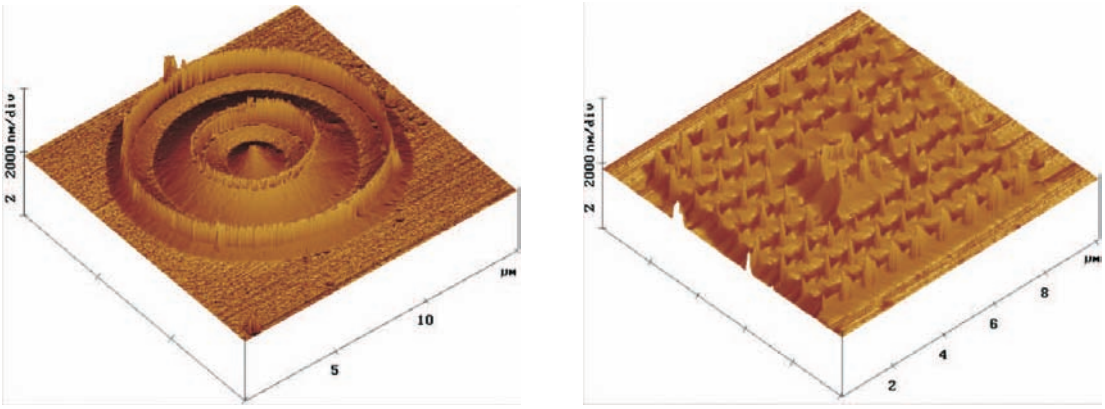

(a) 3-D ring structure (b) Multilevel structure

Figure 4.21: The final 3-D structure etched by the final RIE pattern transfer

4.2.4 3-D Imprint Analysis

The imprints of up to 35 cycles were achieved using the anti-adhesive layer of FOTS was coated on the quartz mold surface in the Imprint 1 process. This is in contrast to only up to 5 imprint cycles were successful without the FOTS. In the Imprint 2 process, up to 26 cycles were achieved with the FOTS coating on the soft mold (Ormocomp), while without FOTS coating, only 3 imprint cycles were successful. Imprint failures mostly because of sticking and particles contamination were observed.

One of the weaknesses of the Ormocomp resist was that it became brittle after a long UV exposure. The material brittleness combined with stress cycles in

the imprint process make the Ormocomp soft mold easily cracked after about 5 imprint cycles. Micro-cracks on the soft mold surface limited the repetition of the imprint cycles.

With a 5 nm coating of sputtered TiO_2 on the soft mold as a permanent anti-sticking layer is formed. The mold surface cleanliness was improved and up to 15 repetitive imprint cycles could be completed. Cracks in the soft mold were observed after 15 imprint cycles, which caused the resist to stick to the mold surface. Figure 4.22(a) shows the sticking problem of the imprinted 3-D ring structure on the Ormocomp resist during the Imprint 1 process, while Figure 4.22(b) shows a similar sticking problem of the imprinted 3-D multilevel structures on the Ormocomp resist.

The imprint pressure must always be at a low level (below 100 mbar) to avoid

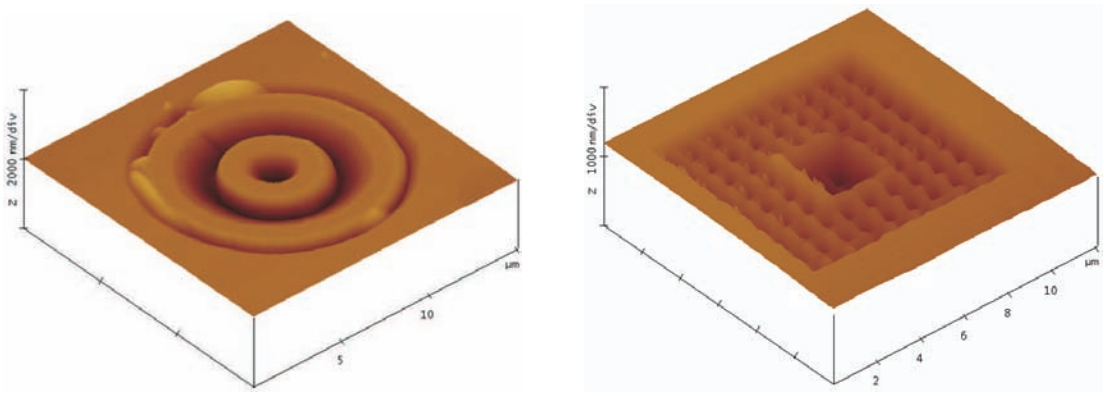

(a) 3-D ring structure (b) multilevel structure

Figure 4.22: The sticking of 3-D imprinted structure on Ormocomp resist.

such sticking issues, soft mold breakage as well as maintaining cleanliness. A better resist system is recommended for a reliable soft mold with an improved ductility and a shorter curing time.

In imprint 2, the disadvantage of a low viscosity $(14mPas)$ mr-UVCur06 resist was its penetration into mold cracks and microcavities causing sticking issues and mold breakages at high stress points.

Other than using a release agent as an anti-sticking layer, the sticking problem can also be minimized by resist surface treatment to change the surface properties.

The final pattern transfer process has not yet achieved satisfactory results be-

cause of difficulties in maintaining a very small oxygen gas proportion in the mixing chamber, and maintaining its flowrate in the RIE system during a long etching time (more than 2 hours). Other RIE etchant gas such as sulfur hexafluoride (SF_6) is proposed for future work replacing CHF_3.

4.3 Summary

The replication of 2-D and 3-D structures has been demonstrated. In 2-D imprinting, two types of mold were used: the transparent mold and the transparent mold with a NiCr absorber. Only a single imprint step is involved in 2-D imprinting while in 3-D imprinting two imprint steps are involved. A 400 nm thick Orcmocomp and mr-UVCur06 resists were used in Imprint 1 and Imprint 2 processes respectively. A 3-D ring with a height of 600 nm and a multilevel pyramid array with each pyramid dimension of one micron square base and 600 nm in height were replicated.

The assistance of anti adhesive coating using FOTS SAM on the surfaces in contact during imprinting was successfully demonstrated. In finding an alternative permanent anti adhesive coatings, Tungsten and TiO_2 were found to be effective. In Imprint 1, coating the quartz mold with a 5 nm sputtered tungsten has protected the mold surface from the stubborn imprint stains. The Ormocomp and mr-UVCur06 resist surfaces were treated with CHF_3 plasma to lowered its surface energy. In imprint 2, coating the Ormocomp soft mold with a 5 nm TiO_2 improved the imprint up to 15 repetitive cycles.

The final pattern transfer process using CHF_3/O_2 plasma has not achieved satisfactory results because of difficulties in maintaining a very small oxygen gas content in the mixing chamber, and maintaining its flow rate in the RIE system during a long etching time (2 hours).

Chapter 5

DISCUSSION AND RECOMMENDATIONS

This chapter discusses the general issues that are important in NIL technology as well as the specific limitations of this research work. Based on these limitations, a number of recommendations are outlined for future work. The directions and the future promises for this technology are also outlined.

NIL is still considered an immature technology where some important issues such as acceptable defects density, suitable resist polymers, master molds, overlay accuracy and throughput are being studied by various research groups and industries around the world. These have been demonstrated by the continuous increase in publications and specialized international conferences on these subjects.

There are stringent requirements imposed by the semiconductor industry which NIL has to meet, however promising applications in new areas are emerging such as in patterned media. As long as the enthusiasm and focus are there, this technology will continue to find new applications and no additional expenses for scaling down.

This work has produced a number of encouraging results, however a few limitations on processes, tools and materials have hindered the anticipated wide spread use of this technique.

UV-NIL study is a huge research area and the scope of 3-D UV-NIL still demands an extensive amount of work before mass production realization. Stud-

ies in this research areas are inter-related which requires comprehension of many aspects of science and engineering such as in plasma chemistry.
Most of the proposed work in this thesis was accomplished except in few area owing to unavoidable limitations especially in the equipment and process used. Hence, a number of recommendations for future work have been outlined at the end.
Even though there are increasing opportunities in NIL technology in terms of potential applications, numerous challenges are waiting ahead. Some of these challenges have become the gating factor in deploying the technology especially in the semiconductor industry. However, success stories such as "Tera Era" Hitachi GST have proved that this technology will be the major technology player in the near future.

5.1 General NIL Issues

As immature technology, NIL including UV-NIL faces a number of important issues waiting to be resolved. Generally, issues in NIL technology can be roughly grouped into four major categories; particle related defects, irregularities in the polymers, overlay accuracy and throughput [113]. Other minor issues are not discussed here. This work has addressed some of the issues such as elimination of the multilevel alignment requirement by using a transparent imprint mold with multilevel features.

5.1.1 Particle Related Defects

One of the disadvantages of 1:1 pattern definition using an imprint is that it replicates the exact size of the defects compared to optical lithography's 4:1 pattern definition where it shrinks the defects size to a quarter of the actual size. Majority of defects are from particle contamination. Defect density is dependent on the minimum size considered as a defect and the sensitivity of the inspection system used to detect the particle defects. As a general guideline, a

defect level of less than one $defect/cm^2$ should be met before it can be deployed as a manufacturing technology especially in semiconductor industries. Figure 5.1 shows the particle defects reduction monitored by Molecular Imprint Incorporation (MII) [114]. Up to date, the defect level down to about 2 $defect/cm^2$ is achievable. However, this has delayed the deployment of this technology into semiconductor manufacturing lines, but some other applications may tolerate a certain defect level such as media storage application and MEMS.

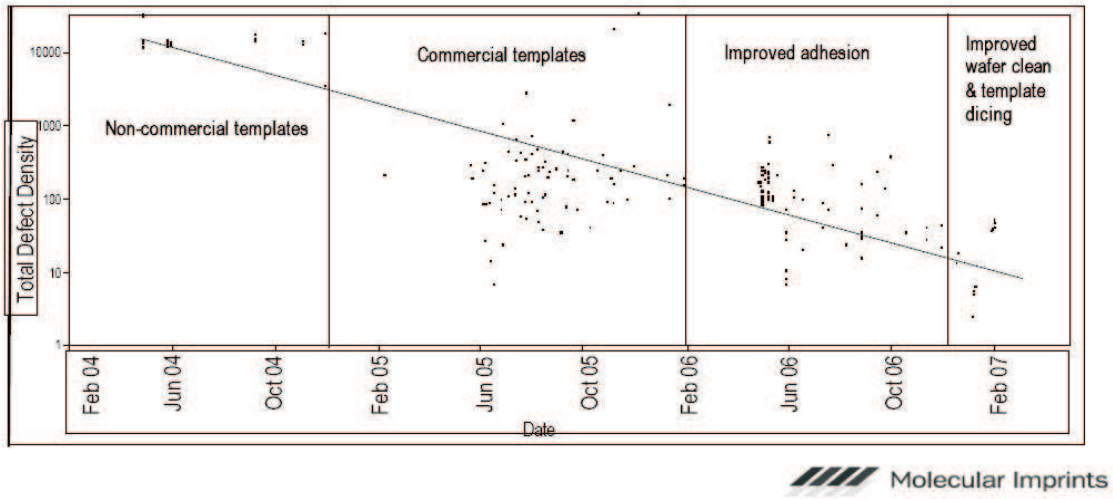

Figure 5.1: The defect density monitored by Molecular Imprint Inc. [114].

5.1.2 Irregularities in Polymers

In achieving a uniform residual resist layer thickness during imprinting, the required resist thickness for the imprint layer must match the mold pattern density to minimize the resist reflow. The concept "drop on demand" by MII where a low-viscosity resist, delivered by ink-jet head has demonstrated better residual resist uniformity compared to spin coated resist e.g. 10nm residual resist. Another approach of "capacity-equalized mold" for a pattern density variation mold has also improved the uniformity [115].

Since NIL involves contacting two material surfaces together in order to replicate the hard surface profile onto soft surface material, resist sticking to the surface material has been an important issue from the early days of this technology.

However, there have been a lot of surface-chemistry engineering activities going on to strengthen and improve the UV cured polymers properties so that the minimum sticking problem is maintained/achieved.

5.1.3 Overlay Accuracies

Overlay accuracy has been an issue for a long time especially on multilevel structures, even with current optical lithography technology. When feature sizes shrink further, overlay becomes more stringent. No alignment system currently exists for NIL that is capable of the alignment required by the semiconductor industry. The semiconductor industry for a 45 nm node requires accuracy of 18 nm, 3σ tolerance [116]. σ is the standard deviation of the placement.

In 1999, alignment accuracy of 1 micron was demonstrated using commercially available equipment [117] for imprinting. Huge efforts have been made in this matter by many research groups around the world with a few techniques being developed [118]. The results were encouraging as accuracy down to 50 nm had been demonstrated by EVG and was improving over time. MII is currently working on $\pm 6nm$ accuracy. This should solve part of the problem of this technology in few years time down the road.

The use of a transparent mold allows not only UV curing through it, but also optical alignment. Alignment in NIL is much better because less distance (no gap between the mold to resist) between mold and substrate as compared to a large gap between the mask and substrate in optical lithography. The contribution of the transparent mold and multilevel structures from this work eliminates the multilevel alignment requirement from current technology.

5.1.4 Throughput

To achieve a higher yield in manufacturing lines, a small size mold is used in repetitive imprint steps on large area substrates. Lower defects and high pro-

cesses yield have been demonstrated by $(S - FIL^{TM})$ technology [30]. MII has produced a series of equipment for this technique [114] which has demonstrated improved capability and reliability as well as process yield. The only setback to this technique was the low throughput of about 5 to 10 wafers per hour (wph) as compared to current optical lithography technology. The semiconductor industry requires a lithography system that can produce about 20 to 25 wph in their manufacturing lines to avoid a bottleneck situation. However, the NIL system throughput is improving from time to time and became less priority because of low tool cost. For a new product introduction which is running in a low volume manufacturing mode, the high throughput requirement becomes less of a priority compared to the quality/yield.

5.2 Limitations of This Work

The 3-D pattern transfer is the most critical process step in this research work. As the aim of this work is to produce micro/nanostructures of optical devices, the general guidelines of the overall surface roughness $R_{q(rms)}$ should be less than 5 nm. However, there was a limitation in the conventional RIE tool where the lowest achievable operating pressure was about 5 to 6 mTorr only. At low operating pressure, a smoother surface and a higher etching rate are expected. Using UC Nanolab's Oxford Plasma 80plus RIE system, the process becomes unstable at a process pressure below 6 mTorr. Because of this limitation, the benefits of very low process pressures (less than 6 mTorr) were unable to be realized.

In the present study, two photoresists were compared for 3-D patterning. In an earlier work, the negative resist of Microresist's ma-2400 series resist and Hydrogen Silsequioxane (HSQ) were chosen to create 3-D structures and to compare the resultant patterns. Unfortunately the unavailability of the HSQ resist at the time of this work has hampered the comparison study.

The manual imprint tools used in this work have less control over imprint parameters such as pressure and de-molding. An attempt to manipulate Karl

Suss mask aligner (MA-6) to function as a semi-automated imprint tool was not achieved because in the MA-6 system, a wafer edge correction (WEC) routine that is performed at every loading made a contact between the mold and the resist prior to the imprint step. In addition, MA-6 releases the mask using a pneumatic controlled system which does not suit the de-molding process requirement of gradual movement. This preset step had reduced the evenness of the resist surface as well as the mold cleanliness, and induces de-molding process failures.

5.3 Recommendations for Future Work

The research work was carried out in two phases; mold fabrication and imprint processes. The mold fabrication process using the EBL technique was well characterized with established tools, but most of imprint works were based on manual tools of which some parameters were difficult to measure. Further work is recommended on proper imprint tools to achieve a better characterized process such as imprint pressure and de-molding.

Achieving a smooth surface in 3-D RIE requires a low process pressure (less than 6 mTorr), which is difficult to realize using conventional RIE. Future work should explore other process options such as ICP-RIE, other gases mixtures. This might yield improvements in process stability, higher etch rate, better profile control and reproducibility. The results of this work are important for many applications including anti-reflection coatings, optical disks and biochips.

A number of things have been observed during the experimental work such as the growth of passivation layers during 3-D etching as discussed in section 3.2.3.2 and shown in Figure C.1 and Figure C.2 of Appendix III. This is the area that requires more understanding but no time to look further.

In 3-D patterning, only one type of resist material was characterized. HSQ or new resist materials should be characterized as a comparison study. This will be explained in details below.

5.3.1 Processes and Equipments

In this work, quartz etching process was carried out using a conventional RIE method which has many limitations. On the other hand, an inductive coupled plasma reactive ion etching (ICP-RIE) dual source system can produce a higher plasma density than the conventional RIE because the power is transferred into the bulk plasma via the magnetic field from the inductive coil. As a result, a higher etch rate, better profile control, uniformity and selectivity can be achieved. ICP-RIE has less radiation damage and contamination, and can operate at a much lower pressure (less than 10 mTorr) which has many advantages especially for etching a high aspect-ratio structure and 3-D structures as in this work. A high etching rate of quartz substrate can be achieved using the ICP-RIE system [119]. Further investigation on its capability is recommended.
Sulfur hexafluoride (SF_6) is another possible RIE etchant gas that can be used to etch quartz together with resist polymer [120]. More work on this area is suggested especially by using the ICP-RIE system.
The results of this imprint work are based on the manual tools that have many limitations in controlling the parameters such as pressure and a method of releasing the mold from the imprinted resist (de-molding). Future work should focus on a more automated system which has better control of the process parameter. Many research imprint systems manufactured by various companies are now available in the market. The EVG 620 UV imprint system which is newly installed at UC Nanolab should be able to perform better process and material characterizations.
Other than the EBL technique to fabricate the 3-D micro/nanostructures, Focus Ion Beam (FIB) technique is the latest attraction [48]. Ion has a larger mass than electron and transfers more energy efficiently to the resist with less scattering. It has lower secondary electron energies and has a shorter range than electron which produces high-resolution patterns without proximity effects.
Plasma is a complex process which requires more understanding in its reactions. The polymerization and sidewall passivation processes are not fully understood. More thoughts and experimental works should be performed to give better understanding of these processes.

5.3.2 Materials

Ormocomp is a very good resist material in UV transmission and suitable to be used directly as optical devices. Its only disadvantage is its brittleness when used as a soft/daughter mold in the imprint process. Long UV exposures made the material too brittle and cracks were propagated from the high stress points when used as a soft mold in the repetitive imprint cycles. The microcracks were causing sticking after about 15 imprint cycles. To be used as an imprint mold, modification of the formulation of this material has been carried out by the manufacturers and the new Ormostamp resist created which is recently become available in the market.

HSQ is another potential resist for 3-D pattern using EBL. The available stock (flowable oxide, Fox16 from Dow Corning) in UC Nanolab was long time expired and the few attempts to define 3-D patterns on it were unsuccessful owing to an increased sensitivity to the proximity effects. The difficulties in getting a fresh sample in small amounts hindered us in studying this material as 3-D pattern resist using EBL. The late arrival of the fresh Fox16 sample at the end of the scheduled work did not help much. Future work should make an attempt to characterize this material or other new material as a 3-D pattern resist for a masking layer and/or as a 3-D mold.

A surface wetting study is very useful for this work as a method to quantify one of the surface properties. More investigation should be carried out on future potential non-stick materials. Titania deposited using pulsed-pressure metal organic chemical vapor deposition (PP-MOCVD) is a potential material as a permanent anti-adhesive coating with a capability of step coverage [121]. A contact angle up to 120^o can be achieved as shown in Figure 5.2 [122].

5.4 Future of NIL Technology

Even though at this moment of time, it is to soon to say that NIL technology will be the absolute replacement for the current optical lithography technology for device manufacturing. IC manufacturer seems still spending times trying to

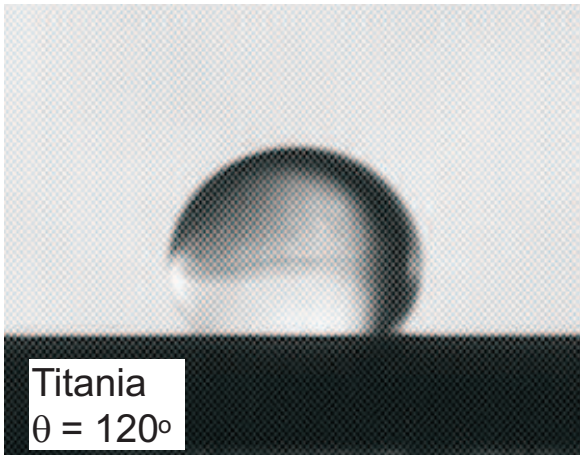

Figure 5.2: The contact angle measurement on PP-MOCVD titania surface

make EUVL working in their manufacturing lines after spend huge capital investments and time. In contrast, the high resolution, low cost and multilevel/3-D capability that demonstrated by NIL technology have promised applications in various fields of science and technology. For example, high resolution lines as small as 5 nm, with pitch of 12 nm has been achieved by Nanonex Inc. as shown in Figure 5.3. This has big potential in future device applications.

In future, this technology should become the first choice for new device fabri-

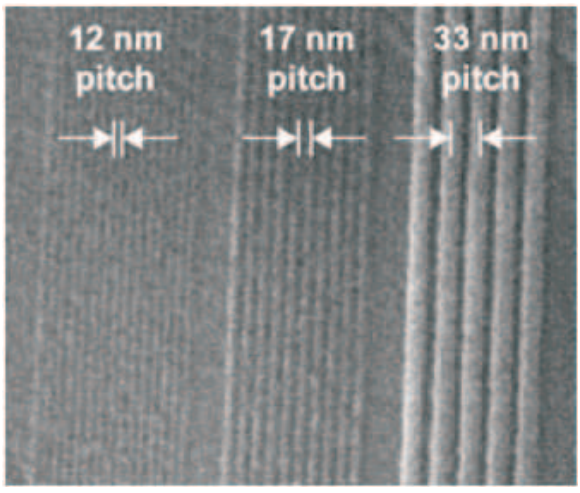

Figure 5.3: Shown on far left are 5 nm lines with pitch of 12 nm imprinted by Nanonex Inc.

cation, for its flexibility in trading between yield, throughput, defect levels, and many other parameters. Research communities around the globe are actively working on researches based on customized device application and fabrication

processes with specific conditions on the targeted results. Here, we can predict that NIL technology is the most suitable for other customized applications.
For example, in recent development, Hitachi Global Storage Technology Inc (Hitachi GST) has adopted UV-NIL technology for producing an 86 nm pitch of magnetic dot arrays in patterned media which is equivalent to about 100 $Gbyte/in^2$ of storage density [123]. Lately, the capability of imprinting 1 $Tbit/in^2$ in ultrahighly packed dot arrays with a dot diameter of less than 15 nm and a dot pitch of 25 nm x 25 nm has been demonstrated [124].
One of the best example of the proven NIL success, is the high volume manufacturing of HDD in the Hitachi GST second generation "Tera Era" product Deskstar 7K1000.B with the magnetic dot arrays of about 30 nm to 50 nm. The limitations were on the track width of the read/write head, not the fabrication process. This product has now been available on the market since July 2008.

5.5 Summary

A number of important issues and recommendations for future work especially on processes and equipment as well as the potential of other materials, have been discussed. NIL is still considered an immature technology where some important issues such as acceptable defects density, suitable resist polymers, overlay accuracy and throughput are being studied by various research groups and industries around the world. These have been demonstrated by the continuous increase in publications and specialized international conferences on these subjects. The contribution of the transparent mold and multilevel structures from this work eliminates the multilevel alignment requirement from current technology.
This work has produced many encouraging results, however a number of limitations have prevented some other major findings such as plasma etching of quartz at a very low operating pressure. There were limitations to the RIE system where the lowest achievable operating pressure for RIE was about 5 to 6 mTorr. The RIE plasma process becomes unstable at a process pressure below 6

mTorr. At low RIE operating pressure, a smoother etched surface and a higher etching rate were expected. The benefits of very low process pressures (less than 6 mTorr) were unable to be realized.

Hydrogen Silsesquioxane (HSQ) is a potential 3-D patterning resist as ma-N2400 series resist but its unavailability had hampered the comparison studies. The manual imprint tools used in this work have less control of the imprint parameters. An attempt to manipulate the MA-6 mask aligner to function as an imprint tool was not achieved.

There are huge opportunities in this new technology in terms of potential applications, however, numerous challenges are waiting ahead. Some of these challenges became the deployment's show stopper in replacing the current technologies. However, success stories such as in Hitachi GST have proved that this technology will be the major technology player in the near future. The future of this technology looks uncertain for semiconductor manufacturing but promising in new application areas.

Chapter 6

CONCLUSIONS

2-D and 3-D patterning using the UV-NIL technique have been demonstrated and the mold making and imprint replication processes for 2-D and 3-D structures have been developed. 2-D and 3-D structures have been fabricated on quartz substrate using EBL and dry etching techniques with simplified process steps. The 2-D structures were fabricated using an additive pattern transfer method while the 3-D structures were fabricated using a subtractive pattern transfer method.

The 3-D mold profiles were created on the ma-N2403 negative tone photoresist using the Raith-150 EBL tool with variable dose controlled exposure. A variable e-beam dose was used to obtain a resist contrast curve to determine the gradient of various 3-D structures. For a 600 nm layer thickness of ma-N2403 resist, the e-beam critical energy was set at 6.25 keV. A higher acceleration voltage of 20 keV was used for the conductive polymer (PEDOT/PSS) top coating method and EBL exposure with line dosages ranging from 0.6 pC/cm to 42.0 pC/cm were used for 3-D resist contrast approach. A linear resist contrast profile was obtained with a negative tone photoresist and subsequently was utilized as the 3-D masking layer. The 3-D pattern was transferred onto the quartz mold substrate by an optimized single-step reactive ion etching (RIE) process with selectivity resist-to-substrate of 1:2 using fluorinated plasma CHF_3/Ar.

The main issues in EBL are surface charging, electrons backscattering and proximity effects. In the fabrication of 2-D structures, this was solved by using thin metallic coatings and conductive polymer PEDOT/PSS as a charge dissipation

layer. 2-D structures with feature sizes below 100 nm and high aspect-ratio of up to 1:10 has been demonstrated. The use of critical acceleration voltage and high accelerating voltage in conjunction with conductive polymer PEDOT/PSS have suppressed the surface charging effects in the fabrication of 3-D structures, where feature size down to 300 nm had been demonstrated. The high surface roughness caused by nanomasking effects in the 3-D etching is the result of the combination of plasma bombardment products, etched electrode particles and dominating polymerization reactions at a high operating pressure. A very low RIE operating pressure was found to produce a smooth etched quartz surface. A surface roughness of below 2 nm was achieved when the RIE process pressure was lower than 6 mTorr.

The replication of 2-D and 3-D structures has been demonstrated. In 2-D imprinting, two types of mold were used: the transparent mold and the transparent mold with NiCr absorber. Only a single imprint step is involved in 2-D imprinting while in 3-D imprinting two imprint steps are involved. A 400 nm thick Ormocomp and mr-UVCur06 resists were used in Imprint 1 and Imprint 2 processes respectively. A 3-D ring with a height of 600 nm and a multilevel pyramid array with each pyramid dimension of one micron square base and 600 nm in height were replicated.

The assistance of anti adhesive coating using FOTS SAM on the surfaces in contact during imprinting was successfully demonstrated. In finding an alternative permanent anti adhesive coatings, Tungsten and TiO_2 were found to be effective. In imprint 1, coating the quartz mold with a 5 nm sputtered tungsten has protected the mold surface from the stubborn imprint stains.

The Ormocomp and mr-UVCur06 resist surfaces were treated with CHF_3 plasma to lowered its surface energy. In imprint 2, coating the Ormocomp soft mold with a 5 nm TiO_2 improved the imprint up to 15 repetitive cycles.

The final pattern transfer process using CHF_3/O_2 plasma has not achieved satisfactory results because of difficulties in maintaining a very small oxygen gas content in the mixing chamber, and maintaining its flow rate in the RIE system during a long etching time (2 hours).

Well-known NIL general issues on defects, polymers, overlay accuracy and

throughput have been taken care of by various research groups around the world and this has been demonstrated by the continuous publications on these subjects.

This work has produced many encouraging results, however a few limitations have prevented some other major findings such as plasma etching of quartz at a very low operating pressure. There are limitations to the RIE system where the lowest achieveable operating pressure for RIE was about 5 to 6 mTorr. The RIE plasma process becomes unstable at process pressure below 6 mTorr. At low RIE operating pressure, a smoother etched surface and a higher etching rate were expected. The benefits of very low process pressures (less than 6 mTorr) were unable to be realized.

Hydrogen Silsesquioxane (HSQ) was a potential 3-D patterning resist as ma-N2400 series resist but its unavailability had hampered the comparison studies. The manual imprint tool used in this work has less control of the imprint parameters. An attempt to manipulate MA-6 mask aligner to function as an imprint tool was not achieved. A number of recommendations for future work especially on processes and equipment as well as the potential of other materials, have been discussed.

There are huge opportunities in this new technology in terms of potential applications, however, numerous challenges are waiting ahead. Some of these challenges have become the gating factor in deploying this technology especially in semiconductor industry. However, success stories such as in Hitachi GST have proved that this technology will be the major technology player in the near future.

The results of this work have been published in the journals and conference proceedings as well as in the oral and poster presentations. This work has contributed essential knowledge of mold making and imprint processes in UV-NIL patterning technique. This thesis has demonstrated that UV-NIL has the capabilities of replicating 2-D and 3-D nanoscale structures that offer application in various fields of science and technology.

Bibliography

[1] K. E. Drexler, "Engine of creation 2.0:," September 22, 2008. [Online]. Available: http://e-drexler.com

[2] R. M. Brydson and C. Hammond, "Generic methodologies for nanotechnology: classification and fabrication," in *Nanoscale Science and Technology*, R. W. Kelsall, I. W. Hamley, and M. Geoghegan, Eds. Wiley, 2005.

[3] L. J. Guo, "Recent progress in nanoimprint technology and its applications," *Journal of Physics D: Applied Physics*, no. 11, p. R123, 2004.

[4] L. W. Liebmann, S. M. mansfield, A. K. Wong, M. A. Lavin, W. C. Leipold, and T. G. Dunham, "Tcad development for lithography resolution enhancement," *IBM Journal of Research and Development*, vol. 45, no. 5, pp. 651–665, 2001.

[5] K. Masaomi and M. Martin, "Immersion and 32nm lithography: now and future," H. Sen, X. Tingwen, L. Yanqiu, and C. Zheng, Eds., vol. 6724. SPIE, 2007, p. 672402, 3rd International Symposium on Advanced Optical Manufacturing and Testing Technologies: Design, Manufacturing, and Testing of Micro- and Nano-Optical Devices and Systems 1.

[6] O. Yasuhiro, N. Toshiharu, N. Hiroyuki, S. Ayako, I. Satoshi, K. Koichi, S. Masahiko, and O. Soichi, "Current status of high-index immersion lithography development," G. F. Donis, Ed., vol. 6520. SPIE, 2007, p. 652006, optical Microlithography XX 1.

[7] G. E. Fuller, "Optical lithography," in *Handbook of Semiconductor Manufacturing Technology*, Y. Nishi and R. Doering, Eds. New York: Marcel Dekker, 2000.

[8] H. Kinoshita and O. Wood, "Euv lithography: An historical perspective," in *EUV Lithography*, V. Bakshi, Ed. SPIE Press, 2008.

[9] S. Sivakumar, *R&D Status and Key Technical and Implementation Challenges for EUV HVM*. Workshop Proceedings of 2009 International Workshop on EUV Lithography.

[10] R. M. Hudyma and R. Soufli, "Projection systems for extreme ultraviolet lithography," in *EUV Lithography*, V. Bakshi, Ed. SPIE Press, 2008.

[11] I. T. R. for Semiconductor (ITRS), "$itrs$ 2003 edition," September 22, 2005. [Online]. Available: http://www.itrs.net/Links/2003ITRS/Home2003.htm

[12] ——, "$itrs$ 2005 edition," February 20, 2006. [Online]. Available: http://www.itrs.net/Links/2005ITRS/Home2005.htm

[13] ——, "$itrs$ 2008 update," February 22, 2009. [Online]. Available: http://www.itrs.net/Links/2008ITRS/Home2008.htm

[14] Y. Ikuo, M. Shinji, O. Takumi, K. Takeshi, I. Masamitsu, N. Tetsuro, and H. Tatsuhiko, "Study of nanoimprint lithography for applications toward 22nm node cmos devices," M. S. Frank, Ed., vol. 6921. SPIE, 2008, p. 692104, emerging Lithographic Technologies XII 1.

[15] A. Fuchs, M. Bender, U. Plachetka, L. Kock, N. Koo, T. Wahlbrink, and H. Kurz, "Lithography potentials of uv-nanoimprint," *Current Applied Physics*, vol. 8, no. 6, pp. 669–674, 2008.

[16] B. LaFontaine, Y. Deng, R.-H. Kim, H. J. Levinson, S. McGowan, U. Okoroanyanwu, R. Seltmann, C. Tabery, A. Tchikoulaeva, T. Wallow, O. Wood, J. Arnold, D. Canaperi, M. Colburn, K. Kimmel, C.-S. Koay, E. McLellan, D. Medeiros, S. P. Rao, K. Petrillo, Y. Yin, H. Mizuno, S. Bouten, M. Crouse, A. van Dijk, Y. van Dommelen, J. Galloway, S.-I. Han, B. Kessels, B. Lee, S. Lok, B. Niekrewicz, B. Pierson, R. Routh, E. Schmit-Weaver, K. Cummings, and J. Word, "The use of euv lithography to pro-

duce demonstration devices," in *Emerging Lithographic Technologies XII*, vol. 6921. San Jose, CA, USA: SPIE, 2008, pp. 69 210P–10.

[17] G. F. Lorusso, J. Hermans, A. M. Goethals, B. Baudemprez, F. V. Roey, A. M. Myers, I. Kim, B. S. Kim, R. M. Jonckheere, A. Niroomand, S. Lok, A. V. Dijk, J. F. d. Marneffe, S. Demuynck, D. Goossens, and K. Ronse, "Imaging performance of the euv alpha semo tool at imec," M. S. Frank, Ed., vol. 6921. SPIE, 2008, p. 69210O, emerging Lithographic Technologies XII 1.

[18] H. Meiling, E. Boon, N. Buzing, K. Cummings, O. Frijns, J. Galloway, M. Goethals, N. Harned, B. Hultermans, R. de Jonge, B. Kessels, P. Kurz, S. Lok, M. Lowisch, J. Mallman, B. Pierson, K. Ronse, J. Ryan, E. Smitt-Weaver, M. Tittnich, C. Wagner, A. van Dijk, and J. Zimmerman, "Performance of the full field euv systems," in *Emerging Lithographic Technologies XII*, vol. 6921. San Jose, CA, USA: SPIE, 2008, pp. 69 210L–13.

[19] S. Uzawa, H. Kubo, Y. Miwa, T. Tsuji, H. Morishima, K. Kajiyama, and T. Hasegawa, "Canon's development status of euvl technologies," in *Emerging Lithographic Technologies XII*, vol. 6921. San Jose, CA, USA: SPIE, 2008, pp. 69 210N–8.

[20] T. Miura, K. Murakami, K. Suzuki, Y. Kohama, K. Morita, K. Hada, Y. Ohkubo, and H. Kawai, "Nikon euvl development progress update," in *Emerging Lithographic Technologies XII*, vol. 6921. San Jose, CA, USA: SPIE, 2008, pp. 69 210M–10.

[21] I. Mori, O. Suga, H. Tanaka, I. Nishiyama, T. Terasawa, H. Shigemura, T. Taguchi, T. Tanaka, and T. Itani, "Selete's euv program: progress and challenges," in *Emerging Lithographic Technologies XII*, vol. 6921. San Jose, CA, USA: SPIE, 2008, pp. 692 102–12.

[22] S. Y. Chou, P. R. Krauss, and P. J. Renstrom, "Imprint of sub-25 nm vias and trenches in polymers," *Applied Physics Letters*, vol. 67, no. 21, pp. 3114–3116, 1995.

[23] ——, "Nanoimprint lithography," *Journal of Vacuum Science & Technology B: Microelectronics and Nanometer Structures*, vol. 14, pp. 4129–4133, 1996.

[24] H. Schift, "Nanoimprint lithography: An old story in modern times? a review," *Journal of Vacuum Science & Technology B: Microelectronics and Nanometer Structures*, vol. 26, no. 2, pp. 458–480, 2008.

[25] J. Haisma, M. Verheijen, K. van den Heuvel, and J. van den Berg, "Mold-assisted nanolithography: A process for reliable pattern replication," *Journal of Vacuum Science & Technology B: Microelectronics and Nanometer Structures*, vol. 14, no. 6, pp. 4124–4128, 1996.

[26] L. Chien-Hung and C. Rongshun, "Nanofabrication with ultrasonic nanoimprint lithography," in *Nanotechnology, 2006. IEEE-NANO 2006. Sixth IEEE Conference on*, vol. 2, 2006, pp. 603–606.

[27] B. Cui, W. Wu, C. Keimel, and S. Y. Chou, "Filling of nano-via holes by laser-assisted direct imprint," *Microelectronic Engineering*, vol. 83, no. 4-9, pp. 1547–1550, 2006, 0167-9317 doi: DOI: 10.1016/j.mee.2006.01.087.

[28] B. Heidari, I. Maximov, and L. Montelius, "Nanoimprint lithography at the 6 in. wafer scale," in *Papers from the 44th international conference on electron, ion, and photon beam technology and nanofabrication*, vol. 18. Rancho Mirage, California, (USA): AVS, 2000, pp. 3557–3560.

[29] J. Ahopelto and T. Haatainen, "Step and stamp imprint lithography," in *Alternative Lithography; Unleashing the potential of Nanotechnology*, C. M. Sotomayor Torres, Ed. Kluwer Academic, 2003.

[30] M. Colburn, S. C. Johnson, M. D. Stewart, S. Damle, T. C. Bailey, B. Choi, M. Wedlake, T. B. Michaelson, S. V. Sreenivasan, J. G. Ekerdt, and C. G. Willson, "Step and flash imprint lithography: a new approach to high-resolution patterning," in *Emerging Lithographic Technologies III*, vol. 3676. Santa Clara, CA, USA: SPIE, 1999, pp. 379–389.

[31] M. Tormen, "Microcontact printing techniques," in *Alternative Lithorraphy: Unleasing the potential of nanotechnology*, C. M. Sotomayor Torres, Ed. Kluwer Academic, 2003.

[32] S. Y. Chou, C. Keimel, and J. Gu, "Ultrafast and direct imprint of nanostructures in silicon," *Nature*, vol. 417, no. 6891, pp. 835–837, 2002, 0028-0836 10.1038/nature00792 10.1038/nature00792.

[33] L. R. Bao, X. Cheng, X. D. Huang, L. J. Guo, S. W. Pang, and A. F. Yee, "Nanoimprinting over topography and multilayer three-dimensional printing," vol. 20. AVS, 2002, pp. 2881–2886, papers from the 46th International Conference on Electron, Ion, and Photon Beam Technology and Nanofabrication 6.

[34] D. J. Resnick, W. J. Dauksher, D. Mancini, K. J. Nordquist, T. C. Bailey, S. Johnson, N. Stacey, J. G. Ekerdt, C. G. Willson, S. V. Sreenivasan, and N. Schumaker, "Imprint lithography for integrated circuit fabrication," *Journal of Vacuum Science & Technology B: Microelectronics and Nanometer Structures*, vol. 21, no. 6, pp. 2624–2631, 2003.

[35] A. Se Hyun, K. Jin-Sung, and L. J. Guo, "Bilayer metal wire-grid polarizer fabricated by roll-to-roll nanoimprint lithography on flexible plastic substrate," *Journal of Vacuum Science & Technology B: Microelectronics and Nanometer Structures*, vol. 25, no. 6, pp. 2388–2391, 2007.

[36] T. Hua, G. Andrew, and Y. C. Stephen, "Roller nanoimprint lithography," *Journal of Vacuum Science & Technology B: Microelectronics and Nanometer Structures*, vol. 16, no. 6, pp. 3926–3928, 1998, papers from the 42nd international conference on electron, ion, and photon beam technology and nanofabrication 6.

[37] K. D. Lee, S. W. Ahn, S. H. Kim, S. H. Lee, J. D. Park, P. W. Yoon, D. H. Kim, and S. S. Lee, "Nanoimprint technology for nano-structured optical devices," *Current Applied Physics*, vol. 6, no. Supplement 1, pp. e149–e153, 2006.

[38] N. Chaix, S. Landis, C. Gourgon, S. Merino, V. G. Lambertini, G. Durand, and C. Perret, "Nanoimprinting lithography on 200mm wafers for optical applications," *Microelectronic Engineering*, vol. 84, no. 5-8, pp. 880–884, 2007.

[39] T. Ouchi, Y. Arikawa, and T. Homma, "Fabrication of copt magnetic nanodot arrays by electrodeposition process," *Journal of Magnetism and Magnetic Materials*, vol. 320, no. 22, pp. 3104–3107, 2008.

[40] A. Pepin, P. Youinou, V. Studer, A. Lebib, and Y. Chen, "Nanoimprint lithography for the fabrication of dna electrophoresis chips," *Microelectronic Engineering*, vol. 61-62, pp. 927–932, 2002.

[41] C. A. Mills, E. Martinez, F. Bessueille, G. Villanueva, J. Bausells, J. Samitier, and A. Errachid, "Production of structures for microfluidics using polymer imprint techniques," *Microelectronic Engineering*, vol. 78-79, pp. 695–700, 2005.

[42] G. Y. Jung, S. Ganapathiappan, X. Li, D. A. A. Ohlberg, D. L. Olynick, Y. Chen, W. M. Tong, and R. S. Williams, "Fabrication of molecular-electronic circuits by nanoimprint lithography at low temperatures and pressures," *Applied Physics A: Materials Science & Processing*, vol. 78, no. 8, pp. 1169–1173, 2004.

[43] P. G. Emma and E. Kursun, "Is $3d$ chip technology the next growth engine for performance improvenment?" *IBM Journal of Research and Development*, vol. 52, no. 6, 2008.

[44] J. M. Keith, N. Gregory, B. Shufeng, and Y. C. Stephen, "Wafer-scale patterning of sub-40 nm diameter and high aspect ratio (more than 50:1) silicon pillar arrays by nanoimprint and etching," *Nanotechnology*, no. 34, p. 345301, 2008.

[45] B. Cui, L. Clime, K. Li, and T. Veres, "Fabrication of large area nanoprism arrays and their application for surface enhanced raman spectroscopy," *Nanotechnology*, no. 14, p. 145302, 2008.

[46] M. LaPedus, "Nano-imprint litho tool shipped to toshiba."

[47] K. Totsu, K. Fujishiro, S. Tanaka, and M. Esashi, "Fabrication of three-dimensional microstructure using maskless gray-scale lithography," *Sensors and Actuators A: Physical*, vol. 130-131, pp. 387–392, 2006, 0924-4247 doi: DOI: 10.1016/j.sna.2005.12.008.

[48] J. Taniguchi, K. Koga, Y. Kogo, and I. Miyamoto, "Rapid and three-dimensional nanoimprint template fabrication technology using focused ion beam lithography," *Microelectronic Engineering*, vol. 83, no. 4-9, pp. 940–943, 2006.

[49] J. Simcic, P. Pelicon, Z. Rupnik, M. Mihelic, A. Razpet, D. Jenko, and M. Macek, "3d micromachining of su-8 polymer with proton microbeam," *Nuclear Instruments and Methods in Physics Research Section B: Beam Interactions with Materials and Atoms*, vol. 241, no. 1-4, pp. 479–485, 2005, 0168-583X doi: DOI: 10.1016/j.nimb.2005.07.058.

[50] F. Romanato, L. Businaro, L. Vaccari, S. Cabrini, P. Candeloro, M. De Vittorio, A. Passaseo, M. T. Todaro, R. Cingolani, E. Cattaruzza, M. Galli, C. Andreani, and E. Di Fabrizio, "Fabrication of 3d metallic photonic crystals by x-ray lithography," *Microelectronic Engineering*, vol. 67-68, pp. 479–486, 2003, 0167-9317 doi: DOI: 10.1016/S0167-9317(03)00104-7.

[51] F. Romanato, M. Tormen, L. Businaro, L. Vaccari, T. Stomeo, A. Passaseo, and E. Di Fabrizio, "X-ray lithography for 3d microfluidic applications," *Microelectronic Engineering*, vol. 73-74, pp. 870–875, 2004, 0167-9317 doi: DOI: 10.1016/j.mee.2004.03.067.

[52] A. Kowalik, K. Gra, Z. Jaroszewicz, and A. Kolodziejczyk, "Multi-step electron beam technology for the fabrication of high performance diffractive optical elements," *Microelectronic Engineering*, vol. 77, no. 3-4, pp. 347–357, 2005, 0167-9317 doi: DOI: 10.1016/j.mee.2004.12.036.

[53] G. Kumaravelu, M. M. Alkaisi, A. Bittar, D. Macdonald, and J. Zhao, "Damage studies in dry etched textured silicon surfaces," *Current Ap-*

plied Physics, vol. 4, no. 2-4, pp. 108–110, 2004, 1567-1739 doi: DOI: 10.1016/j.cap.2003.10.008.

[54] W. L. Chiu, M. M. Alkaisi, G. Kumaravelu, R. J. Blaikie, R. J. Reeves, and A. Bittar, "Sub-wavelength texturing for solar cells using interferometric lithography," *Advances in Science and Technology*, vol. 51, pp. 115–120, 2006.

[55] C. M. Sotomayor Torres, S. Zankovych, J. Seekamp, A. P. Kam, C. Clavijo Cedeo, T. Hoffmann, J. Ahopelto, F. Reuther, K. Pfeiffer, G. Bleidiessel, G. Gruetzner, M. V. Maximov, and B. Heidari, "Nanoimprint lithography: an alternative nanofabrication approach," *Materials Science and Engineering: C*, vol. 23, no. 1-2, pp. 23–31, 2003.

[56] J. Nabity, L. A. Campbell, M. Zhu, and W. Zhou, "E-beam nanolithography integrated with scanning electron microscope," in *Scanning Microscopy for Nanotechnology*, W. Zhou and Z. L. Wang, Eds. Springer, 2007.

[57] Y. Ishii and J. Taniguchi, "Fabrication of three-dimensional nanoimprint mold using inorganic resist in low accelerating voltage electron beam lithography," *Microelectronic Engineering*, vol. 84, no. 5-8, pp. 912–915, 2007.

[58] K. Mohamed, M. M. Alkaisi, and R. J. Blaikie, "Fabrication of three dimensional structures for an uv curable nanoimprint lithography mold using variable dose control with critical-energy electron beam exposure," *Journal of Vacuum Science & Technology B: Microelectronics and Nanometer Structures*, vol. 25, no. 6, pp. 2357–2360, 2007.

[59] S. Nonogaki, T. Ueno, and T. Ito, *Microlithography Fundamentals in Semiconductor Devices and Fabrication Technology*. Marcel Dekker, 1998.

[60] W. Kern and K. K. Schuegraf, "Deposition technologies and applications: Introduction and overview," in *Handbook of thin-film deposition processes and techniques: principles, methods, equipment, and applications*, K. K. Schuegraf, Ed. New Jersey: Noyes Publications, 1988.

[61] K. J. Lesker Co, "Materials guide for thermal evaporation," 7th May 2009. [Online]. Available: http://www.lesker.com/newweb/menu_evapsources.cfm

[62] S. A. Campbell, *The Science and Engineering of Microelectronic Fabrication*, 2nd ed. Oxford University Press, 2001.

[63] W. M. Moreau, *Semiconductor Lithography: Principles, Practices, and Materials*, ser. Microdevices: Physics and Fabrication Technologies. New York: Prenum Press, 1988.

[64] L. C. Sawyer and D. T. Grubb, *Polymer microscopy*. London, New York: Chapman and Hall, 1987.

[65] W. Zhou, R. P. Apkarian, Z. L. Wang, and D. Joy, "Fundamentals of scanning electron microscopy," in *Scanning Microscopy for Nanotechnology*, W. Zhou and Z. L. Wang, Eds. Springer, 2007.

[66] A. J. Gesquiere, D. Y. Kim, S.-J. Park, and P. F. Barbara, "Near-field spectroscopic studies of fluorescence quenching by charge carrier," in *Application of Scanned Probe Microscopy to Polymers.*, ser. ACS symposium series 897, J. D. Batteas, C. A. Michaels, and G. C. Walker, Eds. American Chemical Society, 2005.

[67] D. Rugar, R. Budakian, H. J. Mamin, and B. W. Chui, "Single spin detection by magnetic resonance force microscopy," *Nature*, vol. 430, no. 6997, pp. 329–332, 2004, 0028-0836 10.1038/nature02658 10.1038/nature02658.

[68] R. M. Brydson and C. Hammond, "Generic methodologies for nanotechnology: characterization," in *Nanoscale Science and Technology*, R. W. Kelsall, I. W. Hamley, and M. Geoghegan, Eds. Wiley, 2005.

[69] W.-J. Chang, "Sensitivity of vibration modes of atomic force microscope cantilevers in continuous surface contact," *Nanotechnology*, no. 4, p. 510, 2002.

[70] W.-J. Chang and T.-H. Fang, "The study of afm probe modal sensitivity and nanolithography," in *Trends in Nanotechnology Research*, E. V. Dirote, Ed. New York: Nova Science, 2004.

[71] Y. Sugimoto, P. Pou, M. Abe, P. Jelinek, R. Perez, S. Morita, and O. Custance, "Chemical identification of individual surface atoms by atomic force microscopy," *Nature*, vol. 446, no. 7131, pp. 64–67, 2007, 0028-0836 10.1038/nature05530 10.1038/nature05530.

[72] V. J. Morris, A. R. Kirby, and A. P. Gunning, *Atomic Force Microscopy for Biologist*. London: Imperial College Press, 1999.

[73] C. Hedlund, U. Lindberg, U. Bucht, and J. Soderkvist, "Anisotropic etching of z-cut quartz," *Journal of Micromechanics and Microengineering*, no. 2, p. 65, 1993.

[74] D. L. Flamm, "Introduction to plasma chemistry," in *Plasma Etching*, D. M. Manos and D. L. Flamm, Eds. Academic Press, 1989.

[75] G. S. May and S. M. Sze, *Fundamentals of Semiconductor Fabrication*. John Wiley and Sons, 2004.

[76] R. J. Shul and J. G. Fleming, "Bulk si micromachining for integrated microsystems and mems processing," in *Handbook of Advanced Plasma Processing Techniques*, R. J. Shul and S. J. Pearton, Eds. Springer, 2000, pp. 419–457.

[77] J. Taniguchi, "Diamond and three dimensional nanoimprint lithography," in *New Developments in Nanotechnology Research*, E. V. Dirote, Ed. New York: Niva Science Publishers, 2007.

[78] wikipedia, "Silica," 7th October 2008. [Online]. Available: http://www.wikipedia.org

[79] M. Galleries, "Quartz," 7th August 2008. [Online]. Available: http://mineral.galleries.com/minerals/Silicate/QUARTZ/QUARTZ.htm#p

[80] T. Q. Incorporation., "Cleaning a quartz sample," 7th October 2008. [Online]. Available: http://www.tosohquartz.com

[81] M. Konijn, M. M. Alkaisi, and R. J. Blaikie, "Nanoimprint lithography of sub-100 nm 3d structures," *Microelectronic Engineering*, vol. 78-79, pp. 653–658, 2005.

[82] M. Technology, "Resist for nanoimprint lithography," 20th March 2006. [Online]. Available: http://www.microresist.de/products/ormocers/ormocomp_en.htm

[83] K. Mohamed, "Resist deformation in nanoimprint lithography (n.i.l.)," Master of Engineering (M.E) Thesis, Electrical and Computer Engineering, University of Canterbury, 2005.

[84] W. Zhou, J. Zhang, Y. Liu, X. Li, X. Niu, Z. Song, G. Min, Y. Wan, L. Shi, and S. Feng, "Characterization of anti-adhesive self-assembled monolayer for nanoimprint lithography," *Applied Surface Science*, vol. 255, no. 5, Part 2, pp. 2885–2889, 2008, 0169-4332 doi: DOI: 10.1016/j.apsusc.2008.08.045.

[85] M. Angelopoulus, "Conducting polymers in microelectronics," *IBM Journal of Research and Development*, vol. 45, no. 1, pp. 57–75, 2001.

[86] W.-S. Huang, "Synthesizing and processing conducting polythiophene derivatives for charge dissipation in electron-beam lithography," *Polymer*, vol. 35, no. 19, pp. 4057–4064, 1994.

[87] B. El-Kareh, *Fundamentals of Semiconductor Processing Technology*. Kluwer Academic Publisher, 1995.

[88] S. M. Rossnagel, J. J. Cuomo, and W. D. Westwood, *Handbook of Plasma Processing Technology: Fundamentals, Etching, Deposition, and Surface Interactions*. William Andrew Inc, 1990.

[89] G. S. Oehrlein, Y. Zhang, D. Vender, and M. Haverlag, "Fluorocarbon high-density plasmas. i. fluorocarbon film deposition and etching using

cf[sub 4] and chf[sub 3]," *Journal of Vacuum Science & Technology A: Vacuum, Surfaces, and Films*, vol. 12, no. 2, pp. 323–332, 1994.

[90] C. M. Chan, T. M. Ko, and H. Hiraoka, "Polymer surface modification by plasmas and photons," *Surface Science Reports*, vol. 24, no. 1-2, pp. 1–54, 1996, 0167-5729 doi: DOI: 10.1016/0167-5729(96)80003-3.

[91] J. W. Colburn, "Some fundamental aspects of plasma-assisted etching," in *Handbook of Advanced Plasma Processing Techniques*, R. J. Shul and S. J. Pearton, Eds. Springer, 2000, p. 24.

[92] E. Gogolides, P. Vauvert, Y. Courtin, G. Kokkoris, R. Pelle, A. Boudouvis, and G. Turban, "sio_2 and si etching in fluorocarbon plasmas: A detailed surface model coupled with a complete plasma and profile simulator," *Microelectronic Engineering*, vol. 46, no. 1-4, pp. 311–314, 1999, 0167-9317 doi: DOI: 10.1016/S0167-9317(99)00091-X.

[93] G. Kokkoris, E. Gogolides, and A. G. Boudouvis, "Simulation of fluorocarbon plasma etching of sio_2 structures," *Microelectronic Engineering*, vol. 57-58, pp. 599–605, 2001, 0167-9317 doi: DOI: 10.1016/S0167-9317(01)00549-4.

[94] J.-P. Booth and G. Cunge, "Cfx radical creation and destruction at surface in fluorocarbon plasmas," *Journal of Plasma and Fusion Research*, vol. 75, pp. 821–829, 1999.

[95] O. Joubert, G. S. Oehrlein, and Y. Zhang, "Fluorocarbon high density plasma. v. influence of aspect ratio on the etch rate of silicon dioxide in an electron cyclotron resonance plasma," *Journal of Vacuum Science & Technology A: Vacuum, Surfaces, and Films*, vol. 12, no. 3, pp. 658–664, 1994.

[96] D. D. Cheam and P. L. Bergstrom, "Optimization of focus ion beam patterning and reactive ion etching process of quartz imprint template for ultra violet nanoimprint lithography," in *26th Army Science Conference (ASC)*, JW Marriot Grande Lakes,Orlando, Florida, 2008.

[97] J. W. Thackeray, G. W. Orsula, D. Canistro, and A. K. Berry, "Evaluation of deep uv anr photoresist for 248.4 nm excimer laser photolithography," *Journal of Photopolymer Science and Technology*, vol. 2, no. 3, pp. 429–443, 1989.

[98] J. M. Shaw, J. D. Gelorme, N. C. LaBianca, W. E. Conley, and S. J. Holmes, "Negative photoresist for optical lithography," *IBM Journal of Research and Development*, vol. 41, no. 1/2, 1997.

[99] J. Joo, B. Y. Chow, and J. M. Jacobson, "Nanoscale patterning on insulating substrates by critical energy electron beam lithography," *Nano Letters*, vol. 6, no. 9, pp. 2021–2025, 2006.

[100] M. D. Frey, "Low kv scanning electron microscopy," in *Scanning Microscopy for Nanotechnology*, W. Zhou and Z. L. Wang, Eds. Springer, 2007.

[101] C. Software, "Monte carlo simulation," 28th October 2006. [Online]. Available: http://www.gel.usherbrook.ca/casino/index.html

[102] M. M. Blideran, M. Hffner, B. E. Schuster, C. Raisch, H. Weigand, M. Fleischer, H. Peisert, T. Chass, and D. P. Kern, "Improving etch selectivity and stability of novolak based negative resists by fluorine plasma treatment," *Microelectronic Engineering*, vol. 86, no. 4-6, pp. 769–772, 2008, 0167-9317 doi: DOI: 10.1016/j.mee.2008.12.057.

[103] S. Y. Chou, "Nanoimprint lithography," in *Alternative Lithography: Unleashing the Potentials of Nanotechnology*, C. M. Sotomayor Torres, Ed. Kluwer Academic/Plenum Publishers, 2003.

[104] D. S. Macintyre and S. Thoms, "A study of resist flow during nanoimprint lithography," *Microelectronic Engineering*, vol. 78-79, pp. 670–675, 2005.

[105] S. Merino, H. Schift, A. Retolaza, and T. Haatainen, "The use of automatic demolding in nanoimprint lithography processes," *Microelectronic Engineering*, vol. 84, no. 5-8, pp. 958–962, 2007.

[106] M. Bender, U. Plachetka, J. Ran, A. Fuchs, B. Vratzov, H. Kurz, T. Glinsner, and F. Lindner, "High resolution lithography with pdms molds," *Journal of Vacuum Science & Technology B: Microelectronics and Nanometer Structures*, vol. 22, pp. 3229–3232, 2004.

[107] J. P. Rolland, E. C. Hagberg, G. M. Denison, K. R. Carter, and J. M. De Simone, "High-resolution soft lithography: Enabling materials for nanotechnologies13," *Angewandte Chemie International Edition*, vol. 43, no. 43, pp. 5796–5799, 2004, 10.1002/anie.200461122.

[108] E.-J. Jang, Y.-B. Park, H.-J. Lee, D.-G. Choi, J.-H. Jeong, E.-S. Lee, and S. Hyun, "Effect of surface treatments on interfacial adhesion energy between uv-curable resist and glass wafer," *International Journal of Adhesion and Adhesives*, vol. In Press, Corrected Proof, 0143-7496 doi: DOI: 10.1016/j.ijadhadh.2009.02.006.

[109] V. Trabadelo, H. Schift, S. Merino, S. Bellini, and J. Gobrecht, "Measurement of demolding forces in full wafer thermal nanoimprint," *Microelectronic Engineering*, vol. 85, no. 5-6, pp. 907–909, 2008, 0167-9317 doi: DOI: 10.1016/j.mee.2008.01.086.

[110] A. F. Software, "Abaqus/cae manual," 2003.

[111] K. Mohamed, M. M. Alkaisi, and J. Smaill, "Resist deformation at low temperature in nanoimprint lithography," *Current Applied Physics*, vol. 6, no. 3, pp. 486–490, 2006.

[112] H. Sun, J. Liu, P. Gu, and D. Chen, "Anti-sticking treatment for a nanoimprint stamp," *Applied Surface Science*, vol. 254, no. 10, pp. 2955–2959, 2008, 0169-4332 doi: DOI: 10.1016/j.apsusc.2007.10.047.

[113] R. Wilson, "Can molecular imprint circumvent lithography altogether?" July 10. [Online]. Available: http://www.molecularimprints.com

[114] M. Imprint, "Nanoimprint system," 7th October 2008. [Online]. Available: http://www.molecularimprint.com

[115] H. Hiroshima, "Nanoimprint with thin and uniform residual layer for various pattern densities," *Microelectronic Engineering*, vol. In Press, Corrected Proof, 2009, 0167-9317 doi: DOI: 10.1016/j.mee.2008.11.076.

[116] J. Li and F. Martin, "Accurate alignment technique for nanoimprint lithography," M. S. Richard, Ed., vol. 5752. SPIE, 2005, pp. 429–437, metrology, Inspection, and Process Control for Microlithography XIX 1.

[117] A. Lebib, Y. Chen, J. Bourneix, F. Carcenac, E. Cambril, L. Couraud, and H. Launois, "Nanoimprint lithography for a large area pattern replication," *Microelectronic Engineering*, vol. 46, no. 1-4, pp. 319–322, 1999.

[118] M. Mhlberger, I. Bergmair, W. Schwinger, M. Gmainer, R. Schftner, T. Glinsner, C. Hasenfu, K. Hingerl, M. Vogler, H. Schmidt, and E. B. Kley, "A moir method for high accuracy alignment in nanoimprint lithography," *Microelectronic Engineering*, vol. 84, no. 5-8, pp. 925–927, 2007.

[119] X. Li, T. Abe, and M. Esashi, "Deep reactive ion etching of pyrex glass using sf6 plasma," *Sensors and Actuators A: Physical*, vol. 87, no. 3, pp. 139–145, 2001, 0924-4247 doi: DOI: 10.1016/S0924-4247(00)00482-9.

[120] Y. Morikawa, T. Koidesawa, T. Hayashi, and K. Suu, "A novel deep etching technology for si and quartz materials," *Thin Solid Films*, vol. 515, no. 12, pp. 4918–4922, 2007, 0040-6090 doi: DOI: 10.1016/j.tsf.2006.10.100.

[121] V. Siriwongrungson, M. M. Alkaisi, and S. P. Krumdieck, "Step coverage of thin titania films on patterned silicon substrate by pulsed-pressure mocvd," *Surface and Coatings Technology*, vol. 201, no. 22-23, pp. 8944–8949, 2007, 0257-8972 doi: DOI: 10.1016/j.surfcoat.2007.03.051.

[122] V. Siriwongrungson, *Contact angle measurement on titania surface*. Unpublished Work, 2009.

[123] H. GST, "Terra era," 7th October 2008. [Online]. Available: http://www.HitachiGST.com

[124] S. Hosaka, Z. Mohamad, M. Shirai, H. Sano, Y. Yin, A. Miyachi, and H. Sone, "Nano-dot and -pit arrays with a pitch of 25nm25nm fabricated

by eb drawing, rie and nano-imprinting for 1tb/in2 storage," *Microelectronic Engineering*, vol. 85, no. 5-6, pp. 774–777, 2008, 0167-9317 doi: DOI: 10.1016/j.mee.2007.12.081.

Appendices

Appendix A

List of equipment used in this research work

Figure A.1: The Laurell Technologies spinner system, model WS-400B-6NPP/LITE, used for resist spin coating process.

Figure A.2: The newly installed spinner system from Headway Research Inc.

Figure A.3: The ultrasonic bath from Unisonics for ultrasonic cleaning process.

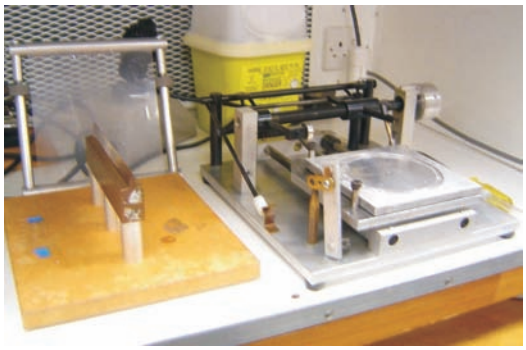

Figure A.4: The in-house designed wafer scriber/cleaver tool.

Figure A.5: The Raith-150 electron beam lithography (EBL) system for direct pattern writing on photoresists and imaging using scanning electron microscopy (SEM).

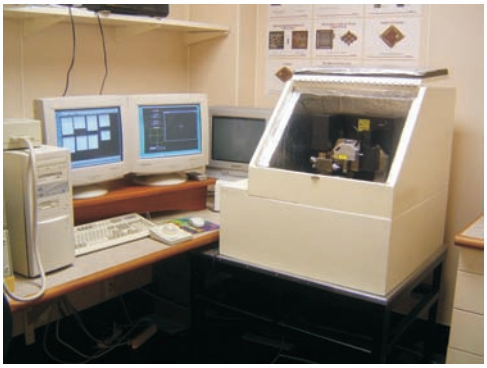

Figure A.6: The atomic force microsopy (AFM) system, Nanoscope IIIa from Digital Instruments, was used for imaging surface topography at nanoscale level.

Figure A.7: The Karl Suss mask aligner system (MA-6) for mask alignment and UV exposure.

Figure A.8: The newly installed EVG620 UV curable Nanoimprint Lithography system for nanoimprint process and optical lithography exposure.

Figure A.9: The Edward 500 Magnetron sputtering system for material deposition using DC, RF sputtering and e-beam evaporation techniques.

Figure A.10: The Balzers BA 510A metal evaporator system for depositing thin metallic layer on samples.

Figure A.11: The conventional Oxford Plasma 80plus reactive ion etching system for pattern transfer process and surface treatment.

Figure A.12: The Veeco Dektak 150 profilometer system for 2-D and 3-D profiles tracing.

Figure A.13: The old ET Plasmafab oxygen plasma system for substrate cleaning.

Figure A.14: The newly installed Emitech K1050X oxygen plasma system for substrate cleaning and residual resist descumming.

Figure A.15: The Tempress 602 dice saw system for cutting substrate materials.

Figure A.16: The stirrer system from Grant Instrument, model Y14, was used for preparing diluted resists.

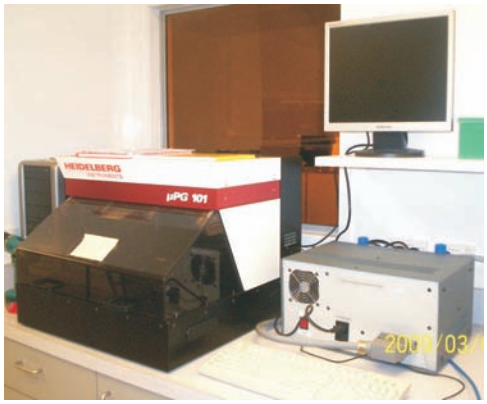

Figure A.17: The mask writer system from Heidelberg Instrument, model μPG 101, for patterning the mask at higher speed.

Figure A.18: The mini furnace from Orton, model SentryXpress 4.0, used for baking samples at high temperatures.

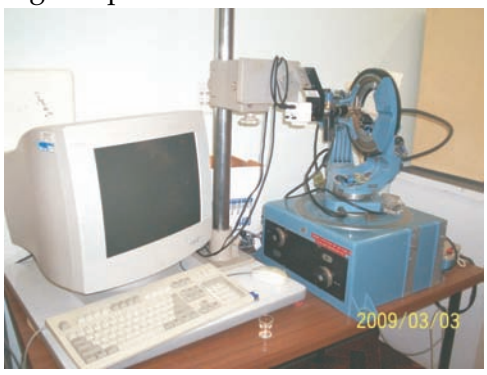

Figure A.19: The UC contact angle measurement system for measuring surface wettability.

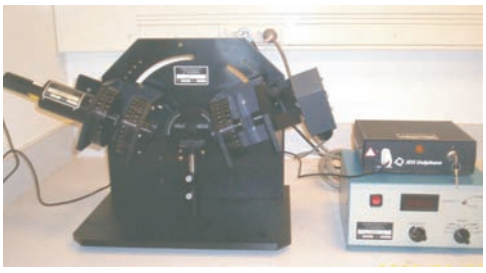

Figure A.20: The manual ellipsometer system from Rudolph Instrument, used for measuring thin film thickness.

Appendix B

Chemicals used in this research work

Table B.1: The list of chemicals for resists, developer and solvents.

Chemical Name	Symbol	Purpose/ Function
Polymethyl methacrylate	PMMA	positive resist
Hydrogen silsesquioxane	HSQ	e-beam negative resist
ma-N2403	ma-N2403	e-beam negative resist
Ormocomp	Ormocomp	UV curable resist
Polydimethylsiloxane	PDMS	UV curable resist
mr-UVCur06	mr-UVCur06	UV curable resist
Methyl Isobutyl Ketone	MIBK	Developer for PMMA
Ormothin	Ormothin	Thinner for Ormocomp dilution
Ormodev	Ormodev	Developer for Ormocomp
ma-T1050	ma-T1050	Thinner for ma-N2400 series resist
Acetone	Ace	Cleaning and lift-off solvent
Methanol	Meth	Cleaning solvent
Isopropyl Alcohol	IPA	Cleaning solvent
N-Methyl-2-pyrrolidone	NMP	Cleaning and lift-off solvent

Table B.2: The list of chemicals for etching and coating.

Chemical Name	Symbol	Purpose/ Function
Trifluoromethane or Halocarbon 23	CHF_3	RIE etchant gas
Sulfur hexafluoride	SF_6	RIE etchant gas
poly(3,4-Ethylenedioxythiophene) /poly(styrenesulfonate)	PEDOT/PSS	Conductive polymer
Polytetrafluoroethylene	PTFE	RIE electrode holder
Tungsten	W	Metallic thin layer
Titania	TiO_2	Non-stick coating
1H,1H,2H,2H-Perfluorooctyl-trichlorosilane (FOTS)	$CF_3(CF_2)_5 -CH_2SiCl_3$	anti adhesive layer

Table B.3: The recipe for wet etching chemicals.

Chemical Etcher Name	Recipe
Aluminium Etcher	80% Orthophosphoric + 10% DI water + 5% Nitric Acid + 5% (Glacial) Acetic acid
Chrome Etcher	165g/l Ammonium Ceric Nitrate + 42g/l 70% perchloric acid
Piranha Etcher	H_2SO_4 + H_2O_2 (5:1)
Buffered Oxide Etcher (BOE) (Silicon Oxide Etcher)	6 parts of 40% NH_4F + 1 part of 40% HF
Gold Etcher	17.0 g KI + 100 ml H_2O + 3.5 g I_2 Dilute 4 parts H_2O: 1 part of above mixture

Appendix C

Other Images

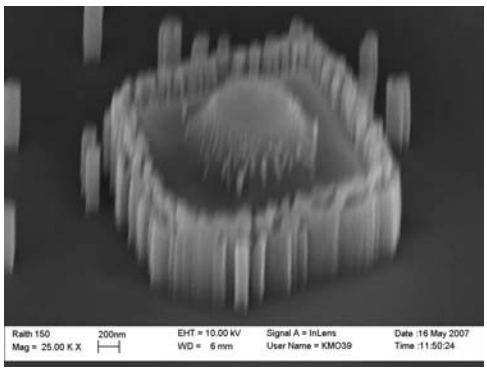

Figure C.1: The multilevel shape of a hemisphere on top of square block with nanomasking effects at the edges.(Quartz substrate)

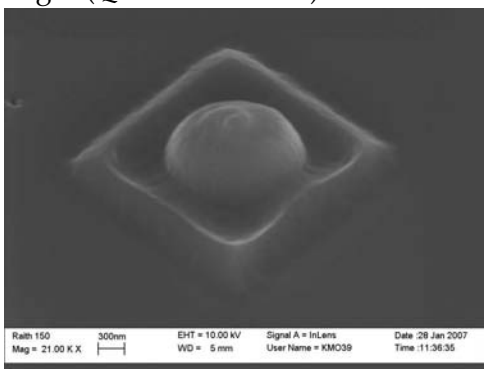

Figure C.3: The multilevel structure of a hemisphere placed on top of the square block showing the trenching effects at the bottom of hemisphere shape. (Quartz substrate)

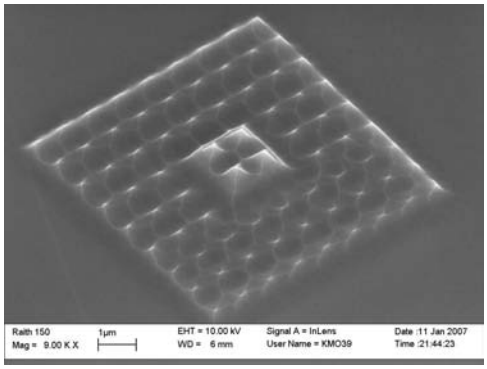

Figure C.5: The multilevel structure of pyramid array on silicon substrate.

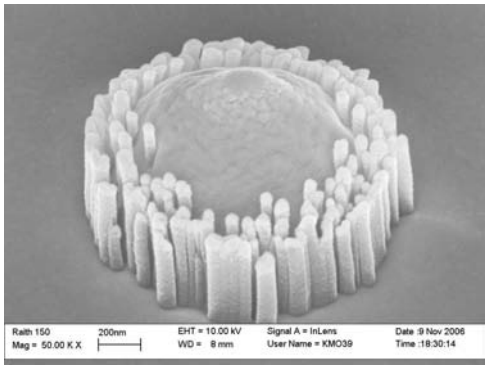

Figure C.2: A single hemisphere shape with nanomasking effects at the bottom. (Quartz substrate)

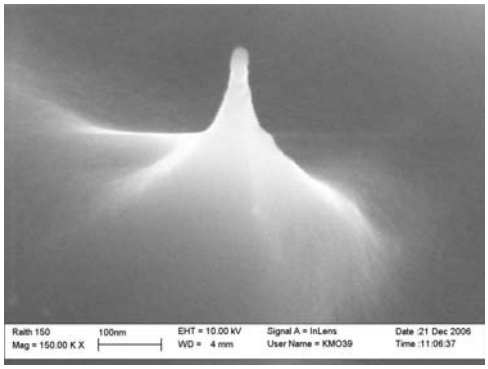

Figure C.4: The silicon tip fabricated after the pattern transfer of a 3-D pyramid shape onto a silicon substrate.

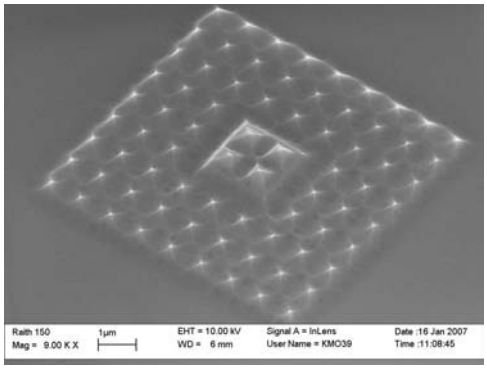

Figure C.6: The multilevel structure of pyramid array on silicon nitride substrate.

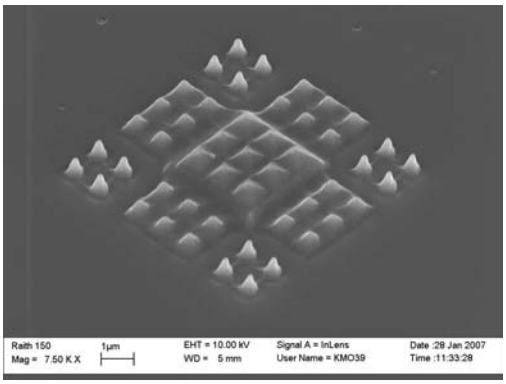

Figure C.7: The SEM image of 3-D multilevel structures with 3 levels demonstrating a more complicated multilevel capability.

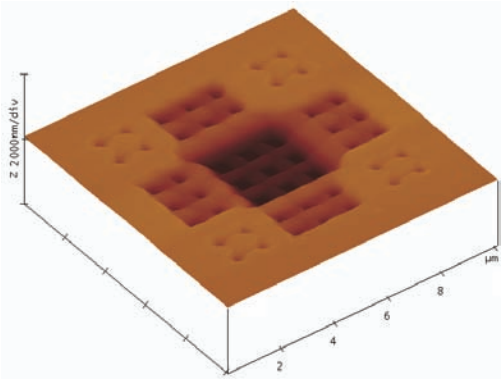

Figure C.8: The AFM image of the imprinted 3 levels structure on an Ormocomp resist.

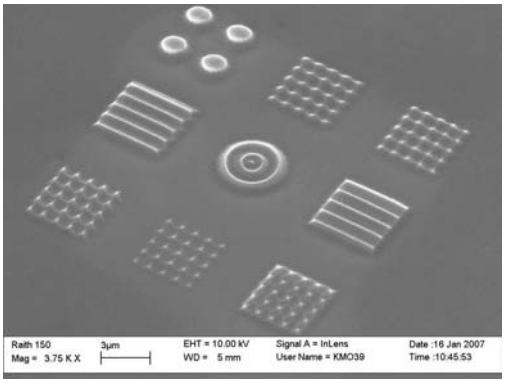

Figure C.9: The SEM image of various 3-D geometrical shapes on quartz mold.

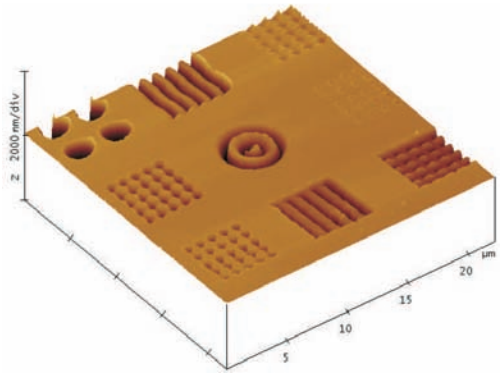

Figure C.10: The AFM image of the imprinted 3-D geometrical shapes on Ormocomp resist.